Studying Intercellular Signaling Underlying Human Diseases Using Open Microfluidic Coculture

Tianzi Zhang

A dissertation

submitted in partial fulfillment of the

requirements for the degree of

Doctor of Philosophy

University of Washington

2020

Reading Committee:

Ashleigh B. Theberge, Chair

Robert E. Synovec

Jesse G. Zalatan

Program Authorized to Offer Degree:

Chemistry

University of Washington

Abstract

Studying Intercellular Signaling Underlying Human Diseases Using Open Microfluidic Coculture

Tianzi Zhang

Chair of the Supervisory Committee:
Professor Ashleigh B. Theberge
Department of Chemistry

This dissertation focuses on the development of innovative open microfluidic cell culture platforms and their application in studying intercellular signaling underlying human diseases in controlled *ex vivo* microenvironments. Chapter 1 introduces the background of open microfluidic capillary systems, including the design considerations and current fabrication techniques, and addresses the advantages of using open microfluidic cell culture systems to study intercellular signaling. Chapter 2 presents a new open microfluidic capillary platform, which patterns biocompatible hydrogel walls along a rail insert set inside established cultureware. The permeable hydrogel walls provide segregation for the cells and support diffusion of soluble factors. Chapter 3 discusses a microscale collagen gel contraction assay with an engineered well plate insert that

uses surface tension forces to load and manipulate small volumes of cell-laden collagen. The system is easily operated with two pipetting steps and the microscale device moves dynamically as a result of cellular forces. Chapter 4 presents an open microfluidic coculture platform consisting of two independent cell culture regions separated by a half wall. The cell types are selectively seeded into the regions and connected with cell culture media. Using the device, we show that human kidney tubular epithelial cells can tune organ-specificity in other endothelial cell types. Chapter 5 shows a preliminary asthma disease coculture model of human lung fibroblasts and primary alveolar macrophages using a similar open microfluidic coculture device to that described in Chapter 4. The preliminary cell culture result indicates that lung fibroblasts exhibit elevated cell contractility when cultured separately with alveolar macrophages in shared cell culture media. Chapter 6 concludes the thesis and proposes some future research directions and interesting metabolomic studies using existing or alternative open microfluidic systems.

TABLE OF CONTENTS

LIST OF FIGURES

ACKNOWLEDGEMENTS

First, I would like to thank my research advisor, Dr. Ashleigh B. Theberge, for her continuous support and guidance in every stage in my PhD study. Her enthusiasm for applying microfluidics to life science problems inspired me to conduct interdisciplinary research in chemistry, biology, and engineering. She is the best mentor that I can ever imagine -- her respect for knowledge, generosity and understanding towards students, and excellent communication skills have always motivated me to become a more professional researcher and a more thoughtful person. I would also like to express my gratitude to Dr. Erwin Berthier and Dr. Ying Zheng, who also mentored me on different projects during my PhD. I could not have achieved my research goals without their continuous support and guidance.

Besides my advisors, I would like to thank my past and present committee members: Dr. Robert E. Synovec, Dr. Jesse G. Zalatan, Dr. Bo Zhang, Dr. Anne B. McCoy, and Dr. Albert Folch for their valuable comments and insightful suggestions.

I sincerely appreciate the research and learning experience with the past and present Theberge-Berthier group members, especially Xiaojing Su, Ashley Dostie, Sam Berry, and John Day. Their intellectual input and dedication really helped my research projects move forward and reach the goal. I would also like to thank fellow group members, Ulri Lee, Tammi van Neel, Amanda Haack, and Dr. Fang Yun Lim, for their generous help with academic writing and scientific insights.

Moreover, I would like to thank my nephrology collaborators at UW Medicine South Lake Union. I really enjoyed working with Daniel Lih, an experienced cell biologist who was always patient, dependable, and coordinated.

I would like to extend my gratitude to the funding organizations and donors of several fellowships and awards I received at the University of Washington, including the Gary and Sue Christian Graduate Fellowship, the Graduate Merit Fellowship, the Alma Mater Travel Award, and the traveling grant awarded by Chemical and Biological Microsystems Society.

Last but not least, I am deeply grateful to my family and friends for their love and emotional support along the way. I am grateful to my parents for offering me the opportunity to study abroad since college and develop my interests in life sciences. I feel incredible lucky to have Nancy and Ray Reasland as my host family in the US and they make me feel at home when my family is thousands of miles away. Thank Catherine Quinn, my dearest friend since college, for being around and hanging out with me during my entire PhD in Seattle. I also feel truly blissful to live with Sishuang Wang and Chenglong Wang in the past five years -- their unconditional support and care help me get through all the emotional ups and downs through my graduate school. All these amazing people I met in the past years have influenced my life and helped me become a who I am today.

DEDICATION

This dissertation is dedicated to my wonderful parents for offering me the chance to exploring the world and trusting me to make my own life decisions.

I would also like to dedicate this to my best friend Chenglong Wang, for all the company, understanding, and encouragement during this unforgettable journey.

Chapter 1. INTRODUCTION

1.1 Open Microfluidic Capillary Systems

Microfluidics is the discipline that manipulates and controls small volumes of fluids in systems with at least one dimension on the micron scale [1-3]. Over the last three decades, microfluidics has evolved as a technology that attracts researchers in both academia and industry, which advances the development of life sciences and biotechnologies. Microfluidic devices enable the utilization of reduced sample and reagent consumption, shorter assay time, and high-throughput processing [4-6]. By leveraging the effects of laminar flow at microscale, microfluidic platforms are capable of performing experiments and studying phenomena that are unreachable using traditional macroscale tools [7, 8].

The interest of cell biologists for microfluidic technology stems from a practical point of view. Traditionally, coculture of cells (i.e., culturing two types of cells in shared cell culture medium) are performed using standardized cell culture vessels, such as culture plates and Transwell inserts placed inside the well plate. Such coculture setups suffer from a few limitations including the fixed culture configurations, the number of cultures in communication, the inability to use alternative surface materials required by certain cell types, and the poorly defined diffusion gradients [9-13]. Innovative microfluidic devices enable biologists to customize and manipulate the microenvironment surrounding the cells in culture, which better mimics the condition in human body. Moreover, the opportunity to create and test numerous individual culture conditions in parallel greatly improves operation efficiencies, which saves on experimental cost, labor, and time. However, due to the complications embedded in the fabrication techniques and operation

requirements, general biology labs could have problems in accessing and adopting the novel microfluidic platforms [6, 7].

Open microfluidic systems contain open air−liquid interfaces (devoid of at least one channel wall), which provides unique opportunities to deliver, handle, and collect biological samples at any time point [13-16]. In open systems, the capillary forces of the liquid in the channel drives the fluid flow without the need for external pressure; this is known as spontaneous capillary flow (SCF) [16, 17]. The conditions for SCF have been well characterized, and certain channel design considerations have been developed, to enable the flow in an open channel. In practice, an open microfluidic device should be designed to allow simple operation. Since these devices do not rely on external actuation or pumping systems, standard tools like automatic pipettes can be deployed by users. Additionally, open microfluidic systems offer unique advantages over closed systems, including single-step fabrication (e.g., soft lithography, 3D printing, and micromilling), surface modification, improved accessibility, and de-bubbling, lowering the barrier of adoption by general biological users [14].

As a class of versatile and translational tools, open microfluidic systems have been developed and applied to a wide range of cell biological studies, including cell signaling, organotypic modeling, single cell culture, metabolomics, and multikingdom cell cultures [6, 7, 9-16]. By understanding of physics of the open microfluidic capillary forces and the advances in engineering and manufacturing methods, open microfluidics will continue to evolve and lead to impactful research discoveries.

1.2 DESIGN CONSIDERATIONS

With at least one boundary removed, open microfluidic systems expose fluid to air or liquid interfaces with a second immiscible liquid. In open systems driven by capillary flow, the microchannel is designed and fabricated such that the fluid flow is driven by surface tension, eliminating the need for external pressure sources. This type of fluid spreading at the contact of wetting walls driven by capillary force is described as spontaneous capillary flow (SCF), which allows fluid movement and control in microscale open systems. In practice, SCF can be predicted by the channel wettability and cross-sectional geometry. Based on the free energy of the fluid, the general equations for SCF can be derived and used as a design guideline for the microscale open channel [16, 17].

1.2.1 *Conditions for SCF in an Open Channel*

The analytical model of SCF in an open microfluidic system has been derived by Casavant et al., which describes the condition required for fluid to flow in a channel without the addition of other forces (e.g., pressure at the inlet port, gravity) [16]. When the channel surface is homogeneous, the contact angle (θ) of the liquid on every channel surface is constant, and the universal condition for SCF can be described as

$$\frac{P_f}{P_w} < \cos(\theta)$$

where P_f, the free perimeter, comprises the total length of air−liquid interfaces on the channel cross-sectional plane at the fluid front; and P_w, the wetted perimeter, comprises the total length of solid−liquid interfaces on the channel cross-sectional plane. Furthermore, when the channel

material is heterogeneous and the contact angle of the liquid on channel surfaces are different, the occurrence of SCF in the system can be determined by the Generalized Cassie law [16, 17].

The condition for SCF sets the boundary condition for the dimensions of the channel relative to the contact angle of the fluid. Specifically, given the contact angle of the liquid flowing in the open channel (i.e., cell culture media) and the geometric relationship (i.e., aspect ratio for a suspended rectangular channel) the channel cross section can be determined [14, 16, 17].

1.2.1 *Evaporation Control*

In open microfluidic systems, evaporation is a common issue due to the existence of air-liquid interfaces [14]. Evaporation control is critical at the microscale, as small amounts of evaporation can have a large impact on media volumes, shifting concentrations and chemical gradients in the microenvironment [18, 19]. As a result, evaporation control should be accounted for in the device design process. Since the loading volumes of the liquid are normally less than 100 μL and the sample for each replicate needs to be pipetted separately, evaporation can have great impact over the device loading process. Therefore, user friendly loading features need to be incorporated into the device design. In addition, it has been shown that encompassing an open microscale device inside a container with sacrificial droplets, such as pure water or phosphate-buffered saline (PBS) solution, can significantly mitigate evaporation [18]. When the system needs to be incubated, the open device can be placed inside a secondary or tertiary humidified container, such as a Petri dish, an Omni Tray, or a BioAssay Dish containing Kimwipes soaked in water or PBS solution. Consequently, the size or the shape of the device needs to be designed to be compatible with the evaporation control platforms mentioned earlier.

1.3 Open Microfluidic System Fabrication

Choosing a suitable fabrication method is important when developing microfluidic systems. The commonly used techniques to fabricate traditional closed or semi-open microfluidic channels include micromachining, injection molding, soft lithography, hot embossing, and laser ablation [2, 3, 5-8]. Devices can then be bonded to a flat surface using heat-based lamination, solvent bonding, ultrasonic or laser welding, or adhesive, to enclose the channel. While bonding methods are well established, they are often a very time-consuming step in the fabrication process, which can be eliminated when fabricating open microfluidics channels. Additionally, open microfluidics allows for fast prototyping using 3D printing without the need to drain uncured polymer as is required for closed channels. Open channel designs typically require less fabrication time and, in some cases, improve fabrication reproducibility [20-23].

1.3.1 *Fabrication Techniques*

Due to the complexity involved in the interaction between cells and their surrounding microenvironment, creating a suitable microscale *in vitro* platform for cell-based studies requires intensive optimization of the original device design. Consequently, affordable fabrication methods that allow for rapid iteration through various designs are favored.

Micromilling is a very effective method for fabricating microfluidic systems with plastics [20]. Specifically, computer numerical control (CNC) milling can automatically convert three-dimensional (3D) computer-aided design (CAD) models to working prototypes, improving the efficiency for design iteration. Compared to stereolithography, hot embossing, and injection

molding, CNC milling offers advantages in start-up cost, design versatility and resolution, and material selection [21-23].

Another simple and direct method for device prototyping and fabrication is 3D printing. The open channel configuration reduces material consumption and printing time, and exposed channel surfaces allow the polymer curing to go more complete without the extra uncured polymer draining process required in closed channel devices. Importantly, 3D printing can achieve complex and detailed structures with high resolution and reproducibility within and across batches of devices [27].

1.3.2 *Surface Treatment*

As an essential part of the microfluidic device preparation for cell culture assays, surface modifications are normally performed on the microscale channels to enhance surface wettability for cell adhesion and proliferation. Subsequently, hydrophilicity of the surface can affect integrin-mediated cell signaling and mechanotransduction. From a device operation aspect, the hydrophilized surface facilitates SCF in the microchannel and minimizes bubble formation during the filling process. For PS based or 3D-printed open microfluidic systems, plasma treatment serves as a practical technique to prime the channel surface [28, 29].

During plasma treatment, a source gas such as free air or oxygen is charged in a low-pressure environment (i.e., vacuum) by an electric current. Reactive oxygen ions are formed and interact with the devices in the chamber to increase the hydrophilicity of the channel surface. The plasma treatment is more homogeneously applied to an open channel system as every point along the channel surface is readily accessible [14]. A limitation of plasma treatment is the reduced shelf life

due to hydrophobic recovery, a reversal of the hydrophilicity of the plasma treated surface over time. To avoid surface deterioration and ensure device functionality, surface treatment is normally done on the same day of the experiment. Due to the necessity to utilize freshly plasma treated devices for cell-based assays, collaborations between engineers and biologists in distant locations may be limited if the group receiving devices does not have the ability to plasma treat the devices.

Additionally, *in vitro* cell adhesion is a complex process that is affected by the presence of ECM proteins, such as Matrigel, collagen, gelatin or other cell culture serum. Coating the device with ECM protein solutions or cell culture media is sometimes required for culturing sensitive cell types [29, 30].

1.4 Key Advantages of Open Microfluidic Systems

The configuration of open microfluidic systems offers freedom in device fabrication and operation along with several other advantages over traditional closed microfluidic systems and are discussed in this section. With careful design consideration and proper choice of material and fabrication method, open microfluidic devices can be easily adopted by researchers without needing specialized training.

1.4.1 *Pipette Accessibility*

One major advantage of open microfluidic platforms is the accessibility of the open channel, which enables researchers to introduce or remove reagents from the device with standard pipetting tools [16]. The direct access to the cell culture regions facilitates a simple workflow for media changes, which can save time during the experiment and minimize the risk of desiccating the cells in culture. Open microfluidic platforms driven by SCF do not need external pumping or tubing equipment,

making them portable from benchtop to benchtop and across laboratories. The air-liquid interface (ALI), enables air bubbles generated in the open system to escape without complex degassing systems [31]. Additionally, an ALI can be an important feature required in experiments or reactions. For example, human pulmonary epithelial cells need to differentiate under ALI to mimic the conditions in the lung [32]. Additionally, the distance between cell culture units in an arrayed microfluidic chip can be designed in accordance with the spacing between the channels of multichannel pipettes, further enhancing the operating efficiency.

1.4.2 *Imaging Capability*

Immunocytochemistry and fluorescence imaging are standard techniques employed in modern biological research to understand biomolecular properties of tissues and cells *in situ*. Cellular structures and key protein expression can be labeled with fluorescent dyes and imaged to provide qualitative information and essential insight for evaluating physiological features of the living or fixed tissues. Traditional 2D imaging normally requires the cells to adhere to a flat substrate with optical transparency, which can be demonstrated by standard cell culture vessels, such as cell culture wells and flasks. Open microfluidic devices can be fabricated from the same material as standard cell culture vessels (i.e., polystyrene, polyethylene, and poly methyl methacrylate (PMMA)) [20, 26].

A main advantage of open microfluidic systems is the capacity to image different cell types grown in a confined area. If the device provides the same plane of focus for both cell types, the operating efficiency and consistency can be assured without manually adjusting the focal plane for each cell type in the device.

1.4.3 *Design Flexibility*

Computer Aided Design (CAD) software, such as SolidWorks and AutoCAD, are widely used to design microfluidic systems. The device development process can take weeks to months of design modification and iteration until the design is optimized and finalized. 3D CAD-based device designing offers great flexibility in design modification and fast prototyping, allowing researchers to customize the system for their own research needs. Additionally, original CAD files can be uploaded to online software provided by rapid injection molding companies to streamline fabrication of devices in large quantities. Rapid injection molding is a fabrication method that improves efficiency, consistency in device fabrication and lowers cost [23].

1.4.4 *Open Microfluidics vs. Transwell Systems*

Transwell systems, which are permeable membrane inserts for well plates, have been widely used as a cell culture tool to study metabolic transport and other intercellular interactions *in vitro*. Two different cell types can be independently loaded into the well plate and the permeable Transwell support to facilitate paracrine signaling. Open microfluidic cell culture platforms embody similar capacities to culture multiple cell types in a shared microenvironment and offer distinct advantages, including the imaging capability and design flexibility discussed in Sections 2-5. Specifically, in a Transwell system, one cell type is seeded on the well plate bottom and the other on the porous membrane that sits above the well plate bottom, making it challenging to image the cell types at the same time. Additionally, the membrane is available in limited materials (polyester and polycarbonate), making it difficult to grow sensitive cell types that require a polystyrene substrate. Pore sizes ranging from 0.4-8 um are available. Open microfluidic systems can avoid this

complication by configuring segregated cell culture regions that are connected by a liquid solution, but that do not allow the migration of cells from one region to the other [33].

1.4.5 *Limitations and Areas for Improvement*

Most current simple open microfluidic systems do not incorporate fluid flow during the culture period, but rather use capillary driven flow only in the initial loading of the device and media changes periodically during culture [16]. Open microfluidic systems are typically operated with a pipette and do not require external pumps, valves or actuation systems to generate fluidic flow, which enables general biological laboratories to operate the devices without training on complicated fluidic generation systems. However, the resulting static fluid in the open system does not provide the capacity of the system to address the effect of shear stress, which refers to forces applied parallel to a surface. For example, as blood flows along the vessel wall *in vivo*, endothelial cells lining the blood vessel wall experience shear stress from the flowing blood, which triggers them to release paracrine signals to adjacent smooth muscle cells and undergo highly complex biochemical interactions [34, 35]. The absence of fluidic flow in open microfluidic systems makes it challenging to incorporate shear stress in cell culture models, therefore, fully recapitulating *in vivo* conditions for investigations on diseases related to shear stress is difficult in open systems.

Consequently, a major design challenge we seek to solve in future work is to incorporate shear flow in open microfluidic systems.

1.5 Novel Advances of Open Microfluidic Tools in Biological Research

The flexibility and functionality of open microfluidic tools have been translated to advance biological research. Great impact has been made in many research areas, including metabolite extraction, hydrogel preparation, gradient generation, cell culture on chip, and perfusion systems for cell culture, etc [16]. The subsections below provide an overview of the areas of interest for the open microfluidic platforms presented in this thesis.

1.5.1 *Suspended Gel Patterning*

For cell culture applications, hydrogel 3D fabrication and patterning techniques have been developed to enable capturing desired biological functions in the microenvironment, such as mechanical responses, organotypic function, or geometric separation. Among the established engineering methods, photopolymerization is a robust technique with the highest resolution (on the order of microns). The limitations are that the precursor hydrogel needs to be chemically functionalized prior to using, and therefore limits the use of native or unmodified gels to address biological questions; also, the photoinitiators could pose cellular damage to some cell types [36, 37]. Inkjet and micro extrusion-based printing is another common method. During printing, the hydrogel encapsulating cells are exposed to shear stress going through the nozzle, which may damage some cell types [38, 39].

Alternatively, SCF flow in the open channel can be utilized as a simple but effective tool to achieve complex hydrogel patterning [33, Chapter 2]. To pattern hydrogel on a flat surface, we developed a patterning device, which in our initial work is typically a 3D printed plastic rail or a hydrophilic

track on a hydrophobic surface. The precursor gel solution flows via SCF without external pressure, and capillary pinning features constrain the pre-gel solution under the rail footprint. Specifically, the patterned hydrogel wall could be used to partition a well plate for coculture studies for two main reasons: 1) the patterned hydrogel wall provides spatial segregation for the neighboring cell types in the microenvironment; 2) the hydrogel wall is permeable to soluble factors, therefore, enabling paracrine signaling between the separated cell types.

1.5.2 *Mechanobiology*

Mechanical forces have long been recognized as fundamental drivers in biological processes, such as embryogenesis, tissue formation and disease regulation. Understanding the interaction between cells and their mechanical environment can help reveal the geometrical dependencies of certain cytoskeleton behavior, direct study of mechanically induced cell behaviors or deformation, or lead to better mimicry of tissue organization like vascularization in a confined environment [40].

The collagen gel contraction (CGC) assay has served as a classic tool in the field of mechanobiology to study cell-induced contraction of extracellular matrix (ECM), which plays an important role in inflammation and wound healing. In a conventional CGC assay, cell-laden collagen is loaded into a cell culture vessel (typically a well plate) and forms a disk-shaped gel adhering to the bottom of the vessel. The decrement in diameter or surface area of the gel is used as a parameter to quantify the degree of cell contractility [41]. Based on a similar idea, we developed a microscale CGC device which consists of a static and a dynamic 3D-printed part [42, Chapter 3]. Cell-laden collagen can be introduced into the system and a collagen bridge could be formed via surface tension. The microscale device moves dynamically as a result of cellular forces. The main advantages of the microscale CGC system include: 1) the system uses markedly less

collagen and cell consumption per each assay (7- to 35-fold reduction compared to conventional assays); 2) the system enables the capture of dynamic cell-cell interaction in real-time.

1.5.3 *Multi-Culture Platforms*

Multi-cell-type (MCT) interaction is a biological process that is responsible for vital physiological responses observed *in vivo*. Due to a lack of commercially available MCT culture tools, innovative multi-culture platforms are required to unravel the contributions of each cell type in the system [42]. Conventional micro- and macro-scale platforms for multi-culture platforms have their own benefits and limitations owing to their capabilities and ease-of-use. It has been a research focus to develop user-friendly multi-culture platforms with low biological and technical barriers. Examples of multi-culture platforms in the literature generally fall into two categories: 1) basic mixing of cells in traditional macroscale well plate; 2) engineered microfluidic embodiments that render 3D culture, perfusion, and compartmentalization for different cell types. The major limitation for the simple mixing approaches is that the mixing does not sustain the delicate control over the nature of the interactions (paracrine or juxtacrine signaling) or patterning of cell-types, and therefore makes it inherently difficult to rationalize changes within the complex mixture. The major limitation for adopting the microfluidic tools is the additional complexity in the experimental setup, which includes specialized equipment such as microfluidic control systems [43, 44].

To reduce the complexity involved in the microfluidic multi-culture embodiments, we developed an open microfluidic coculture system, where two adjacent cell culture regions are separated by a half-wall, and cell culture media can be added atop the wall to initiate paracrine signaling [45, Chapters 4, 5]. The design configuration can be easily customized to adjust the area and volume of the culture chambers or incorporate more cell types into the culture system. We envision that

such simple and flexible multi-culture platforms could also become a potential tool to create *in vitro* modular, multikingdom culture systems that can be used to study soluble factor signaling between mammalian cells, bacteria, and fungi to address more sophisticated biological problems [45, 46].

1.6 REFERENCES

[1] Stone HA, Stroock AD, Ajdari A. Engineering Flows in Small Devices: Microfluidics Toward a Lab-on-a-Chip. *Annu Rev Fluid Mech*. 2004;*36*(**1**):381-411.

[2] Yun H, Kim K, Lee WG. Cell manipulation in microfluidics. *Biofabrication*. 2013;5(**2**):022001.

[3] Mehling M, Tay S. Microfluidic cell culture. *Current Opinion in Biotechnology*. 2014;**25**:95-102.

[4] Beebe DJ, Mensing GA, Walker GM. Physics and Applications of Microfluidics in Biology. *Annu Rev Biomed Eng*. 2002;4(**1**):261-86.

[5] Coluccio ML, Perozziello G, Malara N, Parrotta E, Zhang P, Gentile F, et al. Microfluidic platforms for cell cultures and investigations. *Microelectronic Engineering*. 2019;**208**:14-28.

[6] Velve-Casquillas G, Le Berre M, Piel M, Tran PT. Microfluidic tools for cell biological research. *Nano today*. 2010;5(**1**):28-47.

[7] Oliveira NM, Vilabril S, Oliveira MB, Reis RL, Mano JF. Recent advances on open fluidic systems for biomedical applications: A review. *Materials Science and Engineering*: C. 2019;**97**:851-63.

[8] Sia SK, Whitesides GM. Microfluidic devices fabricated in Poly(dimethylsiloxane) for biological studies. *Electrophoresis*. 2003;24(**21**):3563-76.

[9] Hatherell K, Couraud P, Romero IA, Weksler B, Pilkington GJ. Development of a three-dimensional, all-human in vitro model of the blood–brain barrier using mono-, co-, and tri-cultivation Transwell models. *Journal of Neuroscience Methods*. 2011;199(**2**):223-9.

[10] Miki Y, Ono K, Hata S, Suzuki T, Kumamoto H, Sasano H. The advantages of co-culture over mono cell culture in simulating in vivo environment. *The Journal of Steroid Biochemistry and Molecular Biology*. 2012;131(**3**):68-75.

[11] Lauffenburger DA, Zigmond SH. Chemotactic factor concentration gradients in chemotaxis assay systems. *Journal of Immunological Methods*. 1981;40(**1**):45-60.

[12] Kim HJ, Boedicker JQ, Choi JW, Ismagilov RF. Defined spatial structure stabilizes a synthetic multispecies bacterial community. *Proc Natl Acad Sci USA*. 2008;105(**47**):18188.

[13] Barkal LJ, Theberge AB, Guo C, Spraker J, Rappert L, Berthier J, et al. Microbial metabolomics in open microscale platforms. *Nature Communications*. 2016;7(**1**):10610.

[14] Berthier E, Dostie AM, Lee UN, Berthier J, Theberge AB. Open Microfluidic Capillary Systems. *Anal Chem*. 2019;91(**14**):8739-50.

[15] Lee SH, Heinz AJ, Shin S, Jung Y, Choi S, Park W, et al. Capillary Based Patterning of Cellular Communities in Laterally Open Channels. *Anal Chem*. 2010;82(**7**):2900-6.

[16] Casavant BP, Berthier E, Theberge AB, Berthier J, Montanez-Sauri SI, Bischel LL, et al. Suspended microfluidics. *Proceedings of the National Academy of Sciences*. 2013 June 18;110(**25**):10111-6.

[17] Berthier J, Brakke KA, Berthier E. Theory of Spontaneous Capillary Flows. In: Open Microfluidics. John Wiley & Sons, Inc.; 2016. p. 13-56.

[18] Berthier E, Warrick J, Yu H, Beebe DJ. Managing evaporation for more robust microscale assays Part 1. Volume loss in high throughput assays. *Lab Chip*. 2008;8(**6**):852-9.

[19] Zimmermann M, Bentley S, Schmid H, Hunziker P, Delamarche E. Continuous flow in open microfluidics using controlled evaporation. *Lab Chip*. 2005;5(**12**):1355-9.

[20] Guckenberger DJ, de Groot T,E., Wan AMD, Beebe DJ, Young EWK. Micromilling: a method for ultra-rapid prototyping of plastic microfluidic devices. *Lab chip*. 2015;15(**11**):2364-78.

[21] Lee Y, Choi JW, Yu J, Park D, Ha J, Son K, et al. Microfluidics within a well: an injection-molded plastic array 3D culture platform. *Lab Chip*. 2018;18(**16**):2433-40.

[22] Young EWK, Berthier E, Guckenberger DJ, Sackmann E, Lamers C, Meyvantsson I, et al. Rapid Prototyping of Arrayed Microfluidic Systems in Polystyrene for Cell-Based Assays. *Anal Chem*. 2011;83(**4**):1408-17.

[23] Lee UN, Su X, Guckenberger DJ, Dostie AM, Zhang T, Berthier E, et al. Fundamentals of rapid injection molding for microfluidic cell-based assays. *Lab Chip*. 2018;18(**3**):496-504.

[24] Zhou J, Khodakov DA, Ellis AV, Voelcker NH. Surface modification for PDMS-based microfluidic devices. *Electrophoresis*. 2012;33(**1**):89-104.

[25] Fujii T. PDMS-based microfluidic devices for biomedical applications. *Microelectronic Engineering*. 2002;**61-62**:907-14.

[26] Berthier E, Young EW, Beebe D. Engineers are from PDMS-land, Biologists are from Polystyrenia. *Lab Chip*. 2012 Apr 7;12(**7**):1224-37.

[27] Weisgrab G, Ovsianikov A, Costa PF. Functional 3D Printing for Microfluidic Chips. *Adv Mater Technol*. 2019;4(**10**):1900275.

[28] Flueckiger J, Bazargan V, Stoeber B, Cheung KC. Characterization of postfabricated parylene C coatings inside PDMS microdevices. *Sensors and Actuators B: Chemical*. 2011;160(**1**):864-74.

[29] Tan SH, Nguyen N, Chua YC, Kang TG. Oxygen plasma treatment for reducing hydrophobicity of a sealed polydimethylsiloxane microchannel. *Biomicrofluidics*. 2010;4(**3**):32204.

[30] Halldorsson S, Lucumi E, Gómez-Sjöberg R, Fleming RMT. Advantages and challenges of microfluidic cell culture in polydimethylsiloxane devices. *Biosensors and Bioelectronics*. 2015;**63**:218-31.

[31] de Groot TE, Veserat KS, Berthier E, Beebe DJ, Theberge AB. Surface-tension driven open microfluidic platform for hanging droplet culture. *Lab Chip*. 2016;16(**2**):334-44.

[32] Humayun M, Chow C, Young EWK. Microfluidic lung airway-on-a-chip with arrayable suspended gels for studying epithelial and smooth muscle cell interactions. *Lab Chip*. 2018;18(**9**):1298-309.

[33] Berry SB, Zhang T, Day JH, Su X, Wilson IZ, Berthier E, et al. Upgrading well plates using open microfluidic patterning. *Lab Chip*. 2017 Dec 5;17(**24**):4253-64.

[34] Armistead FJ, Gala De Pablo J, Gadêlha H, Peyman SA, Evans SD. Cells Under Stress: An Inertial-Shear Microfluidic Determination of Cell Behavior. *Biophysical Journal*. 2019;116(**6**):1127-35.

[35] Zhang X, Huk DJ, Wang Q, Lincoln J, Zhao Y. A microfluidic shear device that accommodates parallel high and low stress zones within the same culturing chamber. *Biomicrofluidics.* 2014;8(**5**):054106.

[36] Chan V, Zorlutuna P, Jeong JH, Kong H, Bashir R. Three-dimensional photopatterning of hydrogels using stereolithography for long-term cell encapsulation. *Lab Chip*. 2010;10(**16**):2062-70.

[37] Baroli B. Photopolymerization of biomaterials: issues and potentialities in drug delivery, tissue engineering, and cell encapsulation applications. *J Chem Technol Biotechnol*. 2006;81(**4**):491-9.

[38] Xu T, Zhao W, Zhu J, Albanna MZ, Yoo JJ, Atala A. Complex heterogeneous tissue constructs containing multiple cell types prepared by inkjet printing technology. *Biomaterials*. 2013;34(**1**):130-9.

[39] Derby B. Bioprinting: inkjet printing proteins and hybrid cell-containing materials and structures. *J Mater Chem*. 2008;18(**47**):5717-21.

[40] Chen T, Saw TB, Mège R, Ladoux B. Mechanical forces in cell monolayers. *J Cell Sci*. 2018;131(**24**):jcs218156.

[41] Bell E, Ivarsson B, Merrill C. Production of a tissue-like structure by contraction of collagen lattices by human fibroblasts of different proliferative potential in vitro. *Proc Natl Acad Sci U S A*. 1979;76(**3**):1274-8.

[42] Zhang T, Day JH, Su X, Guadarrama AG, Sandbo NK, Esnault S, et al. Investigating Fibroblast-Induced Collagen Gel Contraction Using a Dynamic Microscale Platform. *Frontiers in Bioengineering and Biotechnology*. 2019;7:196.

[43] Álvarez-García YR, Ramos-Cruz K, Agostini-Infanzón RJ, Stallcop LE, Beebe DJ, Warrick JW, et al. Open multi-culture platform for simple and flexible study of multi-cell type interactions. *Lab Chip*. 2018;18(**20**):3184-95.

[44] Zervantonakis IK, Kothapalli CR, Chung S, Sudo R, Kamm RD. Microfluidic devices for studying heterotypic cell-cell interactions and tissue specimen cultures under controlled microenvironments. *Biomicrofluidics*. 2011;5(**1**):13406.

[45] Zhang T, Lih D, Nagao RJ, Xue J, Berthier E, Himmelfarb J, et al. Open microfluidic coculture reveals paracrine signaling from human kidney epithelial cells promotes kidney specificity of endothelial cells. *Am J Physiol Renal Physiol.* 2020 May 11.

[46] Sackmann EK, Fulton AL, Beebe DJ. The present and future role of microfluidics in biomedical research. *Nature*. 2014;507(**7491**):181-9.

[47] Nash, C., Mavria, G., Baxter, E., Holliday, D., Tomlinson, D., Treanor, D., Novitskaya, V., Berditchevski, F., Hanby, A., Speirs,V. Development and characterisation of a 3D multi-cellular *in vitro* model of normal human breast: a tool for cancer initiation studies. *Oncotarget*. 2015;6(**15**).

Chapter 2. UPGRADING WELL PLATES USING OPEN MICROFLUIDIC PATTERNING

This chapter is mostly adapted from the original publication: Berry, S. B.;‡ Zhang, T.;‡ Day, J. H.; Su, X.; Wilson, I. Z.; Berthier, E.; Theberge; A. B., "Upgrading well plates using open microfluidic patterning." Lab Chip, 2017. 17, 4253. DOI: 10.1039/c7lc00878c (‡ indicates equal contributions).

2.1 ABSTRACT

Cellular communication between multiple cell types is a ubiquitous process that is responsible for vital physiological responses observed *in vivo* (e.g., immune response, organ function). Many *in vitro* coculture strategies have been developed, both in traditional culture and microscale systems, and have shown the potential to recreate some of the physiological behaviors of organs or groups of cells. A fundamental limitation of current systems is the difficulty of reconciling the additional engineering requirements for creating soluble factor signaling systems (e.g., segregated cell culture) with the use of well-characterized materials and platforms that have demonstrated successful results and biocompatibility in assays. We present a new open microfluidic platform, the Monorail Device, that is placed in any existing well plate or Petri dish and enables patterning of segregated coculture regions, thereby allowing the direct upgrade of monoculture experiments into multiculture assays. Our platform patterns biocompatible hydrogel walls *via* microfluidic spontaneous capillary flow (SCF) along a rail insert set inside commercially available cultureware, creating customized pipette-accessible cell culture chambers that require fewer cells than standard macroscale culture. Importantly, the device allows the use of native surfaces without additional modification or treatments, while creating permeable dividers for the diffusion of soluble factors. Additionally, the ease of patterning afforded by our platform makes reconfiguration of the culture

region as simple as changing the rail insert. We demonstrate the ability of the device to pattern flows on a variety of cell culture surfaces and create hydrogel walls in complex and precise shapes. We characterize the physical parameters that enable a reproducible SCF-driven flow and highlight specialized design features that increase the ease of use of the device and control of the open microfluidic flow. Further, we present the performance of our platform according to useful coculture criteria, including permeability and integrity of our hydrogel walls and surface-sensitive cell culture. Lastly, we show the potential of this type of platform to create modular multikingdom culture systems that can be used to study soluble factor signaling between mammalian cells, bacteria, and fungi, as well as the potential for adaptation of this technology by researchers across multiple fields.

2.2 INTRODUCTION

Modeling soluble factor signaling between human cell types and across cells, bacteria, and fungi is essential for studying organ function and disease mechanisms. A powerful approach in modeling this type of signaling utilizes systems that physically separate cell types yet permit soluble small molecules and proteins to diffuse and perform their signaling mechanism. This can typically be accomplished using engineered systems such as Transwell inserts or innovative microfluidic platforms. Both approaches have been enabling for soluble factor signaling and coculture studies, but are fundamentally limited in that they require specifically engineered systems, limiting their versatility and transferability – two important aspects we build upon. For established assays to be compatible with engineered microsystems, the assays must be adapted to match technological requirements that differ between established cultureware and engineered microsystems (e.g., accessibility, workflow for changing media, device material, cell culture surface treatments). In

contrast, we aimed to create a segregated culture device to study heterotypic cellular communication that can simply be inserted into existing culture systems (e.g., well plates) to enable facile augmentation of an established monoculture assay without significant alterations of experimental protocols. We propose a method to perform segregated multiculture and signaling studies through the creation of a hydrogel-wall network patterned using open microfluidics in a well plate-compatible insert.

Cell cocultures have been used to recapitulate specific aspects of in vivo cellular signaling phenomena, providing insight into complex physiological systems (e.g., organs, immune response) [1]. Specifically, segregated coculture, in which cell types are physically separated but are still able to communicate via diffusion of signaling molecules, can capture dynamic, reciprocal signaling between cell types [2, 3] and isolate the effects of soluble factors from the effects of heterotypic contact that include juxtacrine signaling pathways and cell stimulation [4, 5]. Segregated coculture methods are widely available as commercial Transwell inserts which are easy to use and integrate with standard culture plates [6, 7], but are limited by fixed culture configurations, the inability to tune the size of the culture regions, the number of cultures in communication, the use of alternative surface materials (e.g., PC, PET, PTFE), poorly defined diffusion gradients that rapidly decay [8, 9], and the inability to culture multiple cell types on a single surface.

Alternatively, researchers have turned to custom engineered microfluidic systems for segregated coculture, as these systems can provide precise control over cell culture environments, require fewer cells, and can be tailored to mimic physiological conditions [10-20]. These engineering approaches have generated effective and creative segregated coculture platforms, using techniques

such as hydrogel patterning and laminar flow patterning for precise cell seeding and microchannel systems for the isolation of soluble factor effects in complex cocultures [5, 21-26]. For example, Hui et al. [27] created a reconfigurable, interdigitated coculture system that permitted precise temporal and spatial manipulation of coculture. In addition, Lee et al. [28] fabricated a micromolded polydimethylsiloxane (PDMS) device that utilized flow along a rail to pattern gels and selectively seed cells and microbes. Similarly, Patel et al. and others created hydrogel-based barriers that selectively manipulate the chemical and temporal signaling, as well as movement, of cell types in coculture [29-32]. Further, Carney et al. [26] utilized a dual-chambered polystyrene (PS) microfluidic device that allowed transport of signaling molecules through diffusion channels connecting the segregated chambers. These examples represent impressive endeavors to create simple engineering solutions for difficulties associated with segregated coculture, yet they remain limited. Many of these approaches [3, 5, 13-17, 19, 22-24, 28-32] use PDMS, which has been shown to absorb small molecules [33,34] while others use enclosed culture chambers [24, 26, 28], which are only accessible from the inlet/outlet ports, and have not demonstrated compatibility of their platforms with unmodified commercially available tissue-culture surfaces [26, 28]. These customized microsystems are a valuable alternative to commonly used methods and provide important insight into physiological interactions that cannot be easily examined in traditional cultureware. However, despite the remarkable push towards simplifying complex cocultures with these engineered systems, integration of custom microsystems with established cultureware remains difficult. Commercially available well plates and tissue culture treated (TCT) surfaces are easy to handle and use, have been validated through decades of experimentation, and are familiar to biological laboratories [35]. Further, production of cell culture-treated surfaces is a technically challenging and labor-intensive process that has been optimized by industry through decades of

effort. Therefore, there exists a need for an easy-to-use tool that provides investigators with the flexibility to upgrade their model with multiple cell types while maintaining optimized experimental materials and methods.

We developed a segregated coculture technology, called the Monorail Device, that integrates with established cell culture methods and enables the partitioning of cell-culture surfaces in commercially available well plates by flowing biocompatible hydrogels to create hydrogel walls. Importantly, the Monorail Device upgrades simple monoculture assays by adding any number of additional cell-culture wells in controlled configurations on the same plane. Our method builds upon previous work in open microfluidics by incorporating spontaneous capillary flow (SCF) along an open microfluidic channel comprised of a plastic 'rail' insert (channel ceiling), the well plate (channel floor), and two open air interfaces (channel sides) [28, 36, 37]. This type of flow allows the easy patterning of hydrogel and its polymerization, thereby creating permeable cell culture regions. Additionally, the incorporation of SCF as the mechanism of flow eliminates the need for external pumping systems during the hydrogel wall fabrication process. Our platforms are insertable into individual wells, similar to Transwells inserts, and easy to use, as gels and cells can be applied in open wells by simple pipetting. The accessibility to cell culture areas is a key design consideration of the platform; the open chambers and channels demarcated by the hydrogel walls do not have a ceiling and as such are pipette accessible from the top. Thus, cell seeding, media changing, reagent addition, and the removal of media for endpoint analysis (e.g., enzyme-linked immunosorbent assay (ELISA), liquid chromatography-mass spectrometry (LC-MS)) can all be achieved by pipetting directly into the culture regions from the top, just as in a traditional well plate. Additionally, the use of open microfluidics (i.e., simple 'rail' insert) enables straightforward rapid prototyping via 3D printing [38, 39] for platform design and injection

molding (Figure 2.11) for scale-up and reproducible use in biology research environments. We demonstrate the application of our Monorail Device by patterning hydrogel walls onto multiple different surfaces and characterizing the integrity, permeability, flow, and dimensions of the wall. We detail specific design features that improve function within the device and increase the versatility of our design. Importantly, our device can be easily integrated into biological laboratories to fulfill a range of experimental needs, including multikingdom coculture, small molecule diffusion, and surface-sensitive cell culture.

2.3 Materials and Methods

2.3.1 *Devices*

Devices were fabricated using a Form 2 SLA 3D printer (Formlabs, Somerville, MA) or a 770 Series 3 PCNC Mill (Tormach, Waunakee, WI). 3D-printed devices were designed with AutoCAD (Autodesk, San Rafael, CA) and converted to .form files with PreForm 2.11.0 (Formlabs) prior to being printed with Clear V2 (Figure 2.1, 2.2, 2.3a, 2.3b, and 2.6a-c), Black V2 (Figure 2.3c, and 2.4), or High Temp (Figure 2.6d) printer resin (Formlabs). After printing, devices were sonicated in isopropanol (IPA) for 15 min, rinsed with IPA, and UV-cured (Quans 20W UV Lamp) for 10-30 min. Milled devices (used in Figure 2.5) were designed with Solidworks 2016 x64 (Solidworks, Waltham, MA) and converted to .TAP files with Sprutcam (Sprutcam, Naberezhnye Chelny, Russia). Devices were milled from 4 mm thick polystyrene (PS) sheets (Goodfellow USA, Coraopolis, PA), rinsed with deionized water, and sonicated for 10 min in 70% ethanol. All devices and surfaces were plasma treated for 5 min at 0.25 mbar and 70 W in a Zepto LC PC Plasma Treater (Diener Electronic GmbH, Ebhausen, Germany) using ambient air. Original design files are included in the Electronic Supplementary Information (Figure 2.10).

2.3.2 *Characterization of SCF*

Devices of different height and width dimensions, as well as those with integrated design features, were designed as shown in Figures 2.2 and 2.3 with n = 3 replicate devices. After fabrication, devices were inserted into the bottom of a 24 well plate, and an optimized volume of Matrigel (20-35 μL, exact volumes provided in Figure 2.7) was loaded into the device *via* the loading region. All 24 well plates were purchased from the following: polystyrene well plates (Nest Scientific, #702011, Rahway, NJ), tissue-culture-treated (TCT) well plates (Corning Inc., #353047, Corning, NY), glass-bottomed well plates (MatTek Corp., #P24G -1.0-13-F, Ashland, MA), PureCoat™ Carboxyl well plates (Corning Inc., #354775, Corning, NY). For imaging purposes, Matrigel (8.0 - 9.1 mg/mL, Corning Inc., Corning, NY) was mixed 5:1 with red food dye (McCormick, Hunt Valley, MD) to give a final concentration of 6.5 - 6.7 mg/mL Matrigel. We observed no difference in performance between the Matrigel concentrations used. The process of loading, filling, and halting of flow was recorded and imaged using an AmScope MU1403B High Speed Microscope Camera on a SM-3TZ-80S Stereoscope (AmScope, Irvine, CA) set up beneath the well plate for bottom-up imaging. Device width and height dimensions were measured using image measurement tools (ImageJ), and a C112JE Digitmatic Indicator (Mitutoyo, Aurora, IL), respectively. For contact angle measurements, Matrigel was placed on glass (#12-542B, Fisher Scientific, Pittsburgh, PA), PS, plasma-treated PS, or TCT PS and the resulting contact angle was measured using a Kruss DSA25 (Kruss GmbH, Hamburg, Germany). The contact angles were measured and analyzed through ADVANCE Software using an elliptical droplet shape with an automatic baseline and set volume of 2 μL (Kruss GmbH, Hamburg, Germany). All PS contact angle measurements were done on PS Nunc™ OmniTrays™ (Thermofisher, Frederick, MD) since contact angle measurements required imaging from the side, which was not feasible with PS well

plates. Flow experiments on glass were conducted on fabricated well plates in which the PS bottom was replaced with glass microscope slides (#16004-422, VWR International LLC, Radnor, PA). Where indicated in Figure 2.2, surfaces were plasma treated according to the same protocol as described in the previous section.

2.3.3 *Confocal Imaging of Patterned Hydrogel Wall*

Fluorescent Matrigel was prepared by mixing 1 μL of 1 μg/mL AlexaFluor-488 solution (Thermo Fisher, Cat# A33077) with 400 μL of 8.0 mg/mL Matrigel. Devices with and without a trapezoidal rail pinning feature were fabricated *via* the 3D printing protocol described above. The devices were inserted into the bottom of glass-bottomed well plates and loaded with 35 μL of the AlexaFluor-488-dyed Matrigel. After conclusion of flow, the Matrigel wall in devices with and without a trapezoidal rail pinning feature was imaged with a Leica TCS SP5 II Laser Scanning Confocal Microscope. All z-stack images were obtained at an emission wavelength range of 505 nm to 550 nm with an Argon 488 nm laser and a section thickness of 6.229 μm. All the .tif files were processed with Fiji (Version 10, ImageJ) using the following operations: "Transform > Stack-Orthogonal Views".

2.3.4 *Cell Culture*

Benign human prostate stromal cells (BHPrS1) [40] were cultured in RPMI-1640 medium (containing 2 mM L-glutamine) with 5% fetal bovine serum (FBS, Hyclone™), penicillin (100 units/mL), and streptomycin (100 μg/mL). Human umbilical artery smooth muscle cells (HUASMC) (Cell Applications, Cell Applications Inc., San Diego, CA) were cultured in Human Smooth Muscle Cell Growth Medium (#311-500, Cell Applications) and passaged using

Subculture Reagent Kit (#090K, Cell Applications). Human prostate adenocarcinoma cells (LNCaP clone FGC, ATCC, Manassas, VA)[41] were cultured in RPMI-1640 medium with 10% FBS, penicillin (100 units/mL), and streptomycin (100 μg/mL). Human T lymphocyte cells (Jurkat E6.1) (Sigma-Aldrich, St. Louis, MO) were cultured in RPMI-1640 medium with 10% FBS. All mammalian cells were maintained in a 37^{o}C incubator with 5% carbon dioxide. *S. cervesiae* (gift from Dr. Jesse Zalatan and Dr. Alshakim Nelson, University of Washington) were grown on YPD Agar (Sigma-Aldrich) stored at 4^{o}C. *A. fumigatus* (AF293) and *P. aeruginosa* (PA14) (gifts from Dr. Nancy Keller, University of Wisconsin) were grown on glucose minimal media (GMM)[42] with low-gelling temperature agarose (Sigma-Aldrich) and Luria broth (LB) (BD Biosciences, Franklin Lakes, NJ) with low-gelling temperature agarose, respectively, and stored at 4^{o}C. Cells were used at the following passage number: BHPrS1 P8-9, HUASMC P14, LNCaP P59, Jurkat E6.1 P12.

For the initiation and maintenance of cultures in our devices, specialized protocols were developed as described in each section below. To prevent evaporation of media in all of our device cultures, the spaces between wells were filled with 1:1 deionized water/phosphate buffered saline (PBS), and the well plates were stored within a humidified bioassay dish (#240835, Thermo Fisher) with saturated (1:1 water/PBS) Kimwipes. All optimized hydrogel loading volumes are in Table S1 in the ESI.

2.3.5 *Determination of the Permeability of the Hydrogel Wall*

The devices (Figure 2.4b) were inserted into the bottom of a TCT PS 24 well plate. Each device was loaded with 85 μL of 9.1 mg/mL Matrigel, and the plate was incubated for at least 3 min at 37^{o}C after conclusion of flow. Fluorescent dye solution was prepared by mixing AlexaFluor-488 with PBS (final concentration of 237.2 μM). 120 μL of the dye solution was loaded into the

sourcing chamber, 120 μL of PBS was loaded into the receiving chamber (t = 0 h), and the plate was incubated at 37$_o$C. 100 μL of solution in the receiving chamber was collected separately at t = 1 h, 3 h, 5 h, 17.5 h, and 29 h. Samples were diluted by a factor of 50 (t = 1 h, 3 h, 5 h) or 100 (t = 17.5 h, 29 h) with PBS prior to analysis. The fluorescence of each sample was measured using a Multiskan Spectrum UV/Visible Microplate Reader (Thermo Labsystems, Waltham, MA) (n=3 devices per time point).

2.3.6 *Validation of the Hydrogel Wall Integrity for Compartmentalized Cell Culture*

The coculture device (Figure 2.4a) was inserted into the bottom of a TCT PS 24 well plate, loaded with 35 μL of 8.0 mg/mL Matrigel, and incubated for at least 3 min at 37$_o$C after conclusion of flow. BHPrS1 cells and HUASMC were stained with green and red CellTracker Dye at a concentration of 4.55 μg/mL and 6.25 μg/mL for 45 min (ThermoFischer), respectively, and selectively seeded into the outer and inner chambers of the device, respectively. Cells were suspended in culture media at a concentration of 2.3x10$_5$ cells/mL. 14 μL (outer chamber) or 7 μL (inner chamber) of the cell suspension were seeded into each culture chamber to achieve a seeding density of 400 cells/mm$_2$. After overnight adhesion, fluorescent images of the cells along the wall were obtained using a Zeiss Axiovert 200 with a 4x objective and Axiocam 503 mono camera (Carl Zeiss AG, Oberkochen, Germany) (n=3 devices). All the images were processed with Fiji using the following operations: “Subtract Background > Adjust-Brightness/Contrast > Color-Merge Channels > Adjusted-Color Balance”.

2.3.7 *Comparison of LNCaP Morphology on Different Well Plate Surfaces*

The device (Figure 2.5) was placed into the bottom of a TCT PS or a Corning PureCoat™ Carboxyl PS (C-PS) 24 well plate. 40 μL of 9.1 mg/mL Matrigel was loaded into the device and incubated for at least 3 min at 37^{o}C after conclusion of flow. LNCaP cells were thawed from liquid nitrogen storage and seeded directly onto a pre-wetted TCT PS 24 well plate or a C-PS 24 well plate in the presence or absence of the device. Cells were suspended in culture media at a concentration of 2.4x10^{5} cells/mL. In the absence of the device, 320 μL of the cell suspension were seeded into a well containing 200 μL of media to achieve a seeding density of 400 cells/mm^{2} and a final volume of 520 μL. In the presence of the device, 120 μL of cell suspension were seeded into a well containing 75 μL of media to achieve a seeding density of 400 cells/mm^{2} and a final volume of 195 μL. The cells were incubated overnight at 37^{o}C and 5% CO_2, and then imaged with phase contrast using a Zeiss Primovert Microscope ((Carl Zeiss AG, Oberkochen, Germany) and an AmScope MU1403B High Speed Microscope Camera (AmScope, Irvine, CA) (n=3 devices).

2.3.8 *Validation of the Modular Rail-Based Hydrogel Patterning Platform*

The device (Figure 2.6) was inserted into the bottom of a TCT PS 24 well plate, loaded with 50 μL of 8.0 mg/mL Matrigel, and incubated for at least 3 min at 37^{o}C after conclusion of flow. For Figure 2.6c, BHPrS1 cells were suspended in culture media at a concentration of 2.3x10^{5} cells/mL, and 240 μL of the cell suspension were seeded into each outer culture chamber to achieve a seeding density of 400 cells/mm^{2}. Jurkat E6.1 cells were suspended in culture media at a concentration of 4.0x10^{5} cells/mL and 100 μL of the suspension was seeded into the inner culture chamber. The insertable pegs were loaded with 2% BD Bacto™ Agar solution (Fisher Scientific) and allowed to gel at room temperature. A *S. cervesiae* colony was scraped (≈ 1 mm) with a sterile toothpick from

Petri dish culture and streaked onto the center of an agar-filled peg. After overnight incubation at 30 ^{o}C, the yeast-containing peg was loaded into the top of the hydrogel-patterning device, which contained BHPrS1 and Jurkat E6.1 cells. The assembled platform, containing all three cell types, was imaged. The human cells were imaged with phase contrast using a Zeiss Primovert Microscope with a 20x objective and an AmScope MU1403B High Speed Microscope Camera (n=3 devices). The yeast was imaged with an Ultra-High-Resolution SLR camera (Nikon-D5300).

For Figure 2.6d, 100 μL of *A. fumigatus* in liquid GMM were seeded into the bottom of the central chamber of the modular Monorail Device at a concentration of $1x10^{5}$ spores/mL and 250 μL media added to the outer chambers. 3 μL of *P. aeruginosa* were seeded onto LB-agarose (5 μL) in a peg at a concentration of $1x10^{8}$ bacteria/mL and the peg was inserted on top of the *A. fumigatus* culture and maintained at 37°C. Phase contrast images were taken after 24 hours using a Zeiss Primovert Microscope with a 10x objective and an AmScope MU1403B High Speed Microscope Camera (AmScope, Irvine, CA) (n=3 devices). Fluorescence images of *A. fumigatus* stained with Calcofluor white (1 mg/mL, 10 μL + 10 μL 10% KOH, Sigma-Aldrich) were taken after 4 days in coculture; for staining, a peg was removed, the Calcofluor white solution was added directly to the media in the *A. fumigatus* culture in the bottom of the well plate, incubated for 1 minute, and then imaged with a Zeiss Axiovert 200 with a 10x objective and Axiocam 503 mono camera. All fluorescence images were obtained in a single focal plane; as the *A. fumigatus* was not confined to a single plane by Day 4, the focal plane with the highest intensity of Calcofluor white staining was captured in each well. Two fluorescence images were captured for each well at different fields of view; when quantifying the Calcofluor white signal (Figure 2.6d, v), the integrated intensity of both replicate images was averaged. The plotted points represent the average of two images (collected for each of the three replicate wells), and the plotted standard error of the mean (SEM)

is the SEM of the three replicate wells. Fluorescence images were quantified with Fiji following the protocol: “Subtract Background > Adjust Brightness/Contrast > Analyze > Measure > IntDen”. Prism (GraphPad Software) was used to conduct a two-tailed unpaired Student’s t-test (Figure 2.6d, v).

2.4 Results and Discussion

2.4.1 *Spontaneous Capillary Flow along a Rail System*

We created a hydrogel-wall patterning platform that easily integrates into existing cultureware and utilizes SCF along a rail as the principal mechanism of function (Figure 2.1). Operation of our Monorail Device is simple and fast, as wall fabrication *via* SCF requires minimal user interaction through a two-step process: placing the device in a well or on a cell culture surface (Figure 2.1a), similar to a Transwell, and pipetting of the hydrogel into the loading zone (Figure 2.1b and c). In this work, we optimized our platform for use with Matrigel, and we have also used our platform with fibrin and collagen I. Flow within our platform is described by an open microfluidic rail system, in which liquid flows in a channel with no side-walls. The cross-section of the open channel thus defines a wetted perimeter (P_w), comprising of all the solid surfaces, and a free perimeter (P_f), comprising of all the open interfaces. SCF along a rail has been previously modeled[28,36,37] additionally, to describe the specific conditions of flow in our device embodiment, we performed a balance-of-pressure analysis between the inlet surface-tension-based Laplace pressure and the Laplace pressure in the advancing fluid under the rail, which led to the development of an analytical model of the conditions for flow based on the aspect ratio of the open channel (Figure 2.2b).

Our model states that flow within our platform is dependent upon the height (*h*) and width (*w*) of the rail (Figure 2.1d); these two physical parameters can be utilized as guidelines for customizing our open microfluidic system, in which the Laplace pressure affects the performance of a system with different aspect ratios or shapes (Figure 2.1e). Using experimentally measured values for the contact angles of Matrigel on the rail surface ($\theta = 22.3° \pm 1.6°$) and a TCT PS surface ($\theta = 38.4° \pm 1.1°$), we derived a relationship between *h* and *w* which determines the limit between "flow" and "no flow" (illustrated by the boundary between the red and green shaded regions in Figure 2.2b). To validate our model, we characterized conditions for flow in our system using devices of different heights and widths on the TCT PS surface. We use a simple single rail device and a qualitative binary system to differentiate between "flow" and "no flow" conditions: "flow" is defined as complete reproducible flow of Matrigel *via* SCF along the entire length of the rail, whereas "no flow" is defined as no initiation of flow along the rail after reservoir filling or incomplete flow along the rail (Figure 2.2a). According to our model, the region below the boundary (shaded green) represents favorable flow conditions, and the region above the boundary (shaded red) represents conditions for which "no flow" was predicted (Figure 2.2b). Indeed, when we plotted the experimental data of the flow and no-flow observations for devices with a range of heights and widths, we found that the model predicted the conditions for flow well (only one experimental point showed a deviation) and presented an experimental trend, as expected, in which larger widths and smaller heights promoted flow within our platform (Figure 2.2b). We expect this trend to hold for dimensions below those presented in this work, as we were limited by the fabrication capabilities of the 3D printing technology used in this paper (see Methods). However, open microfluidics has been demonstrated and the laws governing open fluid flow have been

validated at scales smaller than those employed here [28, 36], supporting that our method could be extended to smaller length scales achieved with alternative fabrication procedures [43].

Cell-culture platforms are highly tuned towards specific cell types, often matching cell-surface requirements with functionalizing treatments to favorably alter cell adhesion on the culture surface. In order to assess the ability of our platform to adapt to any cultureware surface, we characterized flow on the surface of commonly used cell culture materials (e.g., glass, PS) with different contact angles. We tested the ability of our platform to pattern hydrogel walls on surfaces with a range of contact angles (17.9° – 49.9°) and observed successful hydrogel flow on each surface (Figure 2.2c). These results agree with behavior predicted from our model, in which a device with a height of 0.25 mm and a width of 1 mm would be expected to facilitate SCF on the surfaces tested. The ability of our platform to successfully pattern hydrogel walls on a range of common surfaces illustrates the versatility of our platform. The manipulation of the height, width, and contact angles of the platform can allow our method to be used with a wide range of surfaces.

2.4.2 *Design of the Open Microfluidic Hydrogel Patterning Platform*

The ability to precisely control fluid flow in open channels dictates the shape, size, and ease of use of our platform. To achieve greater control over the fluids and more reproducible filling of the device *via* SCF, we added features to control the capillary forces along the pathway of flow. These features ensure that the hydrogel flows along the rail and accurately patterns the surface; additionally, these regions increase tolerance to pipetting speed and pipette placement by the user. To ensure reproducible initiation of flow, we incorporated a controlled inlet (Figure 2.3a, (ii)) that confines the hydrogel beneath the rail as it flows from the inlet to the end of device; without the controlled inlet, we observed uncontrolled wetting by the inputted fluid in culture chambers and

around the device (Figure 2.3a, (3)). Additionally, the controlled inlet contains a height gradient that directs the hydrogel towards the middle of the inlet (Figure 2.8), thereby enabling the user to load the hydrogel by placing a pipette anywhere in the loading zone. In conjunction with the controlled inlet, we incorporated a region of high capillary favorability (i.e., a capillary sink) at the end of the flow path to ensure controlled flow within the device (Figure 2.3b, (ii)); without the capillary sink, we observed flooding into the culture chambers (Figure 2.3b, (3)). The capillary sink promotes controlled flow because of an increased favorability of the hydrogel to wet a feature with a larger width (resulting from a lower h:w ratio, as h is kept constant from the rail to the sink); therefore, inputted hydrogel preferentially flows to the capillary sink instead of into the culture chambers.

As the channels are open, there is the potential for the fluid to wick vertically up along the sides of the rails, a phenomenon also known as capillary rise (Figure 2.3c, (3)). Indeed, we observed capillary rise within our platform, which led to an increased width at the base of the wall and flooding into the culture chambers while in the process of device filling. At the conclusion of device filling, we observed recession of the hydrogel back towards the rail, leaving a faint residue on the surface where the gel had originally flooded into the culture chamber. To halt the capillary rise of the hydrogel, we improved the pinning ability of the rail by increasing the acuteness of the angles on the sides of the rail, creating a trapezoidal cross section (Figure 2.3c, (ii)). It is important to note that the width at the base of the wall is greater than the width of the rail even with the trapezoidal cross-section, as the bottom surface is not bound laterally (Figure 2.3c, (3)); however, the width at the base is consistent, with the extent of flooding remaining < 260 μm into the chamber, and therefore can be accounted for when designing platform dimensions (Figure 2.8, 2.10). Lastly, another source of error is Concus-Finn filaments (i.e., filaments of fluid in a wedge defined by two

surfaces intersecting) [36, 44] that may occur when rails change direction, split, or merge. The Concus-Finn filaments can be prevented by rounding all the concave angles of the device. By removing wedge-shaped regions conducive to Concus-Finn flow, flow within our device more closely resembled a solid fluid front (i.e., without additional fluid filaments). When combined with the controlled inlet and the capillary sink, these flow-controlling features represent necessary design aspects for the successful execution of SCF in our platform and across different designs.

2.4.3 *Application of Platform for Cell Culture Experiments*

The intrinsic characteristics of hydrogels provide several advantages when used for wall fabrication; hydrogels are permeable, thereby enabling diffusion of soluble factors through the wall, yet are able to maintain a defined shape that can act as a physical barrier for objects like cells. These characteristics support the use of hydrogels as a barrier for segregated coculture systems, as they permit soluble factor signaling while prohibiting physical contact between cell types [32]. To demonstrate the segregation and containment of cells by the hydrogel walls, we selectively stained and seeded benign prostate stromal cells (BHPrS1) and umbilical arterial smooth muscle cells (HUASMC) into separate chambers within a device, separated by the hydrogel wall (Figure 2.4a). After cell incubation and adhesion, we imaged the device and observed no mixing of the cell populations, clearly demonstrating the physical compartmentalization of each cell type. Importantly, this platform can be used with reduced cell numbers (≈2000 cells/chamber), illustrating utility for experiments involving rare or limited cell types (e.g., patient cells).

We then quantified the diffusion of a model small molecule (AlexaFluor-488) through the hydrogel wall to model soluble factor signaling. We generated a diffusion profile by measuring the concentration of AlexaFluor-488 as it diffused through the hydrogel wall from the sourcing

chamber to the receiving chamber (Figure 2.4b). The concentration of AlexaFluor-488 followed the model predicted by the quasi-static Fick law indicating a linear diffusion gradient of AlexaFluor-488 across the hydrogel wall. The diffusion profile demonstrates predictable and controllable signaling across the hydrogel wall. Diffusion time is dependent upon the size of the molecule, the thickness and permeability of the wall, and the distance between the source and the receiver. Therefore, for applications where different diffusion rates are required, the dimensions of the wall and culture chambers and the concentration/type of hydrogel can be adjusted. Importantly, these results support the use of this platform as a method to study intercellular communication while maintaining physical separation of cell types.

The versatility of our Monorail Device extends into applications involving specialized cultureware and sensitive cell types; as a tunable insert, our platform can be incorporated into any "off the shelf" well plate, including those with pretreated and coated surfaces. As a proof of concept, we demonstrate the compatibility of our patterning platform with the human prostate cancer cell line, LNCaP, that is sensitive to culture surface chemistry and that grows better on plates with surface chemistry tuned for improved adherence [45]. Prior work has shown that LNCaP cells exhibit better adherence and spreading on Corning's commercially available PureCoat™ Carboxyl PS (C-PS) than traditional TCT PS [46]. First, we tested and observed successful rail-based hydrogel patterning with our platform on Corning's specialized C-PS well plates. After validation of the compatibility of our platform with the C-PS well plates, we thawed LNCaP cells and directly seeded the cells on TCT PS and C-PS in the absence or presence of hydrogel walls patterned by our platform. As expected based on prior studies [46], we observed morphological differences between LNCaP cells cultured on TCT and C-PS, with LNCaP cells cultured on C-PS displaying more spread out, adherent morphology than the LNCaP cells cultured on TCT PS, which showed

predominantly rounded morphologies (Figure 2.5). The effect was independent of the presence of our platform. In these experiments, we used PS rails fabricated using CNC milling rather than the 3D printed rails used in prior figures because we observed that the 3D printer resin affected LNCaP morphology. We believe this is due to leaching of compounds from the 3D printer resin into the cell culture media; previous work has shown that some printer resins are detrimental to certain cell types [47]. A key advantage of our open microfluidic design is that it is injection moldable (Figure 2.11); in the future, inserts can be injection molded in established cell culture materials (e.g., PS). In summary, these results support the use of our device as a compatible culture platform for sensitive cell types and illustrate its use on custom commercially available culture surfaces beyond traditional TCT plastics.

To further demonstrate the versatility of our Monorail Device in cell culture applications, we created a modular system that can be used to study multikingdom soluble factor signaling (e.g., signaling between bacteria, fungi, and human cells). Coculture of cell types from different kingdoms can be used to decipher complex physiological microenvironments (e.g., human microbiome) and to better understand transkingdom relationships [48-52]. Key challenges of establishing multikingdom cocultures include differential media and culture conditions for each cell type, and the tendency of microbial cultures to overgrow human cultures. These challenges, along with the complexity of existing engineered multikingdom coculture platforms, have made it difficult for multikingdom coculture to expand into most microbiology and cell biology laboratories, with much of the current work accomplished within specialized engineered platforms [53], further illustrating the need for simple and easily-adapted systems that researchers can use to approach these complex environments. Therefore, building upon previously demonstrated reconfigurable systems [27, 54, 55] and Transwell technology, we present a modular

multikingdom coculture platform in which removable coculture "pegs" can be inserted into an existing hydrogel-wall patterned region (Figure 2.6a). Modularity of the individual culture compartments (i.e., peg and hydrogel-patterned well plate) allows users to separately culture each kingdom in its optimized conditions before combining the compartments to initiate soluble factor signaling. Additionally, the ability to load and remove multiple pegs simultaneously allows users to build combinatorial coculture systems (Figure 2.6b). To demonstrate the physical device workflow, we combined a model yeast organism (*S. cerevisiae*) with model adherent and non-adherent human cells (BHPrS1 and Jurkat E6.1 cells, respectively). We cultured the *S. cerevisiae* atop agar-filled pegs while the BHPrS1 and Jurkat E6.1 cells were cultured in their own media in hydrogel-defined culture chambers. After overnight incubation, the three separate cultures were combined by insertion of the *S. cerevisiae*-containing peg into the hydrogel-patterned ring containing human cells (Figure 2.6c.). Further, we recapitulated a separate multikingdom coculture system of two human pathogenic microbes, *A. fumigatus* (fungus) and *P. aeruginosa* (bacterium), demonstrating an additional use of our rail-based hydrogel patterning platform and characterizing the ability of our platform to permit soluble factor signaling in a multikingdom coculture. Prior work has demonstrated that coculture of these two organisms in soluble factor contact results in reduced growth of *A. fumigatus* due to secretion of inhibitory factors by *P. aeruginosa*.[25, 56-58]. Therefore, we examined *A. fumigatus* growth in our modular Monorail Device while in coculture with *P. aeruginosa*. Briefly, *A. fumigatus* was seeded into the inner chamber of a hydrogel-patterned well plate, in which the outer chambers were filled with media, and *P. aeruginosa* was then seeded into LB-agarose-filled pegs and inserted into a peg-holder directly above the *A. fumigatus*. As expected, we observed growth of *A. fumigatus* over four days in monoculture and decreased *A. fumigatus* growth when *A. fumigatus* was cocultured with *P. aeruginosa* (Figure 2.6d).

The inhibition of *A. fumigatus* growth by *P. aeruginosa* demonstrates cellular communication between two different kingdoms, supporting the use of our modular Monorail Device as a platform to study soluble factor signaling in multikingdom cultures. In future work, to study signaling mechanisms between human cells and microbial pathogens, human cell types such as lung endothelial or epithelial cells could be incorporated into separate culture chambers within the modular Monorail Device. The modularity of our proof of concept platform, in addition to the customizability of our rail-based system, demonstrates the potential of our platform as a simple yet versatile tool for studying multikingdom communication.

2.5 CONCLUSION

In this work, we present the creation of a new hydrogel-wall patterning platform, the Monorail Device, that utilizes SCF along a rail to pattern hydrogel walls on commercially available cultureware. The pipette-accessible cell culture chambers, compatibility with a range of cultureware materials, and the potential to reconfigure design geometries facilitate easy integration of our technology into biological laboratories and with established detection methods (e.g., microscopy, ELISA, LC-MS). The ease of use of our device is on par with that of Transwells inserts, and the potential scalability of our technology to existing manufacturing techniques such as injection molding (Figure 2.11) can lower fabrication costs, as our technology relies on SCF instead of specialized fabrication methods to create a cell-segregating membrane. We envision use of this device as a tool to probe underlying mechanisms of cellular communication and multikingdom soluble factor signaling. The platform that we present can further be used for applications that require good control over the cellular micro-environment (e.g. cell migration) as well as applications that require a higher level of complexity, such as host-microbe interactions.

The patterned regions can sustain 2D and 3D cell culture, in which cell-laden hydrogels could be loaded into the culture chambers or used to pattern walls. The use of customizable hydrogels can also enable the selective filtering of specific biomolecules in order to tailor the communication between the cells in culture [32]. We acknowledge the need for further optimization with regards to specific assay requirements, such as extended culture times, incorporating specific cell types depending on the application, and maintaining gel adherence and integrity (or degradability) over time as desired for a given application. Our optimization in the present paper centered on the physical hydrogel patterning capabilities of our platform to create open coculture chambers and we outline foundational technological features that will allow personalized optimization and development of our platform. Ultimately, we aim to create a platform that can be easily translated across fields and adapted by researchers for their own research questions.

2.6 FIGURES

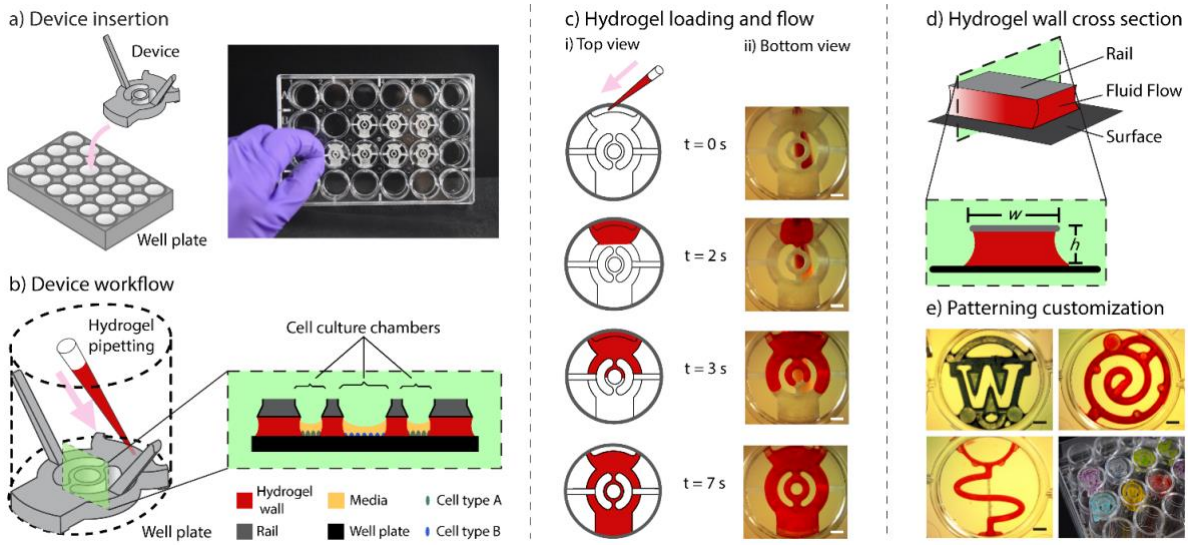

Figure 2.1 Overview of device operation and cross section showing SCF in a rail system. a) Insertion of the Monorail Device into a 24 well plate for hydrogel-wall patterning; image shows the device in a standard 24 well plate. b) Hydrogel is loaded into the inlet, filling the device; the cross section demonstrates a hydrogel-filled device with two separate cell types seeded in the inner and outer culture chambers. c) Schematics (i) and images (ii) of selected time points corresponding to device filling, as imaged through the bottom of a 24 well plate. Corresponding video is included in the ESI. d) Cross section of rail system with SCF. SCF is governed by the physical parameters height (h) and width (w), as well as the contact angles (θ1 and θ2 , not shown) between the gel and the rail and the gel and the bottom surface. e) The patterning method is versatile and can be used to create chambers of diverse geometries. All liquids were dyed red for visualization. Scale bars = 2 mm.

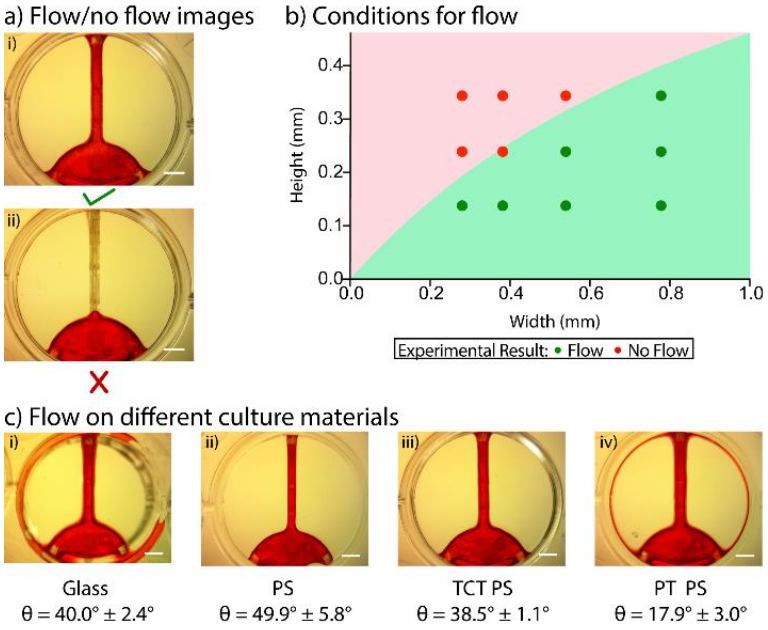

Figure 2.2. Characterization of flow along rails.

a) Representative images showing i) "flow" and ii) "no flow" of Matrigel along rail (n = 3 devices). Scale bar = 2 mm. b) Phase diagram of theoretical (shaded region) and experimental observations (plotted points) of "flow" and "no flow." Theoretical predictions were according to our model (see ESI), wherein the green region represents the region in which flow is expected to occur, and the red region represents the region in which flow is not expected to occur. Experimental results (plotted as red or green points for "no flow" and "flow," respectively) were obtained by varying the height between the rail and well plate or width of the rail in our device (representative of n = 3 devices). All devices were used on tissue culture treated (TCT) polystyrene well plates. Theoretical values were calculated based on contact angles collected on a TCT Omnitray and the 3D printer resin. c) Successful flow conditions on surfaces with varied contact angles. All trials were conducted with the same device design (w = 1 mm, h = 0.25 mm), and images are representative of n = 3 devices. The results show that SCF along the rail occurs on all surfaces tested, as predicted by our model. In image i), the ring of Matrigel along the periphery of the well is due to a gap created from adhering a glass slide to a PS well plate to create a glass-bottomed well. In image iv), the ring of Matrigel along the periphery of the well is due to Concus-Finn flow (i.e., flow along a wedge).36,44 Scale bars = 2 mm.

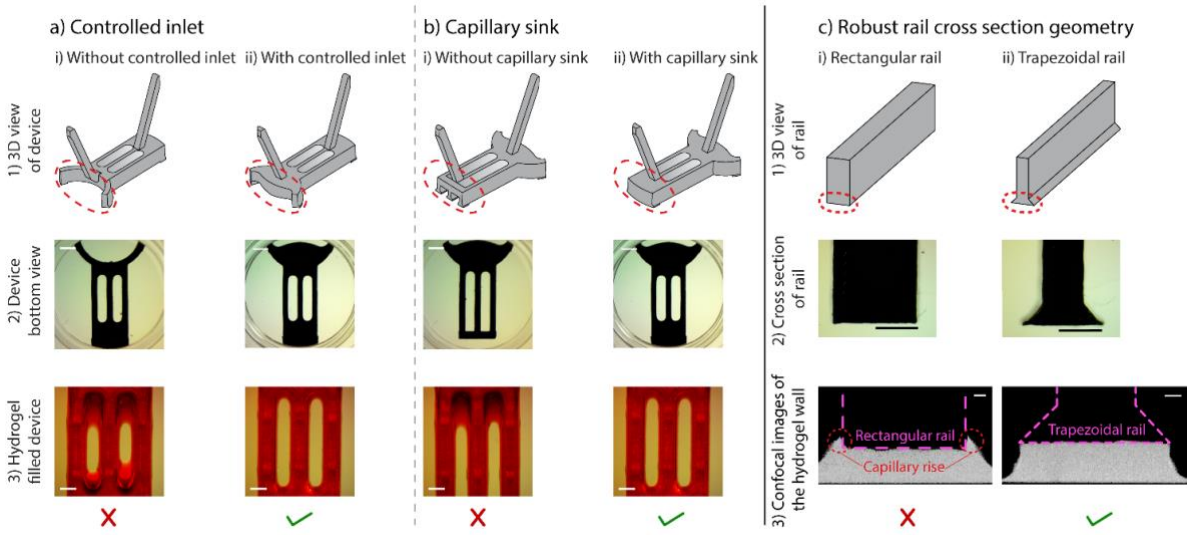

Figure 2.3. Integrated design features for improving control of hydrogel flows. Schematics and images depicting functional design features of our platform include a) a controlled inlet, b) a capillary sink, and c) a trapezoidal rail cross section. For each feature, a 3D schematic (1) and image (2) illustrates the presence or absence of the design feature in the device. For each design, a device containing the design feature and a device without the feature were loaded with hydrogel and allowed to flow to completion (3); devices without the functional design feature experienced flooding of the hydrogel into the culture chamber (a,b) or capillary rise (c, red circles). Devices for a) and b) were used on TCT PS with Matrigel that was dyed red for visualization. Images are representative of n = 3 devices, and videos of each condition are available in the ESI. Scale bar = 2 mm (2), = 1 mm (3). For c), rails for cross sectional images were printed larger for imaging purposes (Scale bar = 1 mm); actual-sized rail images are in the ESI (Figure 2.9). Confocal images of AlexaFluor-488-dyed Matrigel flow were obtained on glass 24 well plates to minimize autofluorescence. Scale bar = 100 μm.

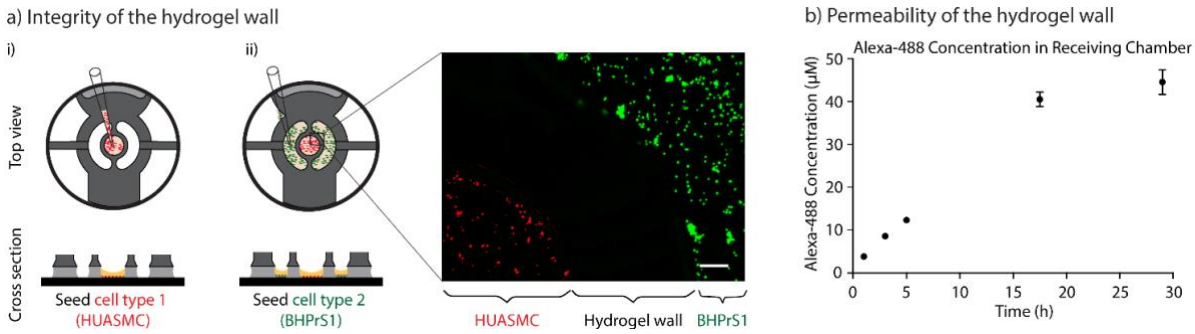

Figure 2.4. Integrity and permeability of patterned hydrogel walls.

A) Integrity of the hydrogel walls is demonstrated by the segregation and containment of cells on either side of the patterned hydrogel wall: i) HUASMC cells stained with CellTracker Red were selectively seeded into the inner culture chamber of the device; ii) BHPrS cells stained with CellTracker Green were selectively seeded into the outer culture chambers of the device. After cell adhesion (overnight incubation), the cells were imaged at the border of the two culture chambers demonstrating the integrity of the hydrogel wall (image is representative of n = 3 devices). Scale bar = 200 μm. B) Permeability of the hydrogel wall was demonstrated via diffusion through the wall. AlexaFluor-488 solution was loaded into the sourcing chamber, and PBS was loaded into a receiving chamber at time = 0 h. The solution in the receiving chambers was collected at t = 1 h, 3 h, 5 h, 17.5 h, and 29 h, and the fluorescence intensity of each sample was measured. Data are expressed as mean ± standard error of the mean (n = 3 devices).

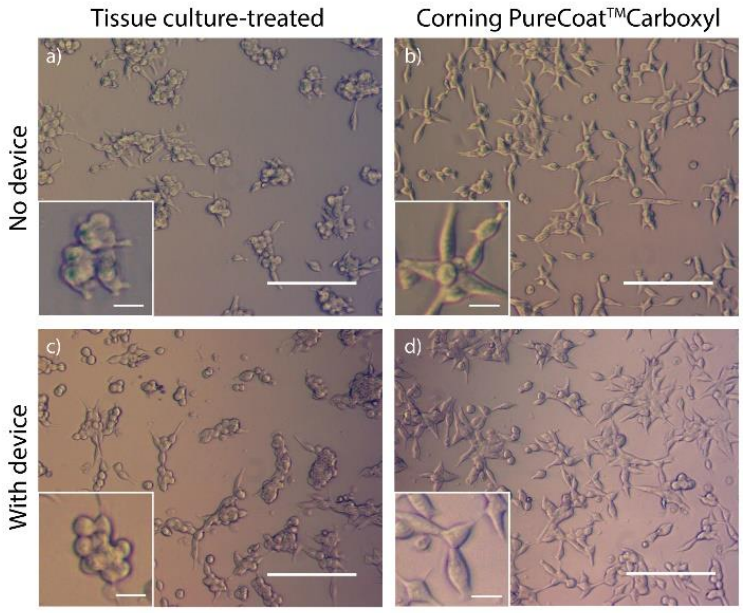

Figure 2.5. Rail-based hydrogel wall patterning technique is compatible with surface-modified commercial well plates designed for sensitive cell types.

Consistent with prior studies,46 LNCaP cells cultured on PureCoatTM Carboxyl well plates exhibited more spread out morphology compared to cells cultured on traditional TCT well plates; this effect was observed when LNCaP cells were cultured in well plates without ((a) and (b)) and with ((c) and (d)) hydrogel wall patterning. Rail devices used in this experiment were micromilled from PS. All images are representative of n = 3 replicates; images were taken between the middle of the culture chamber and the well wall ((c) and (d)) or at a corresponding location off center in the well plate ((a) and (b)). Scale bars = 200 μm, inset scale bars = 20 μm.

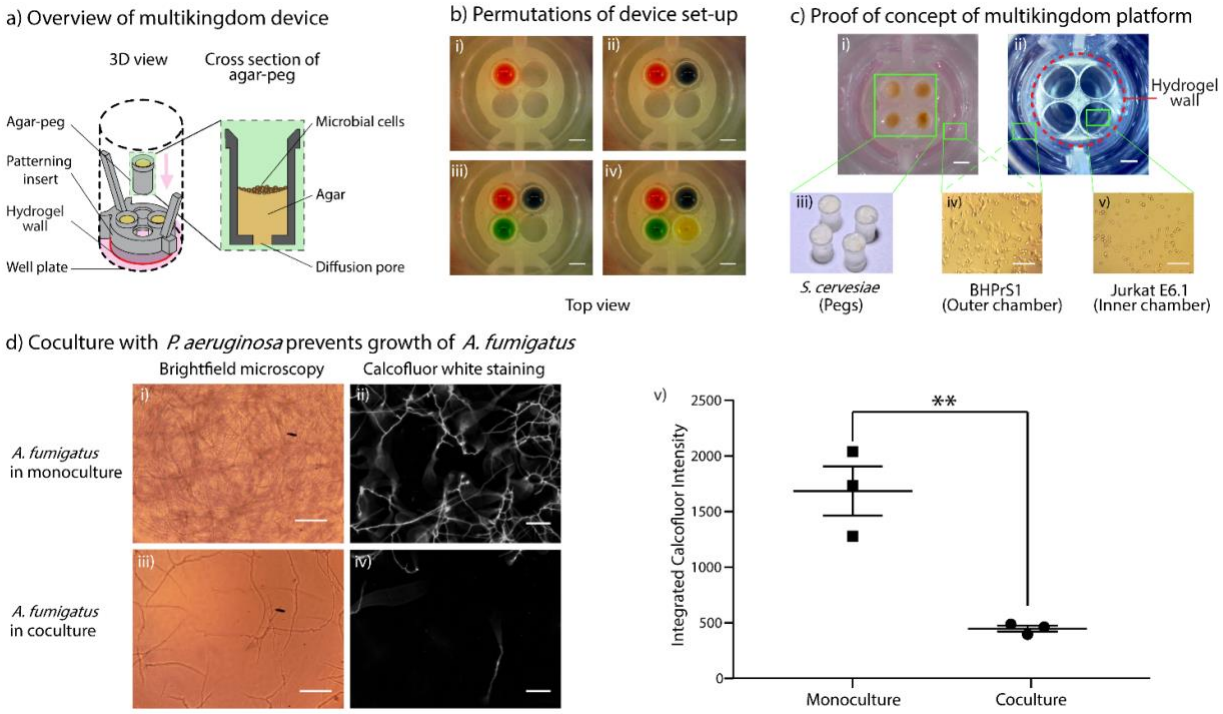

Figure 2.6. Multikingdom coculture in a modular rail-based hydrogel patterning platform. a) An insertable multikingdom coculture platform containing two hydrogel-patterned culture compartments on the well plate surface and four modular "pegs" for temporal or spatial manipulation of multiple cell types. b) Different cell types can be easily added or removed in different permutations to create combinatorial multikingdom cultures; i) Monorail Device with one peg, representing one cell type, while the other ports remain empty; ii-iv) a second, third, and fourth peg can be added as desired. Scale bar = 2 mm. c) A model yeast strain (S. cerevisiae) was cultured on agar-filled pegs (iii) and model human adherent and non-adherent cells (BHPrS1 and Jurkat E6.1, respectively) were cultured separately in a hydrogel-patterned 24 well plate ((iv) and (v)). Jurkat E6.1 cells were seeded into the inner culture chamber of the device, and BHPrS1 cells were seeded into the outer culture chamber. The pegs were then inserted into the device, placing the yeast proximal to the BHPrS1 and Jurkat E6.1 cells. Images are representative of n = 3 devices. The device used for this experiment contained 4 yeast-filled pegs. Scale bar = 2 mm ((i-ii)), 200 μm ((iii - v)). d) Coculture of A. fumigatus with P. aeruginosa inhibits growth of A. fumigatus. Brightfield microscopy images of A. fumigatus in monoculture and coculture (with P. aeruginosa) on Day 1 ((i) and (iii)). Fluorescent images of Calcofluor white stained A. fumigatus in monoculture and coculture on Day 4 ((ii) and (iv)). Quantification of Calcofluor white fluorescent

signal from A. fumigatus in mono- and coculture conveys decreased A. fumigatus growth in coculture (v). Images are representative of n = 3 devices, scale bars = 100 μm. Data is the average of two pegs images per device across three devices plus standard error of the mean (SEM) (error bars). ** indicates significantly different values according to a two-tailed unpaired Student's t-test ($p \leq 0.01$).

2.7 SUPPLEMENTARY INFORMATION

Derivation of theoretical model for conditions for flow in our platform

The pressure in the aqueous phase is generated by surface tension and can be evaluated using the Young-Laplace equation, where ΔP is the pressure difference across a curved air-liquid interface, γ is the interfacial tension, and R_1 and R_2 are the radii of curvature of the interface at a point on the interface in two orthogonal directions (e.g., horizontal and vertical).

The Laplace pressure difference (ΔP) at every interface is zero when the interface is flat ($R_1 = R_2 = \infty$). When the curvature of an interface is concave due to favorable wetting (i.e., contact angle < 90°), the Laplace pressure difference becomes negative. Inversely, when the curvature is convex, the Laplace pressure difference becomes positive. Laplace pressure is a well-defined phenomenon that can be controlled experimentally and used to predict conditions for flow in our system.

Conditions for flow in an open channel have been derived in a general way by Berthier et al [1]. and are known as the spontaneous capillary flow (SCF) equation (in the case of a channel that has the same contact angle on all faces) or as the generalized Cassie angle equation (for the more general case when there are any number of contact angles along the surface of the channel). The current analytical models, however, assume that the pressure at the inlet of the open channel is negligible. The models allow prediction of the theoretical ability for SCF to occur. In order to

refine the conditions for flow in our system, we added a pressure balance analysis between the surface tension-based pressures at the inlet and at the advancing fluid front (assuming the front exists).

The inlet of our system is a rectangular cross-section defined by the insert and the walls of the well plate. The liquid meniscus at the inlet is concave due to the wettability of the insert and well (contact angle < 90°) and the interface will take the shape of a cylinder (as the channel cross-section is long (8.6 mm) and narrow (1 mm)). The radius of curvature along the long edge of the channel inlet is thus infinitely large, while the radius of curvature R_3 along the smaller edge of the inlet is uniquely characterized by two different contact angles with the device insert and the well plate, respectively (Figure 2.7). The pressure of the fluid at the inlet is written as:

$$\Delta P_{\text{inlet}} = \gamma \left(\frac{1}{R_3} \right) \qquad \text{(Eq. 1)}$$

The fluid front advancing under the plastic rail has a more complex geometry. The fluid front is described by a saddle point as the liquid is wetting the rail ceiling and well floor plastics (creating a concave fluid interface in the x-z plane) and is rounded from the top view as the channel does not have any side walls (the interface is convex in the x-y plane) (Figure 2.7). The pressure at the fluid front is described by Eq. 2, where R_1 is chosen to be the radius of curvature in the x-z plane, and R_2 is chosen as the radius of curvature in the x-y plane:

$$\Delta P_{\text{front}} = \gamma\left(\frac{1}{R_1} + \frac{1}{R_2}\right) \quad \text{(Eq. 2)}$$

The condition for flow in our system requires the Laplace pressure of the inlet to be greater than the Laplace pressure at the fluid front in order to drive the fluid towards the area of lowest pressure:

$$\gamma\left(\frac{1}{R_3}\right) > \gamma\left(\frac{1}{R_1} + \frac{1}{R_2}\right) \quad \text{(Eq. 3)}$$

Therefore, the limit of flow will occur when the two pressures are equal:

$$\gamma\left(\frac{1}{R_3}\right) = \gamma\left(\frac{1}{R_1} + \frac{1}{R_2}\right) \quad \text{(Eq. 4)}$$

Or:

$$\frac{1}{R_1} + \frac{1}{R_2} - \frac{1}{R_3} = 0 \quad \text{(Eq. 5)}$$

The radii of curvature in our system are governed by the physical aspect ratio of the channel, which includes the width w of the rail and the gap g_{front} between the rail and the well plate ($g_{\text{front}} = h$), the

gap g_{inlet} between the insert and the well wall, and the contact angles of the fluid on the rail and the well plate surfaces.

We derived an equation for the radius of curvature of the fluid in the advancing filament in the x-z plane in function of the contact angles of the fluid on the well plate (θ_2), the contact angle of the fluid on the rail (θ_1), and the height of the rail (h). Using the geometric relations illustrated in Figure 2.7, we obtain:

$$R_1 = -\left(\frac{h}{\cos\theta_1 + \cos\theta_2}\right) \quad \text{(Eq. 6)}$$

To assess the curvature of radius R_2, we assume that the fluid is minimizing the surface energy, and thus assume that the interface is taking the shape of a large semi-circle of the same radius as the half-width of the rail.

We apply the same reasoning utilized to determine R_1 in Eq. 6 in order to derive R_3, as a function of g_{inlet}, θ_2, and θ_1. Substitution of R_1, R_2, and R_3 into Equation 5 yields:

$$\frac{1}{-\left(\frac{h}{\cos\theta_1 + \cos\theta_2}\right)} + \frac{1}{\frac{w}{2}} - \frac{1}{-\left(\frac{g_{\text{inlet}}}{\cos\theta_1 + \cos\theta_2}\right)} = 0 \quad \text{(Eq. 7)}$$

Where w is the width of the rail, h is the height of the rail, and g_{inlet} is the space between the well and the device at the inlet in mm. Solving for h yields:

$$h = \frac{\cos\theta_1 + \cos\theta_2}{\frac{2}{w} + \frac{\cos\theta_1 + \cos\theta_2}{g_{\text{inlet}}}} \qquad \text{(Eq. 8)}$$

Equation 8 is graphed to give the boundary between the red and green shaded regions in Figure 2.2b, providing a model to predict when flow will occur in our system for devices based on the device dimensions.

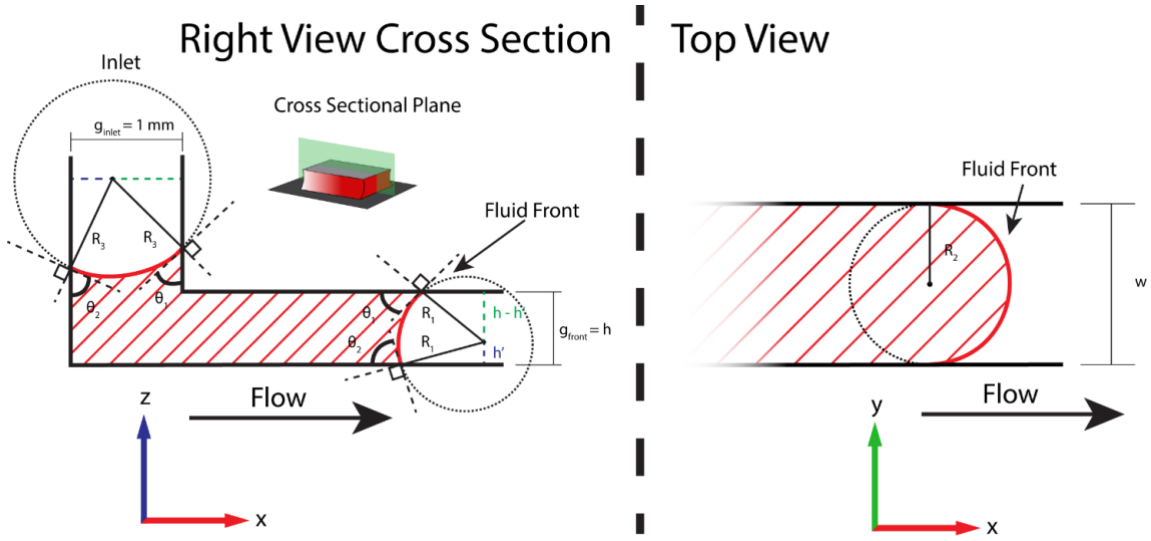

Figure 2.7. Illustrations of radii of curvature for the calculation of Laplace pressure differences in our system.

Perspectives demonstrate the radii of curvature (R), the contact angle between the liquid and the surface (θ), the height of the channel (h), the width of the channel (w), and the gap between the insert and the patterned surface (g).

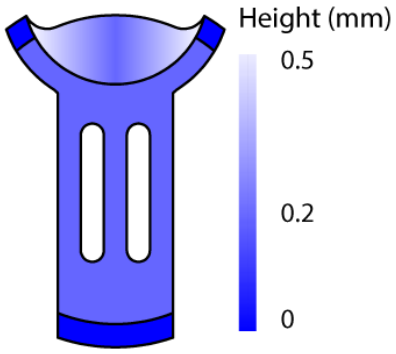

Figure 2.8. Heat map illustrating the height of the rail above the well plate surface. Regions of the device with a lower height to width ratio are more favorable for spontaneous capillary flow (SCF) and tuning the height as shown enables controlled and reproducible hydrogel flow. The height gradient along the loading zone directs flow towards the middle of the flow path while feet (shown in dark blue, h = 0 mm) keep the patterning region off the surface.

a)

Device aspect ratio (designed width vs height)	Measured width of 3D printed rail (mm)	Measured hydrogel wall width (mm)	Difference between measured hydrogel wall width and rail width (mm)
1 mm x .15 mm	0.778 ± .010	1.220 ± 0.028	0.442
.75 mm x .15 mm	0.540 ± .012	0.968 ± 0.035	0.428
.75 mm x .25 mm	0.540 ± .012	1.044 ± 0.014	0.504

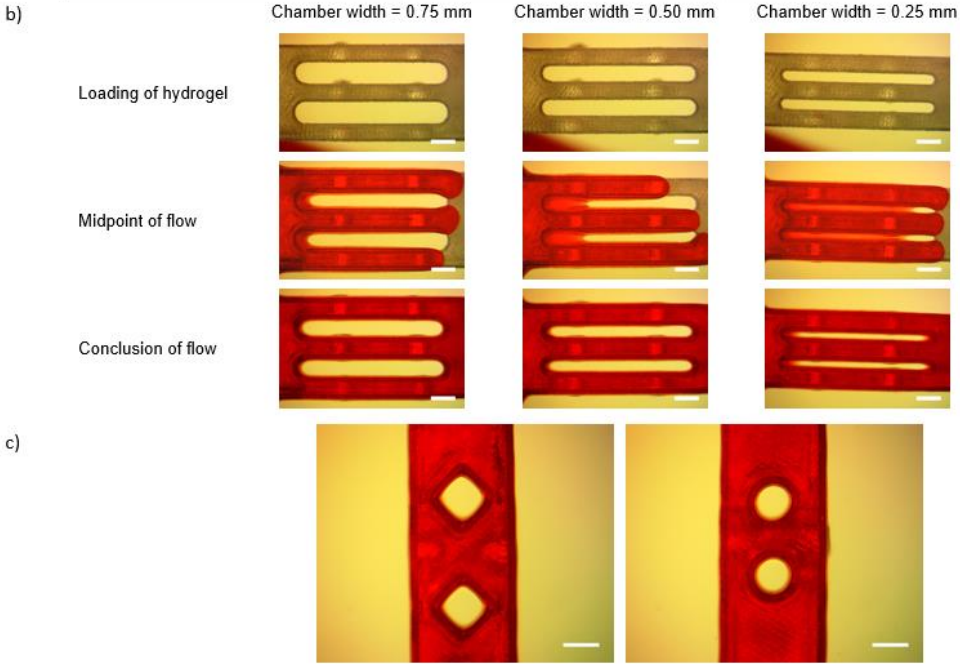

Figure 2.9. Extent of device patterning capabilities on TCT PS.

A) Extent of flooding along a rail. Devices were filled with matrigel dyed with red food dye and imaged from beneath (n = 3 devices). Data presented in the table represent the average width of the wall ± SD for three different device aspect ratios. Height, in addition to width, influences the flooding of the chamber by the wall. B) Limit of culture chamber area due to flooding. Our platform enables fabrication of culture chambers down to a resolution of 0.25 mm width, below which we observed complete flooding of the culture chambers during the flow. At the conclusion of flow, the gel receded from the chamber leaving gel residue on the chamber floor. Images are representative of flow in n = 3 devices on TCT PS at different time points. Scale bar = 1 mm. C) Geometric patterning capabilities of our platforms. Scale bars = 1 mm.

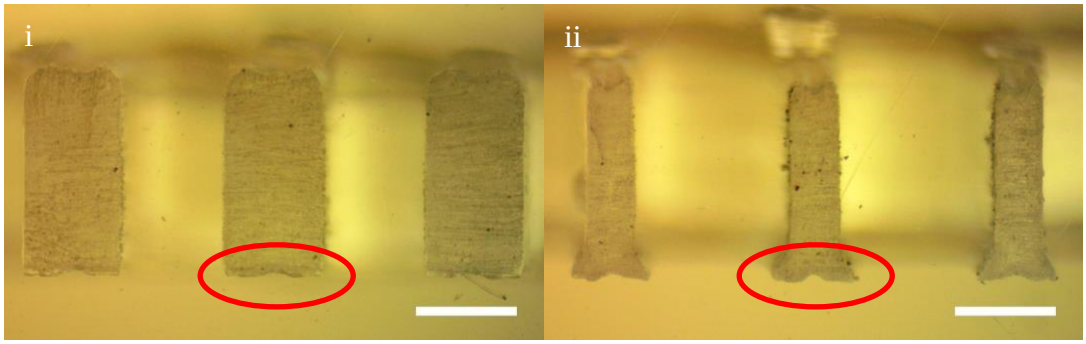

Figure 2.10. Images represent the trapezoidal rail cross section.

Cross sections presented here illustrate the rail without (i) and with (ii) a trapezoidal pinning feature at the scale used in each device. 3D-printed defects can be observed along the base of the rail, which were consistent throughout all devices. Scale bar = 1 mm.

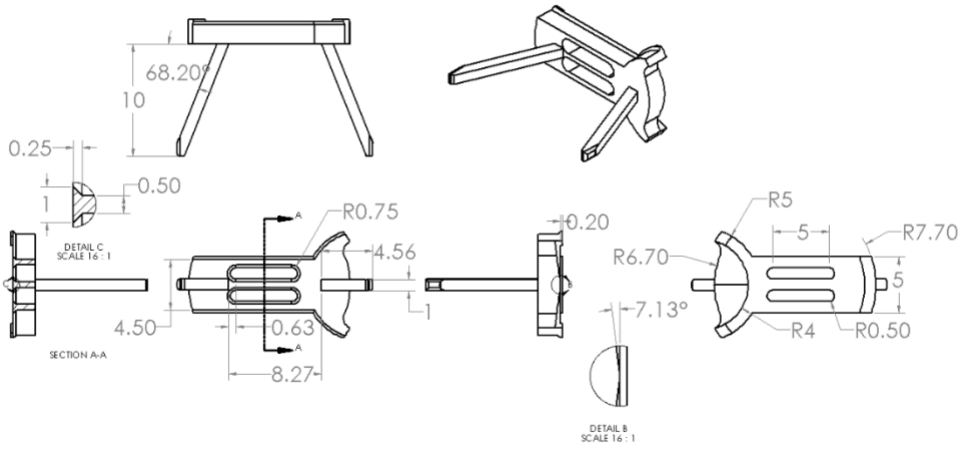

Figure 2.11. Schematic diagrams illustrating the dimensions of our platform.

(All dimensions are in mm. CAD files are also included for all devices in the ESI online.)

2.8 REFERENCES

[1] L. Goers, P. Freemont, K.M. Polizzi, "Co-culture systems and technologies: taking synthetic biology to the next level." *J. R. Soc. Interface,* 2014, **11**, 0065.

[2] D.R. Bogdanowicz and H.H. Lu. "Studying cell-cell communication in co-culture." *Biotechnol. J.* 2013, April, 8(**4**), 395-396.

[3] V.V. Abhyankar, D.J. Beebe, "Spatiotemporal micropatterning of cells on arbitrary substrates". *Anal. Chem*., 2007, **79**, 4066-4073.

[4] S.N. Bhatia, U.J. Balis, M.L. Yarmush, M. Toner, "Microfabrication of hepatocyte/fibroblast co-cultures: Role of homotypic cell interactions." *Biotechnol. Prog*., 1998, May-Jun, **14** (3), 378-387.

[5] H.J. Kim, J.Q. Boedicker, J.W. Choi, R.F. Ismagilov, "Defined spatial structure stabilizes a synthetic multispecies bacterial community." *PNAS*, 2008, Nov., **105**, 18188-18193.

[6] Y. Miki, K. Ono, S. Hata, T. Suzuki, H. Kumamoto, H. Sasano, "The advantages of co-culture over mono cell culture in simulating *in vivo* environment". *Journal of Steroid Biochemistry and Molecular Biology*, 2012, **131**, 68-75.

[7] K. Hatherell, P.O. Couraud, I.A. Romero, B. Weksler, G.J. Pilkington, "Development of a three-dimensional, all-human *in vitro* model of the blood-brain barrier using mono-, co-, and tri-cultivation Transwell models". *Journal of Neuroscience Methods*, 2011, **199**, 223-229.

[8] D.A. Lauffenburger, S.H. Zigmond. "Chemotactic factor concentration gradients in chemotaxis assay systems", *Journal of Immunological Methods*, **40**, (1981), 45-60.

[9] T.M. Keenan, A. Folch. "Biomolecular gradients in cell culture systems", *Lab Chip*, 2008, **8**, 34-57.

[10] A.D. Gracz, I.A. Williamson, K.C. Roche, M.J. Johnston, F. Wang, Y. Wang, P.J. Attayek, J. Balowski, X.F. Liu, R.J. Laurenza, L.T. Gaynor, C.E. Sims, J.A. Galanko, L. Li, N.L. Allbritton, S.T. Magness, "A high-throughput platform for stem cell niche co-cultures and downstream gene expression analysis", *Nature Cell Biology*, 2015, **17**, 340-349.

[11] L.M. Borland, S. Kottegoda, K.S. Phillips, N.L. Allbritton, "Chemical analysis of single cells", *Annu. Rev. Anal. Chem.*, 2008, **1**, 191-227.

[12] S.N. Bhatia, D.E. Ingber. *Nature Biotechnology*, 2014, **32**, 760–772.

[13] S. March, V. Ramanan, K. Trehan, S. Ng, A. Galstain, N. Gural. et al, "Micropatterned coculture of primary human hepatocytes and supportive cells for the study of hepatotropic pathogens". *Nature Protocols*, 2015, **10**, 2027-2053.

[14] S. Takayama, J.C. McDonald, E. Ostuni, M.N. Liang, P.J. Kenis, R.F. Ismagilov, G.M. Whitesides, “Patterning Cells and Their Environments Using Multiple Laminar Fluid Flows in Capillary Networks.” *PNAS*, 1999, May, **96**, 5545-5548

[15] T. Kojima, C. Moraes, S.P. Cavnar, G.D. Luker, S. Takayama, “Surface templated hydrogel patterns prompt matrix-dependent migration of breast cancer cells towards chemokine-secreting cells.” *Acta Biomaterialia*, 2015, **13**, 68-77.

[16] A.P. Wong, R. Perez-Castillejos, J.C. Love, G.M. Whitesides, “Partitioning microfluidic channels with hydrogel to construct tunable 3-D cellular microenvironments.” *Biomaterials*, 2008, **29**, 1853-1861.

[17] C.Y. Li, K.R. Stevens, R.E. Schwartz, B.S. Alejandro, J.H. Huang, S.N. Bhatia, “Micropatterned cell-cell interactions enable functional encapsulation of primary hepatocytes in hydrogel microtissues”. *Tissue Eng. Part A*, 2014, Aug, **20** (15-16), 2200-2212.

[18] E.W.K. Young, C. Pak, B.S. Kahl, D.T. Yang, N.S. Callander, S. Miyamoto, D.J. Beebe, “Microscale functional cytomics for studying hematologic cancers” *Blood*, 2012, **119**, e76-e85.

[19] Y. Torisawa, B. Mosadegh, G.D. Luker, M. Morell, K.S. O’Shea, S. Takayama “Microfluidics hydrodynamic cellular patterning for systematic formation of co-culture spheroids.” *Integr. Bio.*, 2009, **1**, 649-654.

[20] P. Gheibi, K.J. Son, G. Stybayeva, A. Revzin. “Harnessing endogenous signals from hepatocytes using a low-volume multi-well plate”, *Integr. Biol.*, 2017, 9, 427.

[21] C.J. Flaim, S. Chien, S.N. Bhatia, “An extracellular matrix microarray for probing cellular differentiation.” *Nature Methods*, 2005, Feb., **2**, 119-125. Feb. 2005.

[22] C.P. Huang, J. Li, H. Seon, A.P. Lee, L.A. Flanagan, H.Y. Kim, A.J. Putnam, N.L. Jeon, “Engineering microscale cellular niches for three-dimensional multicellular co-cultures”. *Lab Chip*, 2009, **9**, 1740-1748.

[23] Y.S. Torisawa, B Mosadegh, S.P. Cavnar, M. Ho, S. Takayama, “Transwells with microstamped membranes produce micropatterned two-dimensional and three-dimensional cocultures.” *Tissue Eng Part C Methods*, 2011, Jan, 17 (**1**), 61-67.

[24] M. Domenech, H. Yu, J. Warick, N.M. Badders, I. Meyvantsson, C.M. Alexander, D.J. Beebe, “Cellular observations enabled by microculture: paracrine signaling and population demographics.” *Integr. Biol*., 2009, **1**, 267-274.

[25] L.J. Barkal, A.B. Theberge, C.J. Guo, J. Spraker, L. Rappert, J. Berthier, et al., “Microbial metabolomics in open microscale platforms.” *Nature Com*. 2016, Feb, **7**, 10610.

[26] C.M. Carney, J.L Muszynski, L.N. Strotman, S.R. Lewis, R.L. O’Connell, D.J. Beebe, A.B. Theberge, J.S. Jorgenson, “Cellular microenvironment dictates androgen production by murine fetal Leydig cells in primary culture”, Biol Reprod, 2014, Oct., 91 (4), 85.

[27] E.E. Hui, S.N. Bhatia, “Micromechanical control of cell-cell interactions”. *PNAS*, 2007, April, **104**, 5722-5726.

[28] S.H. Lee, A.J. Heinz, S. Shin, Y.G. Jung, S.E. Choi, W. Park, J.H. Roe, S. Kwon. “Capillary based patterning of cellular communities in laterally open channels”, *Anal. Chem.*, 2010, **82**, 2900-2906.

[29] S. Bersini, J.S. Jeon, G. Dubini, C. Arrigoni, S. Chung, J.L. Charest et al. “A microfluidic 3D *in vitro* model for specificity of breast cancer metastasis to bone”, *Biomaterials*, **35**, (2014), 2454-2461.

[30] Y. Gao, D. Majumdar, B. Jovanovic, C. Shaifer, P.C. Lin, A. Zijlstra et al. “A versatile valve-enabled microfluidic cell co-culture platform and demonstration of its applications to neurobiology and cancer biology”, *Biomed Microdevices*, (2011), **13**:539-548.

[31] K.J. Son, P. Gheibi, G. Stybayeva, A. Revzin. “Detecting cell-secreted growth factors in microfluidic devices using bead-based biosensors”, *Microsystems and Nanoengineering* (2017), **3**, 17025.

[32] D. Patel, Y. Gao, K. Son, C. Siltanen, R.M. Neve, K. Ferrara, A. Revzin. “Microfluidic co-cultures with hydrogel-based ligand trap to study paracrine signals giving rise to cancer drug resistance”, *Lab Chip*, 2015, **15**, 4614.

[33] K.J. Regehr, M. Domenech, J.T. Koepsel, K.C. Carver, S.J. Ellison-Zelski, W.L. Murphy, L.A. Schuler, E.T. Alarid, D.J. Beebe, “Biological implications of polydimethylsiloxane-based microfluidic cell culture”, *Lab Chip*, 2009, Aug., 9 (**15**), 2132-2139.

[34] J.N. Lee, C. Park, G.M. Whitesides, “Solvent compatibility of poly(dimethylsiloxane)-based microfluidic devices”, *Anal. Chem*, 2003, 75 (**23**), pp 6544-6554.

[35] E. Berthier, E.W. Young, D.J. Beebe, “Engineers are from PDMS-land, biologists are from polystyrenia.” *Lab Chip*, 2012, 12(**7)**, 1224-37.

[36] B.P. Casavant, E. Berthier, A.B. Theberge, J. Berthier, S.I. Montanez-Sauri, L.L. Bischel, et al. “Suspended Microfluidics.” *PNAS*, 2016, April, **110**, 10111-10116.

[37] J. Berthier, K.A. Brakke, E. Berthier, “Open Microfluidics”. Wiley; 2016

[38] A.K. Au, W. Lee, A. Folch, “Mail-order microfluidics: evaluation of stereolithography for the producton of microfluidic devics.” *Lab Chip*, 2014, **14**, 1294.

[39] A.K. Au, W. Huynh, L.F. Horowitz, A. Folch; “3D-Printed Microfluidics”. *Angew. Chem. Int. Ed*. 2016, **55**, 3862 – 3881.

[40] Franco, M. Jiang, D. W. Strand, J. Peacock, S. Fernandez, R.S. Jackson II, et al. “Altered TGF-β Signaling in a Subpopulation of Human Stromal Cells Promotes Prostatic Carcinogenesis”. *Cancer Res*., 2011, Feb., 71 (**4**), 1272-1281.

[41] D.R. Church, E. Lee, T.A. Thompson, H.S. Basu, M.O. Ripple, E.A. Ariazi, G. Wilding. “Induction of AP-1 Activity by Androgen Activation of the Androgen Receptor in LNCaP Human Prostate Carinoma Cells”. *The Prostate*, 2005, **63**,155-168.

[42] K. Shimizu, N.P. Keller. “Genetic involvement of a cAMP-dependent protein kinase in a G protein signaling pathway regulating morphological and chemical transitions in Aspergillus nidulans”. Genetics, 2001, 157, 591–600.

[43] M. Verhulsel, M. Vignes, S. Descroix, L. Malaquin, D.M. Vignjevic, J.L. Viovy. “A review of microfabrication and hydrogel engineering for micro-organs on chips”, *Biomaterials*, **35**, (2014), 1816-1832.

[44] P. Concus, R. Finn; “On the behavior of a capillary surface in a wedge”. *PNAS*, 1969, June, 2 (**63**), 292-299.

[45] M.S. Liberio, M.C. Sadowski, C. Soekmadji, R.A. Davis, C.C. Nelson; “Differential effects of tissue culture coating substrates on prostate cancer cell adherence, morphology, and behavior”. *PLoS ONE*, 2014, 9(**11**): e112122.

[46] Corning® PureCoat™ Cultureware, Corning Data Sheet CLS-DL-CC-046 REV1, 2013. Web. https://www.corning.com/media/worldwide/cls/documents/CLS-DL-CC-046_REV1.pdf. Accessed 8/12/17.

[47] N. Bhattacharjee, A. Urrios, S. King, A. Folch. “The upcoming 3D-printing revolution in microfluidics”, *Lab Chip*, 2016, **16**, 1720.

[48] S. Saegusa, M. Totsuka, S. Kaminogawa, T. Hosoi; “*Saccharomyces cerevisiae* and *Candida albicans* stimulate cytokine secretion from human neutrophil-like HL-60 cells differentiated with retinoic acid or dimethylsulfoxide”. *Biosci. Biotechnol. Biochem*., 2009, 73, (**12**), 2600-2608.

[49] R. Hatoum, S. Labrie, I. Fliss. “Antimicrobial and probiotic properties of yeasts: from fundamental to novel applications”. *Front. Microbiol*., 2012, **3**, 421.

[50] G.B. Huffnagle, M.C. Noverr. “The emerging world of the fungal microbiome”. *Trends Microbiol*, 2013, July, 7 (**21**), 334-341.

[51] The Human Microbiome Project Consortium. “Structure, function, and diversity of the healthy human microbiome”. *Nature*, 2012, June, **486**, 207-214.

[52] L.J. Barkal, C.L. Procknow, Y.R. Alvarez-Garcia, M. Niu, J.A. Jimenez-Torres, R.A. Brockman-Schneider, et al. “Microbial volatile communication in human organotypic lung models”, *Nat. Comm.*, Accepted.

[53] L.J. Barkal, E. Berthier, A.B. Theberge, N.P. Keller, D.J. Beebe. “Multikingdom microscale models”, *PLoS Pathog*, 2017, **13**, 8: e1006424.

[54] K.H. Spencer, M.Y. Kim, C.C.W. Hughes, E.E. Hui, “A screen for short-range paracrine interactions”, *Integr. Biol.*, 2014, **6**, 382.

[55] N. Rao, G.N. Grover, L.G. Vincent, S.C. Evans, Y.S. Choi, K.H. Spencer, E.E. Hui, A.J. Engler, K.L. Christman, "A co-culture device with a tunable stiffness to understand combinatorial cell-cell and cell-matrix interactions", *Integr. Biol.*, 2013, **5**¸1344.

[56] K. Smith, R. Rajendran, S. Kerr, D. Lappin, W.G. Mackay, C. Williams, G. Ramage. "*Aspergillus fumigatus* enhances elastase production in *Pseudomonas aeruginosa* co-cultures", *Medical Mycology*, 2015, **53**¸645-655.

[57] E. Mowat, R. Rajendran, C. Williams, E. McCulloch, B. Jones, S. Lang, G. Ramage. "*Pseudomonas aeruginosa* and their small diffusible extracellular molecules inhibit *Aspergillus fumigatus* biofilm formation", *FEMS Microbiol Lett*, 2010, **313**, 96-102.

[58] H. Zheng, J. Kim, M. Liew, J.K. Yan, O. Herrera, J.W. Bok, N.L. Kelleher, N.P. Keller, Y. Wang. "Redox metabolites signal polymicrobial biofilm development via the NapA oxidative stress cascade in *Aspergillus*", *Current Biology*, 2015, **25**, 29-37.

Chapter 3. INVESTIGATING FIBROBLAST-INDUCED COLLAGEN GEL CONTRACTION USING A DYNAMIC MICROSCALE PLATFORM

This chapter is mostly adapted from the original publication: Zhang, T.;‡ Day, J. H.;‡ Su, X.; Guadarrama, A. G.; Sandbo, N. K.; Esnault, S.; Denlinger, L. C.; Bertheir, E.; Theberge, A. B., "Investigating Fibroblast-Induced Collagen Gel Contraction Using a Dynamic Microscale Platform." Frontiers in Bioengineering and Biotechnology, 2019;7:196. DOI: 10.3389/fbioe.2019.00196 (‡ indicates equal contributions).

3.1 ABSTRACT

Mechanical forces have long been recognized as fundamental drivers in biological processes, such as embryogenesis, tissue formation and disease regulation. The collagen gel contraction (CGC) assay has served as a classic tool in the field of mechanobiology to study cell-induced contraction of extracellular matrix (ECM), which plays an important role in inflammation and wound healing. In a conventional CGC assay, cell-laden collagen is loaded into a cell culture vessel (typically a well plate) and forms a disk-shaped gel adhering to the bottom of the vessel. The decrement in diameter or surface area of the gel is used as a parameter to quantify the degree of cell contractility. In this study, we developed a microscale CGC assay with an engineered well plate insert that uses surface tension forces to load and manipulate small volumes (14 μL) of cell-laden collagen. The system is easily operated with two pipetting steps and the microscale device moves dynamically as a result of cellular forces. We used a straightforward one-dimensional measurement as the gel contraction readout. We adapted a conventional lung fibroblast CGC assay to demonstrate the functionality of the device, observing significantly more gel contraction when human lung

fibroblasts were cultured in serum-containing media versus serum-free media ($p \leq 0.05$). We further cocultured eosinophils and fibroblasts in the system, two important cellular components that lead to fibrosis in asthma and observed that soluble factors from eosinophils significantly increase fibroblast-mediated gel contraction ($p \leq 0.01$). Our microscale CGC device provides a new method for studying downstream ECM effects of intercellular cross talk using 7-35 folds less cell-laden gel than traditional CGC assays.

3.2 INTRODUCTION

Fibroblasts are key mesenchymal cells in connective tissue which synthesize extracellular matrix (ECM) components and provide structural support for the extracellular environment [22]. As part of the tissue self-repair mechanism, fibroblasts interact with surrounding ECM proteins through a variety of inflammatory mediators and differentiate into a more contractile phenotype known as myofibroblasts [14, 22, 35]. However, overreactive myofibroblasts generate and deposit excessive ECM proteins in the interstitium, contributing to fibrotic diseases such as asthma and idiopathic pulmonary fibrosis [13, 16]. Therefore, understanding the mechanobiology of fibroblasts in ECM and the underlying signaling mechanisms is essential to developing therapies for diseases involving fibrosis. The goal for this study is to develop a microscale assay that captures and reflects dynamic fibroblast-ECM interactions.

The fibroblast-induced collagen gel contraction (CGC) assay was established by Bell et al. to study fibroblast-matrix interactions [3] and has been modified and widely used over the past four decades. The traditional CGC assay is performed by embedding fibroblasts into a three-dimensional (3D) gel matrix, such as collagen or fibrin, on the bottom of a well plate, which is then manually separated from the well plate surface (for example by scraping a pipette tip around the perimeter

of the well) to loosen the gel puck from the well plate walls and enable contraction [8, 32]. The contractile forces generated by fibroblasts propagate throughout the collagen matrix and arrange collagen fibers to higher density structure with decreased matrix volume [24]. As a result, measuring the decrease in size of a gel matrix puck by imaging and subsequent analysis provides a direct way to assess fibroblast contractility.

Addressing some complications in the existing CGC assay workflow could help researchers meet a diverse set of experimental needs. For example, deformation of gel shape and ambiguous post-contraction gel borders make the exact gel area difficult to define [6]; the requirement of relatively large cell samples precludes the assay from use with limited primary cells [34]; large volumetric consumption of gels (>100 μL per replicate in a 96 well plate) is relatively expensive [15, 40]; and the friction between gel and substrate upon gel contraction is not well defined, potentially adding variation to the data [7, 41]. Through the years, numerous tools and technologies have been developed to improve these shortcomings. For example, automated image analysis programs have been used to improve accuracies for the geometric gel shape readout [6, 23]. Leung et al. developed a high-throughput microscale aqueous two-phase droplet fabrication method in conventional 384-well plate which effectively reduced the gel droplet to 10-15 μL [28]. Ilagan et al. used glass capillary to cast cell-laden collagen which was subsequently detached from the glass surface by pipetting force, significantly reducing friction and converting three-dimensional parameters into a single, linear measurement [21]. The recent efforts to develop new CGC assay platforms have underscored the utility of the assay and motivated our work to develop a new microscale CGC assay that builds on past improvements and enables a combination of new experimental features.

Microfluidics has emerged as a versatile toolbox that researchers have used to develop a wide variety of assay platforms [33, 42]. Our goal was to use microfluidics to create a microscale CGC assay that addresses the needs in objective gel shape quantification, reducing cell and gel consumption, minimizing friction between the plastic culture substrate and the gel, and enabling segregated coculture to study paracrine signaling. Here, we describe a microscale CGC platform based on 24 well plate insert that enables the study of dynamic cell-matrix interactions. The device is characterized by a two-step pipetting operation and a simple angle measurement as a contractility readout. We demonstrate a proof of concept use of this technology with a serum stimulation experiment. Further, we validate our device for coculture by testing the hypothesis that soluble factors secreted by eosinophils induce increased gel contraction by lung fibroblasts as has been previously observed using the traditional CGC assay [45]. In the future, we envision that we and other researchers could use our technology to address additional research questions relating to paracrine signaling in lung fibrosis as well as fibrosis in other organs such as the regulation of epithelial-to-mesenchymal transition in kidney fibrosis and the role of stellate cell activation in hepatic fibrosis.

3.3 Materials and Methods

3.3.1 *Devices Fabrication*

Devices were fabricated using a Form 2 SLA 3D printer (Formlabs, Somerville, MA). 3D-printed devices were designed with Solidworks and converted to .form files with PreForm 2.11.0 (Formlabs) prior to being printed with Form 2 Clear V4 Resin (Formlabs). After printing, devices were sonicated in isopropanol (IPA) for 15 min, rinsed with fresh IPA, and UV-cured (Quans 20 W UV Lamp) for 2 hours. Original design files are included in the ESI.

3.3.2 *Cell Culture*

Human fetal lung fibroblasts (HFL-1) were obtained from the American Type Culture Collection (Rockville, MD, USA). The cells were cultured in a T-75 tissue culture flask (Falcon; Franklin Lakes, NJ, USA) with F-12K Medium (Kaighn's Modification of Ham's F-12 Medium, ATCC® 30-2004) supplemented with 10% heat-inactivated fetal bovine serum (FBS; GIBCO&SOL; BRL Life Technologies), penicillin (100 units mL−1), and streptomycin (100 μg/mL). Fibroblasts were used between the 4th and 10th passage. Confluent fibroblasts were trypsinized (Trypsin-EDTA; GIBCO/BRL Life Technologies, 0.05% trypsin 0.53 mM EDTA), resuspended in serum free F-12K medium at a working concentration of 3×106 cells/mL, and kept on ice prior to use in the CGC assay.

AML14.3D10 cells (cell line was generously provided by Cassandra Paul (Wright State University, Dayton, OH)), a differentiated human myeloid leukemic cell line that displays typical morphology and enzymatic activity of normal eosinophils [1, 2, 11] (Ackerman et al., 2000; Baumann and Paul, 1997; Esnault et al., 1998), were grown in T-75 tissue culture flasks in RPMI 1640 media containing 8% FBS, supplemented with 2 mM L-glutamine, 1 mM sodium pyruvate, 0.05 mg/mL gentamycin, and 5.5×10-5 M 2-mercaptoethanol. Eosinophil concentration was maintained between 1×105 - 1×106/mL in the flask. All cells were maintained in a 37 °C incubator with 5% carbon dioxide.

3.3.3 *HFL-1 Collagen Gel Contraction Assay in the CGC Device and 96 Well Plate*

Two parts of HFL-1 in serum free F-12K media (3×106 cells/mL) were mixed together with one part of type I collagen (9.4 mg/mL; Corning, Corning, NY, USA) and one part of 1×HEPES to a

final concentration of 2.35 mg/mL of collagen, 1.5×106 fibroblasts/mL. CGC devices were assembled and inserted into 24 well plates. 14 μL of fibroblast-laden collagen was loaded into the loading channel, contacting the free-swinging arm head and swinging it into the loading channel (as shown in Figure 3.1 i)). 40 μL of F-12 K media supplemented with 10% FBS (for all conditions) was pipetted into the retraction tube to contact the free-swinging arm (Figure 3.1 ii)); the media was then quickly withdrawn to pull the free-swinging arm back into the retraction tube (Figure 1iii)). The plate was incubated for 15 min at 37 °C. For monoculture experiments (Figure 3.2), 2 mL F-12 K media with or without 10% FBS was gently loaded into each well of the 24 well plate; for coculture experiments (Figure 3.3), 7×105 eosinophils were resuspended with 2 mL of serum-free F-12K media then gently added into each well. The plate was incubated overnight.

For the CGC assay in 96 well plate, 100 μL of the fibroblast-laden collagen was loaded into each well. The plate was incubated for 1 h at 37 °C. 100 μL F-12 K media with or without 10% FBS was gently loaded into each well of the 96 well plate. To initiate contraction, the gel disc in each well was manually separated from the well plate surface by scraping a pipette tip around the perimeter of the well. The plate was incubated overnight.

3.3.4 *Measurement of CGC Device Angle*

The top view of each device was imaged using a MU1403B Microscope Camera mounted on an Amscope SM-3TZ-80S stereoscope (Amscope, Irvine, CA). Each device was imaged after setup and media addition (initial angle, θi) then placed into incubator, and imaged with the same setup (position, lighting condition, and same Amscope parameters) after 24 h (final angle, θf). The brightness of each image was adjusted with Fiji (ImageJ, version 2.0.0), and the CGC device angle was determined by the pivot point of the rotation axis and two side faces of collagen in contact

with the device (as depicted in Figure 3.1B and Figure 3.2A). The initial and final angles were measured automatically with ImageJ for each device, respectively.

3.3.5 *Viability Test*

After overnight incubation, live/dead labeling reagent (LIVE/DEAD® Viability/Cytotoxicity Kit for mammalian cells, Invitrogen, L3224) was added into each well to a final concentration of 0.01 mM Calcein AM (labelling reagent for live cells, green) and 2 nM Ethidiumhomodimer-1 (labelling reagent for dead cells, red). The plate was incubated for 20 min. For fibroblast imaging, the device was removed from the well plate and mounted on a 3D printed imaging support ("microscope jig" in Figure 3.4; original design file is included in the ESI.). Eosinophils settled on the well plate bottom were imaged directly in the well plate (Figure 3.4(iii)). All images were taken with a Zeiss Axiovert 200 equipped with an Axiocam 503 mono camera (Carl Zeiss AG, Oberkochen, Germany).

3.3.6 *Statistical Analysis*

Data are presented as the percentage of the initial angle (i.e., θf /θi). Data are plotted as the mean of three independent experiments ± the standard error of the mean (SEM); each plotted point on the graphs in Figures 3.2B and 3.3B represents an independent biological experiment and is the mean of three devices within each experiment (the data for each set of experiment is provided in Figure 3.5). Differences between two groups of data were evaluated using a two-tailed unpaired Student's t-test (Prism, GraphPad Software).

3.4 RESULTS

3.4.1 *Device Design and Workflow*

The underlying principle of our device is that it moves dynamically in response to cell-induced collagen gel contraction. As shown in Figure 3.1A, the device is composed of two parts: a base insert (which contains the loading channel and retraction tube) and a free-swinging arm. The free-swinging arm rests on a pivot point that juts out from the base insert, which allows the arm to rotate freely inside the well. When mechanical force is applied by cell-mediated collagen gel contraction, the device is dynamically reconfigured via rotation of the free-swinging arm, as shown in Figure 3.1B. The movement of the device can then be used as a quantitative metric for cell contractility by measuring the change in CGC device angle as described below. To begin the device workflow, cell-laden collagen gel precursor solution is pipetted into the loading channel of the device, where it flows through a closed tube to an opening that is positioned adjacent to the head of the free-swinging arm (Figure 3.1B i)). As the gel precursor solution is added, it forms a droplet at this opening, which grows until it meets the head of the free-swinging arm. Surface tension then pulls the head of the arm into the droplet. In the next step, media is pipetted into the retraction tube of the device (Figure 3.1B ii)). The media is pipetted in excess of the 30 μL inner volume of the tube such that the media wets the tail of the free-swinging arm. Upon immediate withdrawal of the media from the retraction tube (which does not remove all the media in the retraction tube), the wetted arm tail is pulled into the retraction tube by surface tension (Figure 3.1B iii)). The resulting surface tension force at the arm tail pulls the spherical droplet into a hyperboloid, or bridge, at the arm head. An approximate calculation of this surface tension force is provided in the supporting information (Figure 3.10), which is 1 mN. To ascertain the reliability of the retraction system, we varied the volume of medium loaded into the retraction tube (30-50 μL), and found that the wetted

arm tail was successfully pulled into the retraction tube with a loading volume greater than 35 μL; at 30 μL, which is equal to the inner volume of the tube, the arm tail was not fully retracted due to an incomplete wetting of the arm tail (Figure 3.6). After the collagen bridge is formed, the device is incubated at 37 °C to polymerize the collagen hydrogel, setting the three-dimensional geometry of the bridge. The well is then filled with media (Figure 3.1B iv)). The surface tension force exerted by the media in the retraction tube is nullified because the air-liquid interface that applied this force is submerged in media; this allows the device to move freely in response to the force that the cells exert when contracting the gel. Finally, the initial angle (θ_i) is measured (Figure 3.1B v)), and the final angle (θ_f) is measured after 24 hours of incubation (Figure 3.1B(vi)). To evaluate the consistency of the 3D printed device and reproducibility of θ_i, devices 3D printed on four different days were loaded with collagen-cell media mixture, and θ_i was measured. The data suggested that the average θ_i was 32°± 0.5°, indicating an overall consistency in device loading.

Quantification of gel contraction in our assay is done by comparing the initial angle, θ_i (as shown in Figure 3.1B v)), with the final angle, θ_f (as shown in Figure 3.1B vi)), after a period of incubation (typically 24 h) during which the cells contract the collagen gel. Importantly, our device design maximizes the dynamic range of our CGC assay measurement by forming the hyperboloid collagen bridge (through the use of the retraction tube as discussed in Figure 3.1B ii), iii)), which increases the initial angle (θ_i) that the device takes and increases the maximum potential change in angle that can occur due to cellular forces contracting the gel. Additionally, retraction of the collagen bridge is not affected by gel-substrate friction due to the dynamic nature of our device.

3.4.2 *Viability Test*

We evaluated the viabilities of fibroblasts and eosinophils in the coculture system after 24 h of incubation. Images from a live/dead stain are included in the ESI (Figure 3.4 iii)).

3.4.3 *FBS Augments Fibroblast Gel Contraction in Our Device*

We used a simple fetal bovine serum (FBS) stimulation experiment as a proof-of-concept to validate that the microscale platform is capable of quantifying collagen gel contraction due to a known treatment; the comparison between fibroblast-mediated gel contraction under serum-free and serum-containing conditions is frequently used in macroscale CGC assays as a validation experiment [29, 46]. Human fetal lung fibroblast (HFL-1)-laden collagen was loaded into the CGC device in both 10% FBS and serum-free media conditions. The initial angle of the CGC device (θi, as shown in Figure 3.1B v)), was measured immediately after cell culture media was added into each well. After 24 h of incubation, the angle was measured again (θf, as shown in Figure 3.1B vi)). The difference in the gel contraction can be clearly seen by eye (Figure 3.2A). In the absence and presence of FBS, the CGC device angle decreased to 69% and 41% of initial angle, respectively (Figure 3.2B). The gel contraction was reported as the average of three independent experiments performed on different days (the data for each independent experiment is provided in Figure 3.5A); the presence of FBS in the media resulted in significantly more collagen gel contraction than in serum-free conditions. Collagen without fibroblasts was loaded into the device as a negative control, and there was no significant change in the angle (Figure 3.9). We also performed a traditional CGC experiment with HFL-1 using a 96 well plate format. The result showed that the gel surface area decreased to 47% and 27% over 18 hours of incubation in either serum free media or media containing 10% FBS, respectively (Figure 3.8). Therefore, our small

scale CGC system offers a comparable dynamic range as the conventional well plate CGC assay, while the gel consumption is 7-fold smaller.

3.4.4 *Eosinophils Cocultured With Fibroblasts Augment Collagen Gel Contraction in Our Device*

Following a similar CGC device loading workflow, we established an eosinophil-fibroblast coculture using our platform to test the hypothesis that soluble factors secreted from eosinophils increase fibroblast-mediated collagen gel contraction as observed in prior work by Zagai et al. [45] using the traditional CGC assay. We used the eosinophil cell line model AML14.3D10, a differentiated human myeloid leukemic cell line that displays typical morphology and enzymatic activity of normal eosinophils [1, 2]. Eosinophils were maintained in RPMI media supplemented as described in the Materials and Methods section (as recommended for this cell line) and resuspended into serum-free F-12K media prior to loading to the well plate for coculture (Figure 3.3A). Eosinophils were loaded into the culture media surrounding the device after the fibroblast-laden collagen was established in the device (Figure 3.3A (iv)); this setup allows us to study soluble-factor mediated signaling while keeping the eosinophils and fibroblasts physically separate from each other. The CGC device angle was measured at the starting point of the culture and after 24 h incubation as described previously. In the absence and presence of eosinophils, the CGC device angle decreased to 90% and 60% of initial angle, respectively (Figure 3.3B). The gel contraction was reported as the average of three independent experiments performed on different days (the data for each independent experiment is provided in Figure 3.5B); the presence of eosinophils resulted in significantly more collagen gel contraction than in monoculture. Differences were observed between the absolute values of percentage of initial angle in the monoculture serum-free conditions across Figures 3.2 and 3.3, likely due to higher passage number

cells used in Figure 3.3; we discuss this further in the Discussion section. Collagen without fibroblasts was loaded into the device with the presence of eosinophils as a negative control for coculture, and there was no significant change in the angle (Figure 3.9).

3.5 DISCUSSION

In the fields of regenerative medicine, tissue engineering, and organotypic models, cell-encapsulating microfluidic hydrogels have been widely employed as an effective model to study cell behaviors in ECM environment [4, 9, 19, 20, 26, 30]. Specifically, the 3D culture of fibroblasts in native type I collagen gels has enabled researchers to integrate cell behaviors with surrounding matrix components, capturing some key aspects of cell-extracellular matrix interactions that are lost in simple 2D culture on plastic substrates [4, 9].

Here, we designed a dynamic microscale CGC system, and identified three ways in which we could build on and improve traditional CGC assays: 1) reduced cell and gel consumption, 2) straightforward measurements of collagen gel contraction that are not dependent on scale calibration or ambiguous gel boundaries, and 3) the ability to perform coculture experiments to study how paracrine signaling (soluble-factor mediated signaling) between fibroblasts and other cell types affects fibroblast contractility. In this study, we developed a dynamic microscale CGC platform that integrates these criteria through use of a small gel volume (14 µL in comparison to over 100 µL typically used in traditional CGC assays [17, 40], a simplified quantitative readout (CGC device angle), and compatibility with coculture.

Importantly, existing cell-based assays developed around the traditional CGC assay can be readily translated to our microscale CGC assay because both assays share similar protocols for cell-laden

collagen preparation. Prior systems for microscale gel droplet fabrication have achieved impressive advances in terms of miniaturization, which often involve engineering with new biomaterials or reagents such as polyethylene glycol or dextran that allow for rapid polymerization of droplets and careful management of evaporation [28, 33]. Since the gel polymerization conditions are pH-sensitive and thermally driven, the addition of new materials in the process requires intensive testing of precise gelling conditions [12]. Moreover, washing steps are required to remove the additional materials from the droplet, increasing the time and labor involved in the fabrication process [28, 33]. Our CGC device serves as an alternative surface-tension driven method to manufacture microscale gel droplets (and ultimately stretch the droplets into hyperboloid bridges), eliminating the possible complications involved in adding new materials.

Gel area quantification has been a hurdle to the accuracy and reproducibility of the CGC assay largely due to the difficulties in characterization of gel boundaries, as well as aberrancies in gel shape post-contraction [5, 6]. Although atomic force microscopy (AFM) and traction force microscopy (TFM) serve as alternative quantification methods for cell contraction force measurement bypassing the gel border delineation issue, the instruments are normally unfamiliar to common users in traditional biological laboratory settings [38]. The CGC device we present in the study measures the change in CGC device angle, which converts the 3D change in gel volume to single parameter that is straightforward to measure. Three reference points are clearly and easily identified in digital images of the device, and the angle is calculated automatically using image processing software (see Methods section and Figures 3.1B and 3.2A).

Previous studies have identified a group of soluble factors including transforming growth factor-β (TGF-β), that contribute to fibroblast myodifferentiation, leading to increased expression of α-

smooth muscle actin and a contractile phenotype typified by increased collagen gel contraction [15, 18, 25]. Myodifferentiation and fibrosis are particularly important in airway remodeling and asthma as they can lead to exacerbated symptoms and progressive damage [15, 18]. To better understand how fibroblasts are affected by soluble factors from other types of cells in airway remodeling, researchers have conducted mixed coculture (embedding additional cell types into the fibroblasts-laden collagen), conditioned media coculture (feeding fibroblast-laden gel matrix with supernatants collected from other types of cells), and segregated Transwell coculture CGC experiments [13, 31, 44]. These studies revealed that mast cells, red blood cells, and eosinophils can promote fibroblast contraction in mixed 3D coculture, or in conditioned media culture through paracrine signaling; whereas blood monocytes and lung epithelial cells attenuate fibroblast-mediated gel contractility, an important aspect of tissue repair [10, 39].

Given the importance of paracrine signaling in myodifferentiation illuminated by prior work, we developed an eosinophil-fibroblast paracrine signaling coculture model to demonstrate the ability to conduct coculture experiments with our microscale CGC assay (Figure 3.3A). Our coculture system enabled eosinophils, which settled to the bottom of the well plate physically separate from the fibroblast-laden gel suspended in our device above, to communicate with fibroblasts through shared media. In contrast to culture systems that involve transfer of conditioned media from one cell type to another, the shared media in our coculture model enables bidirectional signaling and signaling based on short-lived factors that may degrade in conditioned media studies [36] (Ruth et al., 1999). Here, we cocultured HFL-1 with AML14.3D10, which is a well-characterized mature eosinophil surrogate (Figure 3.3A) [2]. Previous studies have identified eosinophil cationic protein as an important biomarker for airway inflammation, which is largely released from mature eosinophils [27, 44, 45]. Using our microscale CGC device, we found that the presence of

eosinophils caused significantly increased fibroblast contractility (Figure 3.3B), which agreed with the previous mixed coculture experiments where eosinophils were mixed in with fibroblasts in collagen gel [45].

It is worth noting that we observed a decrease in HFL-1 contractility (in the monoculture, serum-free condition) in the second set of experiments (Figure 3.3B, $\theta_f/\theta_i = 90 \pm 2\%$) compared to the first set of experiments (Figure 3.2B, $\theta_f/\theta_i = 69 \pm 5\%$), as the cells were at higher passage numbers in the second set of experiments. Thus, it is important to set up separate controls within each set of experiments (as we did in Figures 3.2 and 3.3); the comparison between the treatment and the control within experiments should be considered rather than the absolute value of the percentage of initial angle, which can vary across passage numbers.

In conclusion, this paper presents a novel platform that translates a traditional CGC assay to a microscale assay, minimizing fibroblast and gel consumption. Utilizing surface tension, the device enables generation of a suspended cell-laden gel with two standard pipetting steps. Gel contraction quantification is simplified to a single angle measurement. Moreover, we established an eosinophil-fibroblast coculture model using the CGC device and showed that the platform sustained segregated coculture and paracrine signaling to recapitulate aspects of immune-fibroblast-ECM interactions. Importantly, our platform captures bidirectional and time-sensitive paracrine signaling interactions which are sometimes lost in stepwise conditioned media studies due to decay of short-lived cytokines and other signaling molecules. Finally, our device fits within a standard well plate and cell culture incubator, increasing its translation to biology laboratories.

3.6 FIGURES

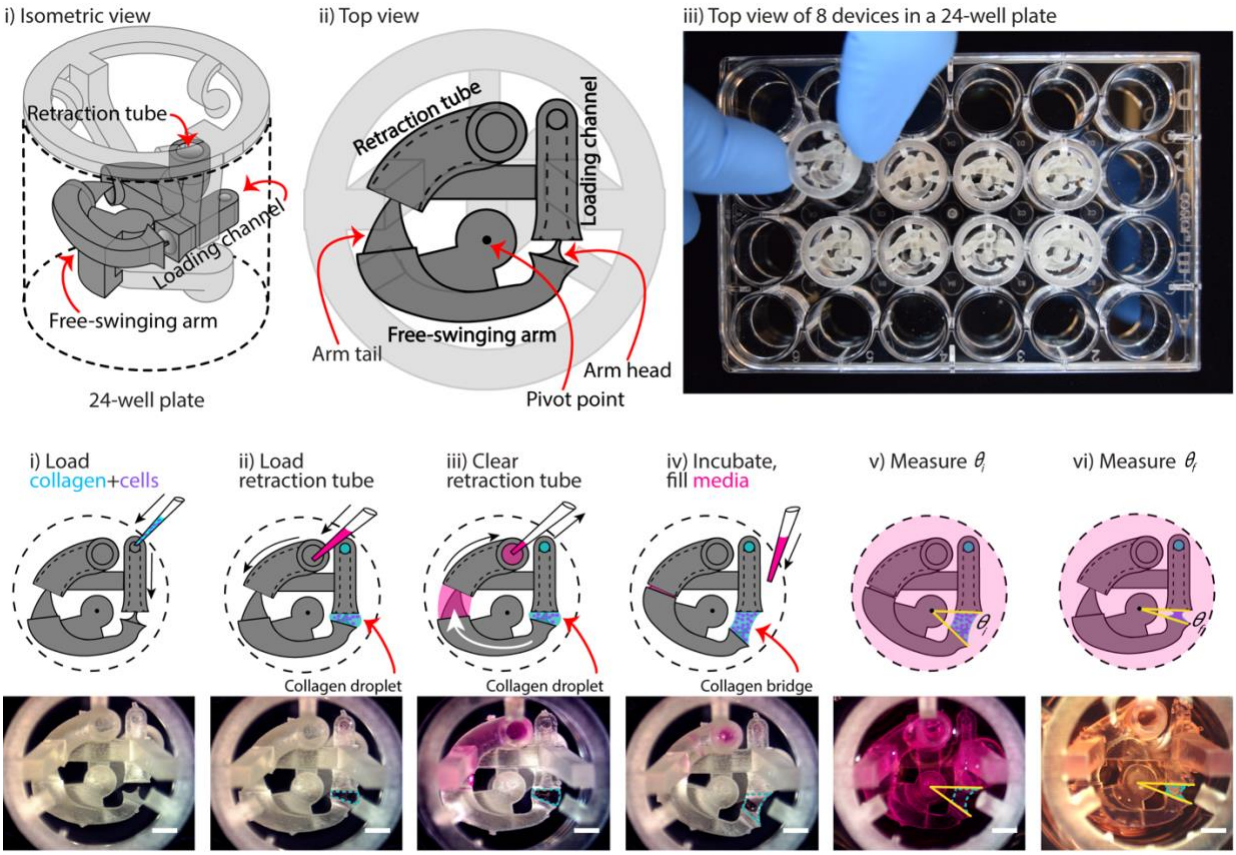

Figure 3.1. Overview of device configuration and operation.

Overview of device configuration and operation. (A) Overview of collagen gel contraction (CGC) device. (i,ii) Schematic drawing of an assembled CGC device, which consists of a collagen loading channel, a free-swing arm, and a retraction tube. (iii) Top down picture showing inserting an assembled CGC device in a 24-well plate. (B) Top view of CGC device operation workflow. i) 14 μL of cell-laden collagen is loaded into the loading channel; after filling the loading channel, a collagen droplet is formed in between the loading channel and arm head. ii) and iii) 25 μL of cell culture media is pipetted in and out of retraction tube; the arm tail is pulled back into the retraction tube with the flow of the media, causing the collagen droplet to extend into a collagen bridge. iv) The system is incubated at 37 °C for 15 min for collagen to gel; cell culture media is loaded directly into the well plate from top. v) and vi) The top view of the device is captured to determine the angle at starting point (θi) and end point (θf), respectively. The change in θ reflects cell contractility. Scale bars: 2 mm.

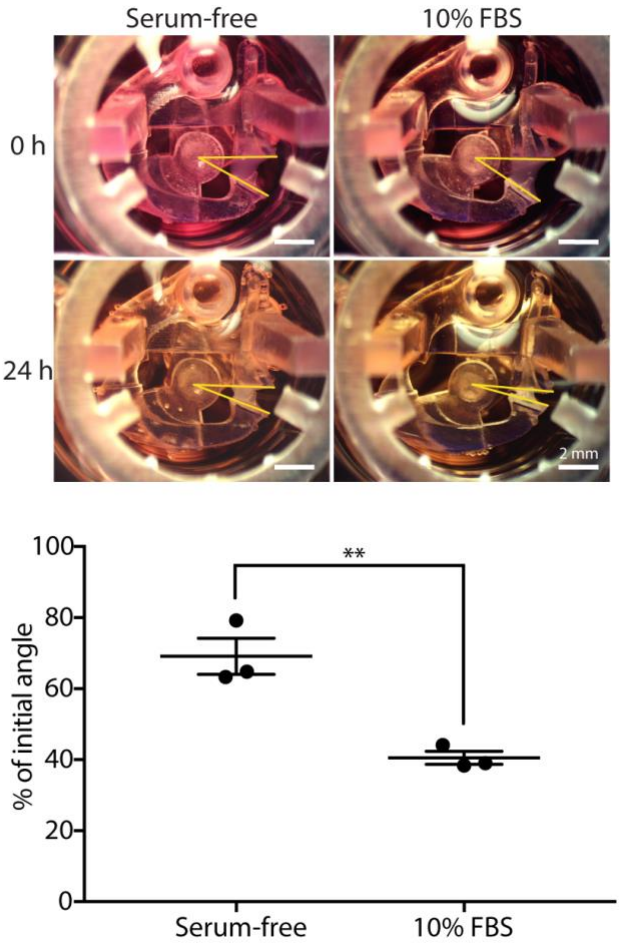

Figure 3.2. CGC device characterization using fibroblast contraction in differential serum conditions.

(A) Representative images showing the contracting angle, θ, of the same device immediately after loading the cell-laden gel and cell culture media (0 h, top) and after 24 h in culture (bottom), in both serum-free media (left) and media containing 10% FBS (right) (scale bars: 2 mm). (b) fibroblasts (HFL-1) cultured in media containing 10% FBS contract collagen gel more than fibroblasts cultured in serum-free media. Each data point represents the average of three devices from an independent experiment; three independent experiments were performed. Error bars: SEM of three independent experiments; * indicates significantly different values according to a two-tailed paired Student's t-test ($p \leq 0.05$).

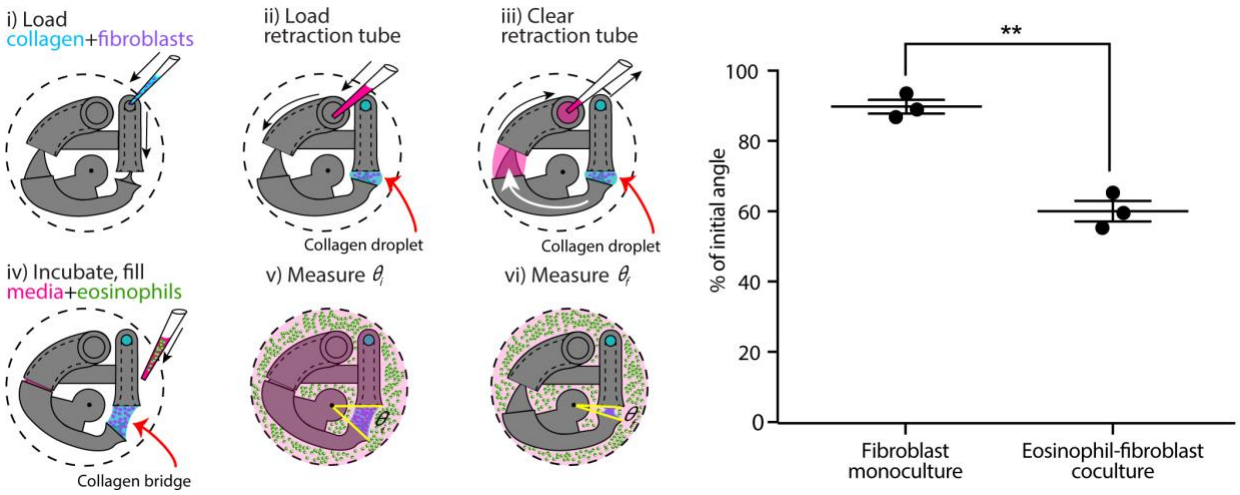

Figure 3.3. CGC device application in a coculture system with human fibroblast cells (HFL-1) and eosinophil model cell line (AML14.3D10) to evaluate the effect of soluble factor signaling from eosinophils on fibroblast gel contraction.

(A) Schematics of the coculture configuration and workflow. i) Fibroblast-laden collagen is loaded into the CGC device in a 24-well plate. ii) and iii) Cell culture media is pipetted in and out of retraction tube and the arm tail is pulled back into the retraction tube. iv) The system is incubated for the collagen to gel; eosinophils are suspended in serum-free F-12K media at a concentration of 3.5 ×107 cells/mL; 2 mL of serum-free media (for monoculture) or cell suspension (for coculture) is added into each well. v) and vi) Top view image is taken to measure θi and θf, respectively. (B) Coculture of fibroblasts with eosinophils augments HFL-1 collagen gel contraction in serum-free media. Each data point represents the average of three devices from an independent experiment; three independent experiments were performed. Error bars: SEM of three independent experiments; ** indicates significantly different values according to a two-tailed paired Student's t-test ($p \leq 0.01$).

3.7 SUPPLEMENTARY INFORMATION

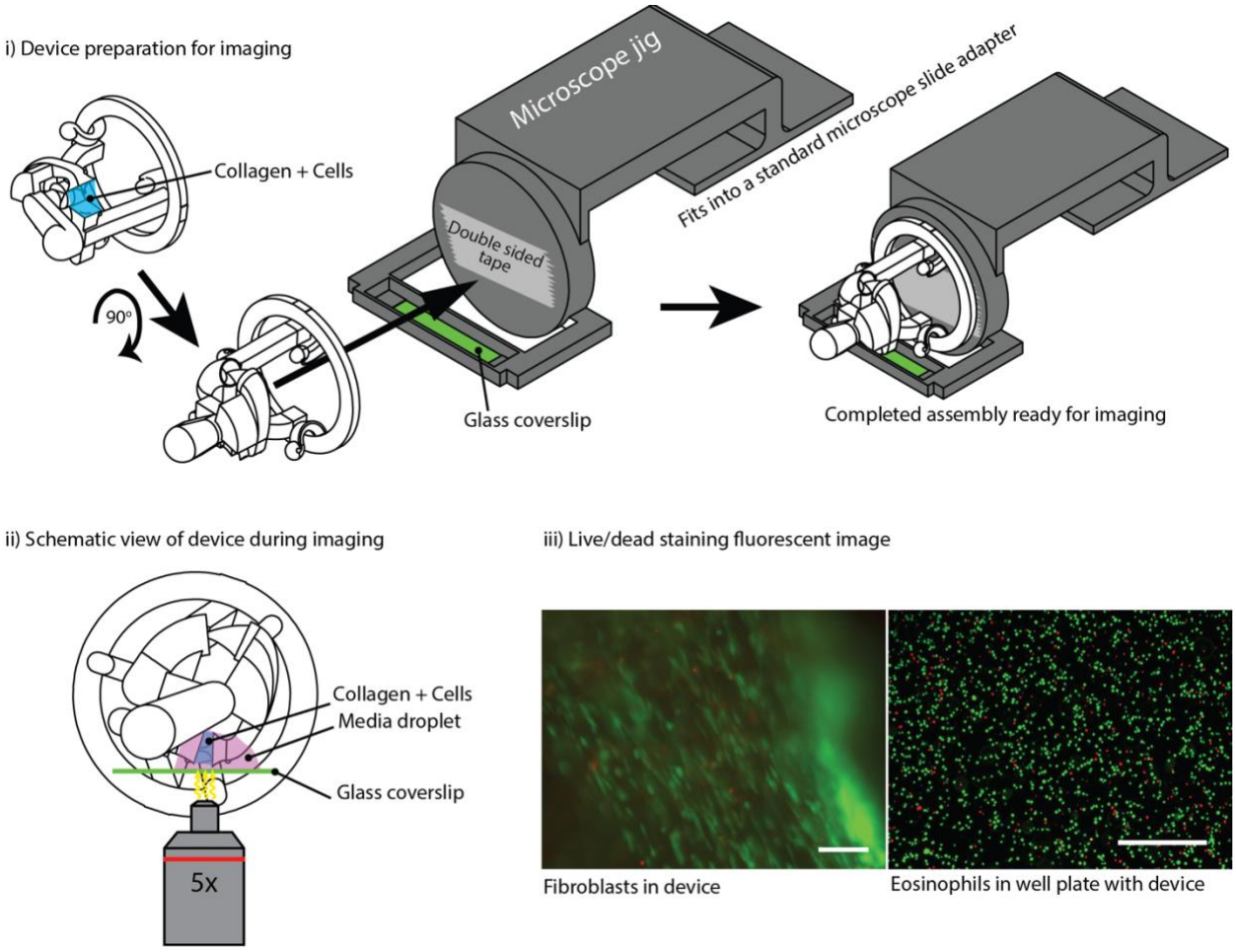

Figure 3.4. Imaging in CGC device.

i) Imaging in device requires a microscope jig, which positions the collagen bridge directly above a glass slide. ii) Schematic view of imaging in device. Microscope jig is omitted for simplicity. iii) Fluorescence images of fibroblasts in collagen and eosinophils in the well plate (green: live, red: dead, scale bars: 100 μm).

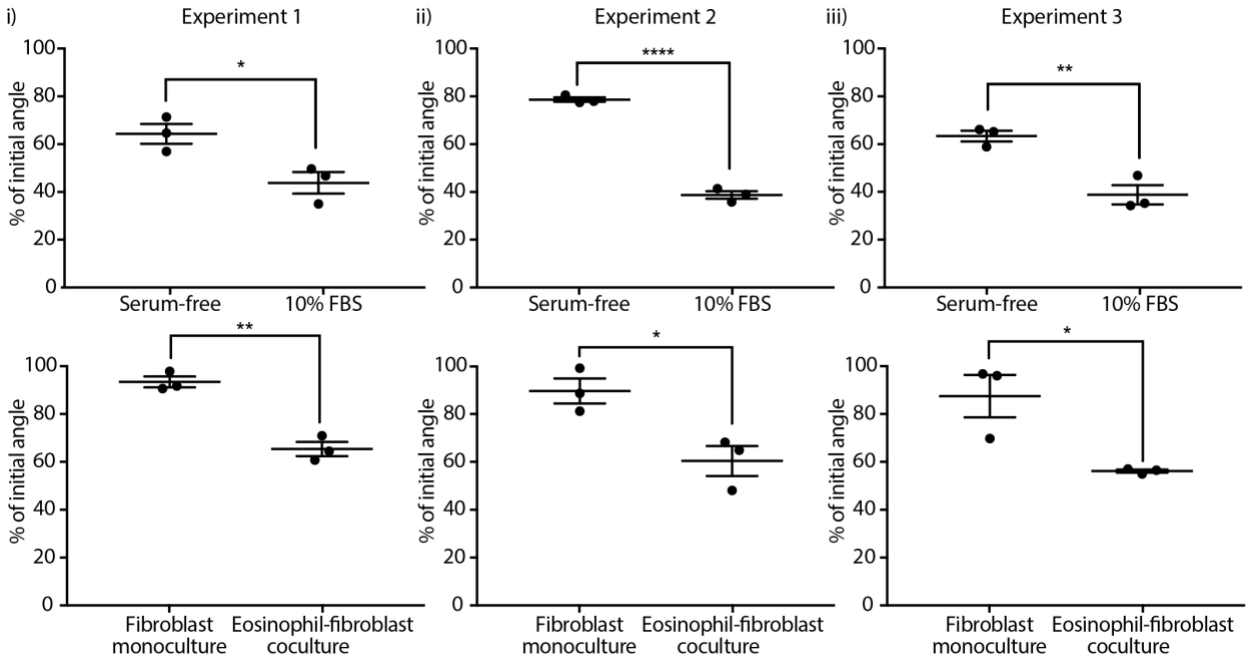

Figure 3.5. Complete set of data collected across three independent experiments; each data point plotted is from a replicate device within an independent experiment.

These are the complete data sets data corresponding to (A) Figure 3.2B and (B) Figure 3.3B. Error bars: SEM of three device replicates; p-value indicates significantly different values according to a two-tailed unpaired Student's t-test (*$p \leq 0.05$, **$p \leq 0.01$, ****$p \leq 0.0001$).

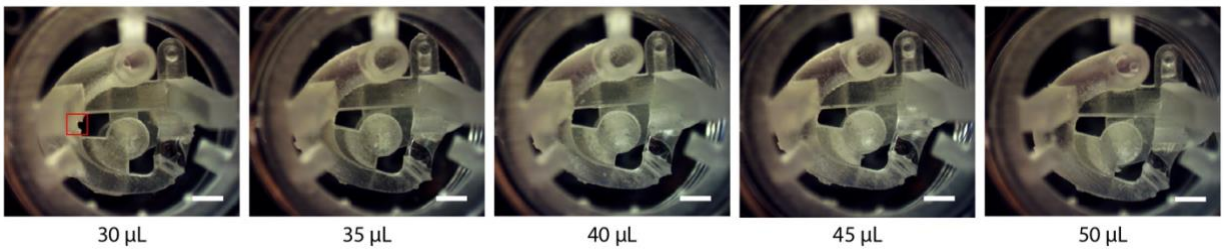

Figure 3.6. Determination of the volume of media required when loading the retraction tube such that the free-swinging arm is pulled back and the collagen droplet extends into a collagen bridge (step ii) and iii) of Figure 3.1).

Each image is the representative of four devices for each loading volume. The loading was successful with a volume of 35, 40, 45, and 50 µL of media. With a loading volume of 30 µL, there was not enough media to bring the tail of the swing arm completely back into the retraction tube, resulting in a small gap (red box). Scale bars: 2 mm.

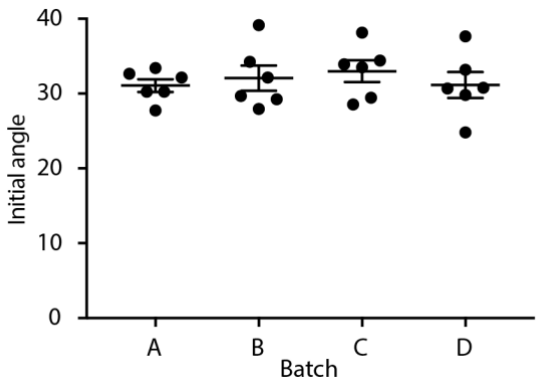

Figure 3.7. The initial angle of six devices (each plotted as a separate data point) containing collagen with no cells from four different batches (3D printed on different days). Error bars represent SEM.

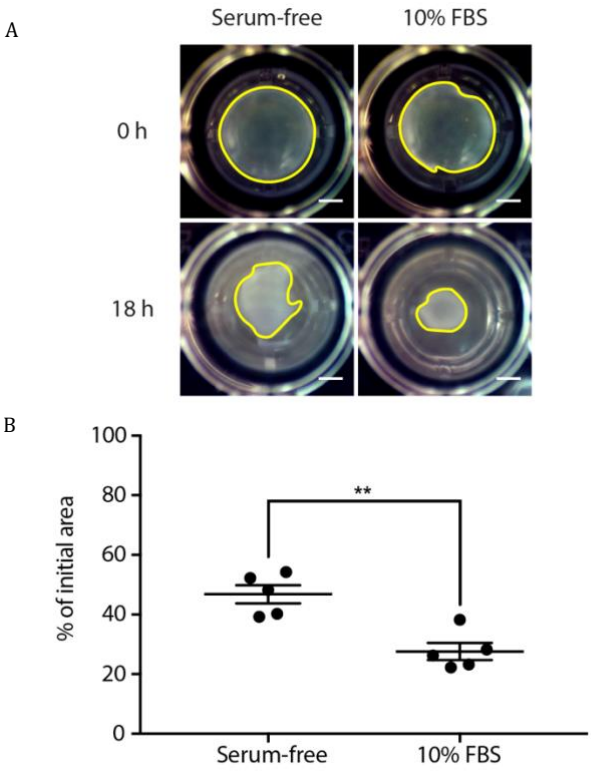

Figure 3.8. HFL-1 induced collagen gel contraction in a 96 well plate, using the standard macroscale collagen gel contraction assay.

(A) The gel contours are traced in yellow, showing gel disc distortion. (B) Each data point represents the percentage of initial gel area of each replicate from an independent experiment.

Error bars: SEM of 5 replicates; p-value indicates significantly different values according to a two-tailed unpaired Student's t-test (**p ≤ 0.01). Scale bars: 1 mm.

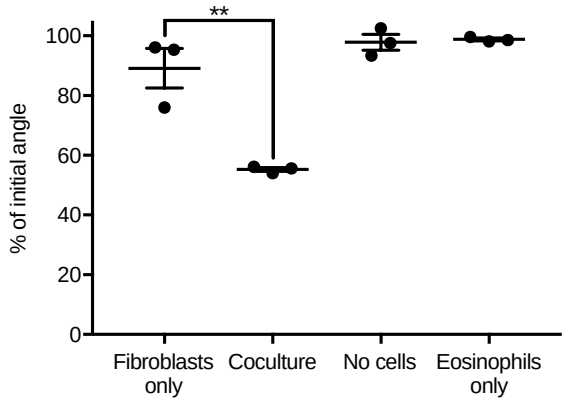

Figure 3.9. HFL-1 mediated collagen contraction in serum-free media under four different culture conditions.

"No cells" and "Eosinophils only" conditions are used as negative controls. Each data point represents a single device from the same experiment. Error bars: SEM; ** indicates significantly different values according to a two-tailed unpaired Student's t-test (p ≤ 0.01); only the "Fibroblasts only" and "Coculture" conditions were compared.

Approximate determination of surface tension forces in CGC device.

The force provided by the surface tension of media in the retraction tube is equal and opposite to the force applied by the surface tension of the collagen bridge. This force can be calculated using the following equation:

$$F = PA = \gamma(\frac{1}{r_1} + \frac{1}{r_2})A$$

Where P is the Laplace pressure associated with the air-liquid interface, A is the surface area of that interface, $\gamma$is the surface tension of the liquid, and r_1 and r_2 are the characteristic radii of

curvature that describe the interface. If we assume that the collagen bridge is approximately cylindrical, and that its surface tension is equal to the surface tension of pure water, then we can calculate the surface tension force applied by the collagen bridge:

$$\gamma = 72 \times 10^{-3} \ \frac{m\mathrm{N}}{\mathrm{m}}$$

$$r_1 = 1.014 \times 10^{-3} \ \mathrm{m}$$

$$r_2 \cong \infty$$

$$A \cong \left(2 \times 10^{-3} \left(\frac{3.172 + 1.477}{2}\right)(\pi \times 1.014 \times 10^{-3})\right)$$

Note that the surface area of the collagen bridge is approximated as the area of two trapezoids with width of parallel edges given by measurements 2 and 3 from Figure S7, and height given by half the circumference of the cylindrical bridge.

$$F = PA = 72 \times 10^{-3} \left(\frac{1}{1.014 \times 10^{-3}} + \frac{1}{\infty}\right)\left(2 \times 10^{-3} \left(\frac{3.172 + 1.477}{2}\right)(\pi \times 1.014 \times 10^{-3})\right)$$

Using these assumptions, and by measuring the diameter of the collagen bridge in FIJI image processing software, we find that the collagen bridge applies a force of approximately 1 mN, and thus the media in the retraction tube also applies 1 mN in opposition. However, the surface tension force applied by the media in the retraction tube is nullified when the device is submerged in media at the beginning of an experiment, thus enabling the device to move dynamically based on forces exerted by the cells on the collagen.

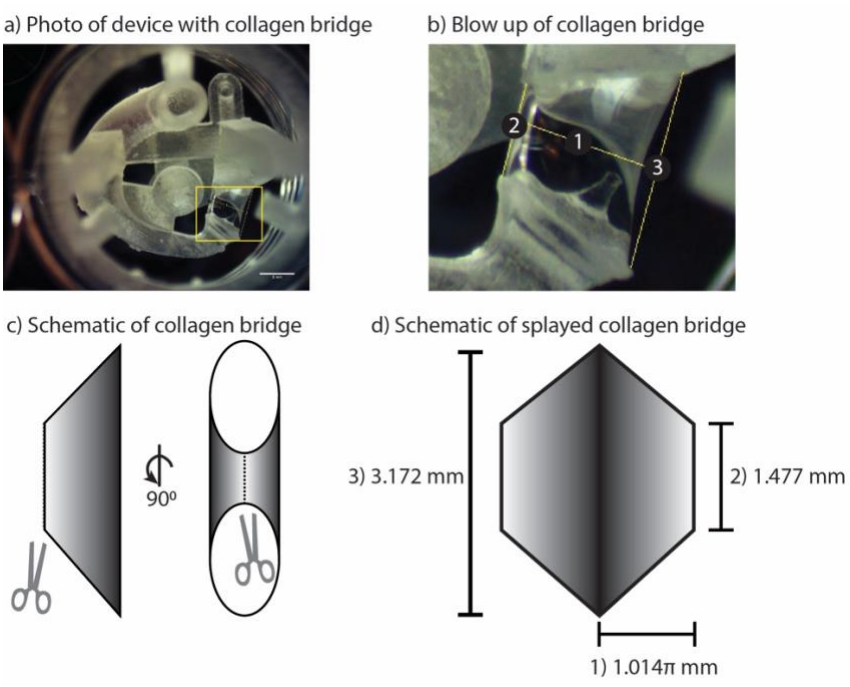

Figure 3.10. Photo used to make retraction force approximation and corresponding schematic representation of surface area approximation.

a) Photo of device used for approximation with b) inset of collagen bridge. Yellow lines indicate where measurements were taken. c) Schematic of 3D shape used to approximate collagen bridge (cylinder with angled end caps). d) Schematic of approximate 2D (splayed out) surface geometry of collagen bridge. Measurements from b) were used to calculate the area of this shape. Scale bar: 2 mm.

3.8 REFERENCES

[1] Ackerman S. J., Du J., Xin F., Dekoter R., McKercher S., Mak I. R., et al. (2000). Eosinophilopoiesis: to be or not to be (an eosinophil)? That is the question: transcriptional mechanisms regulating eosinophil genes and development. *Respir. Med*. **94**, 1135–1138.

[2] Baumann M. A., Paul C. C. (1998). The AML14 and AML14.3D10 cell lines: a long-overdue model for the study of eosinophils and more. *Stem Cells.* **16**, 16–24.

[3] Bell E., Ivarsson B., Merrill C. (1979). Production of a tissue-like structure by contraction of collagen lattices by human fibroblasts of different proliferative potential in vitro. *Proc. Natl. Acad. Sci. U.S.A.* **76**, 1274–1278.

[4] Bhatia S. N., Ingber D. E. (2014). Microfluidic organs-on-chips. *Nat. Biotechnol*. **32**, 760–772.

[5] Chapuis J. F., Agache P. (1992). A new technique to study the mechanical properties of collagen lattices. *J. Biomech.* **2**5, 115–120.

[6] Chen H. C., Yang T. H., Thoreson A. R., Zhao C., Amadio P. C., Sun Y. N., et al. . (2013). Automatic and quantitative measurement of collagen gel contraction using model-guided segmentation. *Meas. Sci. Technol*. **24**:85702.

[7] Chen M. Y., Sun Y. L., Zhao C., Zobitz M. E., An K. N., Moran S. L., et al. . (2008). Substrate adhesion affects contraction and mechanical properties of fibroblast populated collagen lattices. *J. Biomed. Mater. Res. B Appl. Biomater*. **84**, 218–223.

[8] Dallon J. C., Ehrlich H. P. (2008). A review of fibroblast-populated collagen lattices. *Wound Repair Regen*. **16**, 472–479.

[9] Duval K., Grover H., Han L. H., Mou Y., Pegoraro A. F., Fredberg J., et al. . (2017). Modeling physiological events in 2D vs. 3D cell culture. *Physiology (Bethesda)*. **32**, 266–277.

[10] Epa A. P., Thatcher T. H., Pollock S. J., Wahl L. A., Lyda E., Kottmann R. M., et al. . (2015). Normal human lung epithelial cells inhibit transforming growth factor-β induced myofibroblast differentiation via prostaglandin E2. *PLoS ONE* **10**:e0135266.

[11] Esnault S., Jarzembowski J. A., Malter J. S. (1998). Stabilization of granulocyte-macrophage colony-stimulating factor RNA in a human eosinophil-like cell line requires the AUUUA motifs. *Proc. Assoc. Am. Physicians.* **110**, 575–584.

[12] Forgacs G., Newman S. A., Hinner B., Maier C. W., Sackmann E. (2003). Assembly of collagen matrices as a phase transition revealed by structural and rheologic studies. *Biophys. J*. **84,** 1272–1280.

[13] Fredriksson K., Lundahl J., Palmberg L., Romberger D. J., Liu X. D., Rennard S. I., et al. . (2003). Red blood cells stimulate human lung fibroblasts to secrete interleukin-8. *Inflammation.* **27**, 71–78.

[14] Grinnell F. (1994). Fibroblasts, myofibroblasts, and wound contraction. J. *Cell Biol*. **124**, 401–404.

[15] Grinnell F. (2000). Fibroblast-collagen-matrix contraction: growth-factor signalling and mechanical loading. *Trends Cell Biol*. **10**, 362–365.

[16] Grinnell F. (2003). Fibroblast biology in three-dimensional collagen matrices. *Trends Cell Biol*. **13**, 264–269.

[17] Gullberg D., Tingstrom A., Thuresson A. C., Olsson L., Terracio L., Borg T. K., et al. . (1990). Beta 1 integrin-mediated collagen gel contraction is stimulated by PDGF. *Exp. Cell Res*. **186**, 264–272.

[18] Hinz B., Phan S. H., Thannickal V. J., Galli A., Bochaton-Piallat M. L., Gabbiani G. (2007). The myofibroblast: one function, multiple origins. *Am. J. Pathol*. **170**, 1807–1816.

[19] Huang G., Wang S., He X., Zhang X., Lu T. J., Xu F. (2013). Helical spring template fabrication of cell-laden microfluidic hydrogels for tissue engineering. *Biotechnol. Bioeng*. **110**, 980–989.

[20] Huang G., Zhang X., Xiao Z., Zhang Q., Zhou J., Xu F., et al. (2012). Cell-encapsulating microfluidic hydrogels with enhanced mechanical stability. *Soft Matter*. **8**, 10687–10694.

[21] Ilagan R., Guthrie K., Quinlan S., Rapoport H. S., Jones S., Church A., et al. . (2010). Linear measurement of cell contraction in a capillary collagen gel system. *BioTechniques*. 48, 153–155.

[22] Jeffery P. (2001). Remodeling in asthma and chronic obstructive lung disease. *Am. J. Respir. Crit. Care Med.* **164**, S2–S38.

[23] Jin T., Li L., Siow R. C. M., Liu K. (2015). A novel collagen gel-based measurement technique for quantitation of cell contraction force. *J. R. Soc. Interface*. **12**. 10.1098

[24] Jonas O., Duschl C. (2010). Force propagation and force generation in cells. *Cytoskeleton (Hoboken)*. **67**, 555–563.

[25] Kendall R. T., Feghali-Bostwick C. (2014). Fibroblasts in fibrosis: novel roles and mediators. *Front. Pharmacol*. **5**:123.

[26] Khetan S., Burdick J. A. (2011). Patterning hydrogels in three dimensions towards controlling cellular interactions. *Soft Matter*. **7**, 830–838.

[27] Koh G. C., Shek L. P., Goh D. Y., Van Bever H., Koh D. S. (2007). Eosinophil cationic protein: is it useful in asthma? A systematic review. *Respir. Med*. **101**, 696–705

[28] Leung B. M., Moraes C., Cavnar S. P., Luker K. E., Luker G. D., Takayama S. (2015). Microscale 3D collagen cell culture assays in conventional flat-bottom 384-well plates. *J. Lab. Autom*. **20**, 138–145.

[29] Lijnen P., Petrov V., Fagard R. (2001). In vitro assay of collagen gel contraction by cardiac fibroblasts in serum-free conditions. *Methods Find. Exp. Clin. Pharmacol*. **23**, 377–382.

[30] Ling Y., Rubin J., Deng Y., Huang C., Demirci U., Karp J. M., et al. . (2007). A cell-laden microfluidic hydrogel. *Lab Chip*. **7**, 756–762.

[31] Margulis A., Nocka K. H., Wood N. L., Wolf S. F., Goldman S. J., Kasaian M. T. (2009). MMP dependence of fibroblast contraction and collagen production induced by human mast cell activation in a three-dimensional collagen lattice. *Am. J. Physiol. Lung Cell. Mol. Physiol*. 296:236.

[32] Mikami Y., Matsuzaki H., Takeshima H., Makita K., Yamauchi Y., Nagase T. (2016). Development of an in vitro assay to evaluate contractile function of mesenchymal cells that underwent epithelial-mesenchymal transition. *J. Vis. Exp*. 2016:53974.

[33] Moraes C., Simon A. B., Putnam A. J., Takayama S. (2013). Aqueous two-phase printing of cell-containing contractile collagen microgels. *Biomaterials*. **34**, 9623–9631.

[34] Redden R. A., Doolin E. J. (2003). Collagen crosslinking and cell density have distinct effects on fibroblast-mediated contraction of collagen gels. *Skin Res. Technol*. **9**, 290–293.

[35] Royce S. G., Cheng V., Samuel C. S., Tang M. L. K. (2012). The regulation of fibrosis in airway remodeling in asthma. *Mol. Cell. Endocrinol*. **351**, 167–175.

[36] Ruth J. H., Esnault S., Jarzembowski J. A., Malter J. S. (1999). Calcium ionophore upregulation of AUUUA-specific binding protein activity is contemporaneous with granulocyte macrophage colony-stimulating factor messenger RNA stabilization in AML14.3D10 cells. *Am. J. Respir. Cell Mol. Biol.* **21**, 621–628.

[37] Sackmann E. K., Fulton A. L., Beebe D. J. (2014). The present and future role of microfluidics in biomedical research. *Nature*. **507**, 181–189.

[38] Schierbaum N., Rheinlaender J., Schäffer T. E. (2019). Combined atomic force microscopy (AFM) and traction force microscopy (TFM) reveals a correlation between viscoelastic material properties and contractile prestress of living cells. *Soft Matter*. **15**, 1721–1729.

[39] Sköld C. M., Liu X. D., Umino T., Zhu Y. K., Ertl R. F., Romberger D. J., et al. . (2000). Blood monocytes attenuate lung fibroblast contraction of three-dimensional collagen gels in coculture. *Am. J. Physiol. Lung Cell. Mol. Physiol*. 279:667.

[40] Timpson P., McGhee E. J., Erami Z., Nobis M., Quinn J. A., Edward M., et al. (2011). Organotypic collagen I assay: a malleable platform to assess cell behaviour in a 3-dimensional context. *J. Vis. Exp.* 2011:e3089.

[41] Vernon R. B., Gooden M. D. (2002). An improved method for the collagen gel contraction assay. *In Vitro Cell. Dev. Biol. Anim*. **38**, 97–101.

[42] Whitesides G. M. (2006). The origins and the future of microfluidics. *Nature*. **442**, 368–373.

[43] Wygrecka M. F. A. U. D. B., Kosanovic D. F., Petersen F. F., Taborski B, FAU, von Gerlach, von Gerlach S. F., et al. . (2013). Mast cells and fibroblasts work in concert to aggravate pulmonary

fibrosis: role of transmembrane SCF and the PAR-2/PKC-alpha/Raf-1/p44/42 signaling pathway. *Am. J. Pathol*. **182**, 2094–2108.

[44] Zagai U., Dadfar E., Lundahl J., Venge P., Sköld C. M. (2007). Eosinophil cationic protein stimulates TGF-beta1 release by human lung fibroblasts in vitro. *Inflammation.* **30**, 153–160.

[45] Zagai U., Sköld C. M., Trulson A., Venge P., Lundahl J. (2004). The effect of eosinophils on collagen gel contraction and implications for tissue remodelling. *Clin. Exp. Immunol*. **135**, 427–433.

[46] Zhu Y. K., Liu X. D., Sköld M. C., Umino T., Wang H., Romberger D. J., et al. (2001). Cytokine inhibition of fibroblast-induced gel contraction is mediated by PGE2 and NO acting through separate parallel pathways. *Am. J. Respir. Cell. Mol. Biol*. **25**, 245–253.

Chapter 4. PARACRINE SIGNALING FROM HUMAN KIDNEY EPITHELIAL CELLS PROMOTES KIDNEY SPECIFICITY OF ENDOTHELIAL CELLS

This chapter is mostly adapted from the original publication: Zhang, T.; Lih, D.; Nagao, R. J.; Xue, J.; Bertheir, E.; Himmelfarb, J.; Zheng, Y.; Theberge, A. B., "Open microfluidic coculture reveals paracrine signaling from human kidney epithelial cells promotes kidney specificity of endothelial cells". American Journal of Physiology-Renal Physiology.

4.1 ABSTRACT

Endothelial cells (ECs) from different human organs possess organ-specific characteristics that support specific tissue regeneration and organ development. EC specificity are identified by both intrinsic and extrinsic cues, among which, parenchyma and organ-specific microenvironment are critical contributors. These extrinsic cues are, however, largely lost during ex vivo cultures. Outstanding challenges remain to understand and re-establish EC organ-specificity for in vitro studies to recapitulate human organ-specific physiology. Here, we designed an open microfluidic platform to study the role of human kidney tubular epithelial cells in supporting EC specificity. The platform consists of two independent cell culture regions segregated with a half wall; culture media is added to connect the two culture regions at a desired timepoint, and signaling molecules can travel across the half wall (paracrine signaling). Specifically, we report that in the microscale coculture device, primary human kidney proximal tubular epithelial cells (HPTECs) rescued primary human kidney peritubular microvascular EC (HKMEC) monolayer integrity and fenestra formation, and HPTECs upregulated key HKMEC kidney-specific genes (HNF1B, AJAP1, KCNJ16) and endothelial activation genes (VCAM1, MMP7, MMP10) in coculture. Co-culturing

with HPTECs also promoted kidney-specific genotype expression in human umbilical vein ECs (HUVECs), and human pluripotent stem cell-derived ECs (hPSC-ECs). In comparison to the culture in HPTEC conditioned media, co-culture of ECs with HPTECs showed increased upregulation of kidney specific genes, suggesting potential bidirectional paracrine signaling. Importantly, our device is compatible with standard pipettes, incubators, and imaging readouts, and could also be easily adapted to study cell signaling between other rare or sensitive cells.

4.2 INTRODUCTION

During human development, ECs acquire tissue-specific properties based on cues from the local microenvironment while organs undergo vascularization; *in vitro* cell culture systems often lack microenvironmental cues, making it challenging to maintain endothelial cell identity [20]. Therefore, a better understanding of how to preserve endothelial cell morphologic phenotypes and gene expression profiles in *ex vivo* environments is important to building more physiologically relevant endothelial cell-based disease models for pathological research. Specifically, the human kidney is a highly vascularized organ, and the peritubular capillaries play an important role in maintaining normal renal function of selective reabsorption and secretion, in addition to providing oxygen and nutrients to the tubules and surrounding cells [1, 27, 33]. The loss of renal microvasculature integrity has been recognized as a classic finding contributing to progressive renal diseases, including tissue ischemia, tubular dysfunction, inflammation, and fibrosis [27, 32, 36]. Reabsorption occurs through both passive and active transport, from the proximal tubular epithelial cells lining the tubule, across the extracellular matrix (ECM) separating the tubules, through the ECs and into the adjacent peritubular capillaries [9].

The interplay between human kidney proximal tubule epithelial cells (HPTECs) and human kidney peritubular microvascular ECs (HKMECs) is a complex process largely regulated by soluble factors in the tubulo-interstitium [27, 34, 38]. The understanding of human kidney microvasculature injury and regeneration mechanisms has been of great interest in the past several decades, and a group of growth factors have been identified that mediate the intercellular interaction [52, 53, 55]. Importantly, vascular endothelial growth factor (VEGF) is an angiogenic and vascular permeability factor, which is critical to the survival and proliferation for ECs [23, 28]. However, due to the challenge of isolating primary HKMECs from fresh tissues and the unavailability of an established HKMEC cell line, much of our understanding has come from cell culture models using non-renal human cell lines, such as human umbilical vein ECs (HUVECs), or animal cells. For example, Kim et al [28] showed that human kidney epithelial cells generate VEGF which promoted branching angiogenesis of HUVECs *in vitro*; Zhao et al. [62] discovered that mouse renal proximal tubular epithelial cells helped mouse renal peritubular ECs maintain phenotypes in coculture. More recently, our group [33] successfully isolated and purified HKMECs and discovered that the significant difference between HKMECs and HUVECs in morphology, phenotype and transcriptional profiling. Further, we [37] reported that ECs from different human organs exhibit organ-specific gene expression profiles, which correlate with specific cell functions, including metabolic rate, angiogenic potential, and barrier properties. However, compared to freshly isolated cells, most of organotypic gene expression is lost during *in vitro* expansion, which highlighted the importance of both employing specific endothelial cell types and identifying ways to enhance organotypic properties during *in vitro* culture.

We sought to test whether soluble factors from HPTECs could be used to maintain kidney-specific gene expression and morphology in HKMECs cultured *in vitro* using a microfluidic coculture

platform, and further to understand if non-parenchymal tissues (i.e., non-kidney ECs) are plastic to develop organ-specificity through paracrine signaling with parenchymal cells (i.e., kidney epithelial cells). Emerging as an alternative tool for coculture studies, microfluidic platforms reduce cell and reagent consumption and offer better control over the configuration of the cell culture regions. Despite the rapid development of microfluidic technologies, many microfluidic platforms require handling expertise and equipment such as pumps and valves, creating significant obstacles for general biological laboratories to adopt microfluidic cell culture devices [8, 48, 61]. In this study, our goal was to create a user-friendly microfluidic device not only suitable for our coculture objectives, but also translatable to other cell culture schemes and easily adoptable by general biology researchers.

Here, we present an open microscale coculture platform that contains two cell culture chambers segregated by a polystyrene half wall. Paracrine signaling is initiated by connecting the two chambers with additional cell culture media, which overflows the half wall. We separately cultured HPTECs with three different endothelial cell types in the device and evaluated key endothelial cell organ-specific features under differential culture conditions. Our findings suggest that coculture with HPTECs supports maintenance of key organ-specific genes in primary human kidney ECs (HKMECs) and enhances kidney-specific gene expression in non-kidney-derived cells (human umbilical vein ECs (HUVECs), and human pluripotent stem cell-derived ECs (hPSC-ECs) over three days in culture. This work also serves as a proof of concept to demonstrate that the presented device could become a simple and efficient platform to study paracrine signaling effects across different cell types.

4.3 MATERIALS AND METHODS

4.3.1 *Open Microfluidic Coculture Device Fabrication*

Devices were fabricated using a Series 3 PCNC Mill (Tormach, Waunakee, WI) or a DATRONneo (Datron Dynamics, Germany). The devices were designed with Solidworks 2017 ×64 (Solidworks, Waltham, MA) and converted to .TAP files with Sprutcam (Sprutcam, Naberezhnye Chelny, Russia) or to .simpl files with Fusion 360 (Autodesk, San Rafael, CA). Devices were milled from 2 mm thick polystyrene (PS) sheets (Goodfellow USA, Coraopolis, PA). After milling, the device was washed thoroughly with dish soap and water, followed by 70% ethanol and DI water then air dried. A piece of 1.2 mm PS plastic (Goodfellow USA, Coraopolis, PA) was cut (65×50 mm square), cleaned, and solvent bonded to the bottom surface of the device according to the protocol adapted from Young et al. [60]. Briefly, a hot plate (Torrey Pines Scientific, HP60) was pre-heated to 65 °C; the bottom of the milled device was mated to the top surface of 1.2 mm PS square; small amounts of acetonitrile (ACN; A998-4, Fisher Chemicals) was pipetted gently through the hollow regions of the device until the liquid filled the entire mated area between the PS square and the device. Weight (2 kg) was placed on the top for about 30 s to facilitate the reaction between solvent and the polymer interface. The bonded device was sonicated with 70% ethanol at 68 °C for 15 min and rinsed with DI water and air dried. The device was plasma treated for 5 min at 0.25 mbar and 70 W in a Zepto LC PC Plasma Treater (Diener Electronic GmbH, Ebhausen, Germany) using oxygen, followed by 10 min of UV sterilization. An engineering drawing of the device with dimensions is included in Figure 4.6. Original design files are included in the ESI.

4.3.2 *Isolation and Cell Culture of HPTEC and HKMEC*

This work was approved by the University of Washington Institutional Review Board (IRB447773EA). Human HPTECs and HKMECs were isolated from surgically dissected kidney tissues from fetal donors (donor A: 125 days, male; donor B: 113 days, male; donor C: 127 days, female; donor D: 110 days, female), as we reported previously [33]. Kidneys were minced in serum-free EBM2 endothelial growth medium (Lonza) with 0.2 mg/mL Liberase and 100 U/mL DNase (Roche). The minced kidneys were incubated for 30 min at 37 °C in a shaking water bath. The tissue homogenate was filtered through a 40 μm cell strainer. For HKMEC enrichment, EpCAM-positive cells were depleted first from the cell suspension using EpCAM microbeads (Miltenyi Biotec). EpCAM-negative cells were cultured on gelatin-coated T-75 flasks in EBM2 media supplemented with antibiotic/antimycotic (Invitrogen), 10% FBS (Invitrogen), 10 μg/mL ECGS (Cell Biologics), 50 ug/mL heparin (Sigma), and 40 ng/mL VEGF (R&D Systems). Cells were cultured at 5% CO_2 and 37 °C until confluent, and HKMECs were sorted as CD144-positive population on BD FACSAria II at the UW SLU Flow Cytometry Facility. After sorting, HKMECs were cultured in EBM2 media supplemented with antibiotic/antimycotic (Invitrogen), 10% FBS (Invitrogen), 10 μg/mL ECGS (Cell Biologics), 50 μg/mL heparin (Sigma), and 20 ng/mL VEGF (R&D Systems) at 5% CO_2. For HPTEC enrichment, EpCAM-positive cells were collected using EpCAM microbeads from the cell suspension. HPTECs were then cultured in T-75 flasks in DMEM/F12 (Corning) supplemented with antibiotic/antimycotic (Invitrogen), ITS-X (Invitrogen), and 50 nM hydrocortisone (Sigma-Aldrich) at 5% CO_2 and 37 °C. Cells between passage 1-5 were used for coculture experiments.

HKMECs and HPTECs were plated on the center (17 μL) and side chamber (37 μL) of the coculture device at a density of 1×10^5 cells/cm^2 and 4.35×10^4 cells/cm^2 with their own media, respectively. 24 hours after initial cell plating, the two chambers were connected using 100 μL HKMEC media +/- VEGF (20 mg/mL), which was replaced every 24 h. Throughout culturing, the devices were kept in a primary container (a 86×128 mm OmniTray, or a 100×150 mm Petri Dish (Thermo Scientific)). Sacrificial PBS droplets (total volume of 1 mL) were pipetted around the devices to mitigate evaporation. The primary container was placed in the center of a 245×245 mm BioAssay Dish (Corning) with 100 mL PBS. The peripheral of the primary container was wrapped tightly with moisten Kim Wipe. The secondary container was incubated at 5% CO_2 and 37°C.

For HKMECs and HPTECs conditioned media culture experiment, HPTECs were plated on the side chambers of the device and recovered overnight. On the next day, HPTECs were fed with 100 μL HKMEC media supplemented with 20 mg/mL VEGF. HKMEC were plated on the center chambers of separate wells. After overnight recovery, HPTEC conditioned media was collected and filtered to remove any HPTEC debris. 100 μL of conditioned media was added to the wells containing HKMECs. The conditioned media was collected and changed every 24 h.

4.3.3 *Cell Culture of HUVEC and hPSC-EC*

HUVECs (Lonza) were cultured in EBM (Lonza) supplemented with EGM Endothelial Cell Growth Medium SingleQuots Kit (Lonza) and used at passage 3-6. The coculture procedures for HUVEC-HPTEC were the same as HKMEC-HPTEC coculture described above using HUVEC media. Human pluripotent stem cells (hPSC) (WTC line, a gift from Dr. Murry, University of Washington) was first differentiated to posterior-like ECs according to the protocol adapted from Palpant et al. [41] and Redd et al. [44] with low Activin A and high BMP4 for 10 days. Then these

cells were trypsinized and plated into co-culture device (at center well) to allow for attachment and growth into confluency. HPTECs were plated into the outer well of the device at day 11, and co-cultured with hPSC-EC for additional two days in hPSC-EC media [41]. At day 13, five devices were fixed with PFA for immunostaining, and additional 5 devices were lysed for RNA collection.

4.3.4 *Cell Staining and Imaging*

The ECs in the study were washed with PBS, blocked with PBS containing 2% BSA for 1 h, and incubated with 0.1% Triton X-100 for 5 min. The cells were washed and incubated at 1:50 dilution over night at 4°C with primary antibodies: mouse anti PV-1, rabbit anti VECad, and sheep anti vWF (Abcam). The samples were washed and incubated at 1:200 dilution for 1 hour at room temperature with secondary antibodies: goat anti mouse 488, goat anti rabbit 568, and donkey anti sheep 568 goat anti-rat secondary antibody (Thermo Fisher). The secondary antibodies were removed, a 1:1000 dilution of DAPI (Invitrogen) was added and incubated for 5 min. The samples were washed twice, mounted with PBS, and covered with a glass slip to prevent sample dehydration during imaging. The protected device was fitted directly into the mounting frame for fluorescence microscopy.

4.3.5 *RNA Isolation, RT-PCR, and qPCR Analysis for ECs*

RNA was collected and purified using the RNAeasy Mini Kit (Qiagen), and residual DNA was removed by on-column DNase digestion (Qiagen). RNA quantity and quality were measured with NanoDrop ND 1000 Spectrophotometer. RT-PCR was performed using Biometra T-Personal Thermal Cycler with iScript Reverse Transcription Supermix (Bio-Rad). qPCR was performed using the Real-time PCR System (Applied Biosystems) with Fast SYBR Green Master Mix

(Applied Biosystems) and primers (RealTimePrimers). The gene expression was quantified according to MIQE guidelines, and the expression of each gene was determined relative to reference gene GAPDH [10].

4.3.6 *Microscopy and Image Processing*

ECs were imaged using a Nikon High Resolution Widefield microscope with a high-resolution CCD camera. Brightness/contrast adjustments were made uniformly across all images in Fiji (ImageJ). To calculate the cell size for HKMECs monoculture without VEGF condition, a random cell region on 10x image was chosen and cells were counted, and average cell size was determined by region area/DAPI count. For other culture conditions where HKMECs were confluent, the average cell size was determined by field of view/total DAPI count.

4.3.7 *Statistical Analysis*

Quantitative data was graphed and analyzed using GraphPad Prism 7 software. In Figure 4.2C, each plotted point represents the average of approximately 3.5×10^4 cells – 8.0×10^4 cells analyzed within a device. HKMEC cell size was compared using a one-way an ANOVA test followed by Tukey's multiple comparisons. In Figures 4.3 and 4.4, statistical tests were run to compare the expression in coculture vs. monoculture (all VEGF-free) as follows: Due to the distribution of data from multiple human donors, the coculture expression ratios for the three donors were log transformed to better fulfill the assumptions of the *t*-test. The log transformed coculture data were then compared to 0 using a two-tailed one-sample *t*-test using “QuickCalcs one-sample *t*-test” on the GraphPad website. (Note that the coculture data had previously been normalized to

monoculture data, which was set to 1 as described in the figure captions; log(1)=0 hence we compared to 0 using the one-sample *t*-test.)

4.4 Results and Discussion

4.4.1 *Open Microfluidic Device Design and Workflow*

Open microfluidic systems are characterized by the introduction of an air-liquid interface, where liquid flows in microscale channels devoid of at least one side-wall [2, 5, 6, 13]. Unlike typical microfluidic devices with enclosed culture chambers, open devices offer increased pipette accessibility at any point along the culture chamber and simpler fabrication processes, such as straightforward micro-milling and injection molding, allowing open microfluidic devices to become efficient tools with versatility and transferability across different research disciplines [11, 18, 30, 31, 40, 49, 58].

In the present study, we develop a user-friendly platform to maintain and evaluate kidney endothelial cell organ-specificity under various microenvironments. Our device consists of two cell culture regions, a center chamber and a side chamber, segregated by a half wall (Figure 4.1A, Figure 4.6A). The width and height of the side chamber are designed to allow filling by a single pipette-dispensing step based on the concept of spontaneous capillary flow in open microchannels (see SI for equation describing the conditions for capillary flow and illustrations in Figure 4.6). Two cell types are selectively pipetted into the center (ECs) and the side (HPTECs) chamber, respectively; after adherence, the cells are placed into paracrine signaling contact by filling cell culture medium over the half wall (Figure 4.1B). The notched features for each chamber are designed to accommodate a pipette tip for ease of use when pipetting media. Figure 4.1C shows a

device with 5 by 4 array of the wells. The replicating wells allow for testing multiple culture conditions in a single experiment. Additionally, the dimensions of the device plate are designed to fit into a standard petri dish (88 mm in diameter, shown in Figure 4.1C) to maintain sterility and control evaporation during incubation. The device plate dimensions (60×50 mm) are also compatible with universal microscope mounting frames for convenient endpoint imaging.

Importantly, the coculture device is fabricated with polystyrene, which is the standard material for cell culture due to its biocompatibility and good optical properties for medium resolution imaging, which is used for standard kidney endothelial cell immunocytochemistry and morphology studies [17]. In contrast to microfluidic platforms made of polydimethylsiloxane (PDMS), the device used in this work mitigates problems with oligomer leaching and adsorption of small molecules (such as potential drugs or toxicants that this device could be used to screen in future studies) (7, 25, 45, 54). The ECs (HKMECs, HUVECs, and hPSC-ECs) and HPTEC coculture model presented in this study demonstrates that the coculture device, and our culture protocols to avoid evaporation and ensure nutrient availability in microscale culture, are compatible with cells from different sources. Additionally, to demonstrate the versatility of the device for culturing different cells in the side chamber, we cultured freshly isolated human pericytes in the side chamber and HKMECs in the middle chamber for 72 hours; this is a biologically relevant coculture model because kidney pericytes play a profound role in inflammation and the renal pericyte-endothelial cross-talk contributes to fibrogenesis during kidney disease progression [29]. The results showed that incorporation of pericytes increased HKMEC density in the device (Figure 4.7).

Although Transwells have been widely used in coculture studies to study soluble factor signaling, our open microfluidic coculture system offers additional features that address several limitations

of the Transwell system. Specifically, our system provides a tissue culture-treated polystyrene substrate to culture both cell types, avoiding the potential complication of culturing sensitive cell types on Transwell insert membrane; the coculture device enables imaging both cell types in the same plane of focus, enabling efficient imaging during culture; the open microfluidic design allows for a simple workflow for media changes, minimizing the operation time and the risk of drying the cells in culture; finally, the size and the ratio of the two cell culture regions can be tuned easily in the computer aided design (CAD) file, offering the flexibility for researchers to customize the system suitable for their own research purpose. However, a potential limitation for this present open microfluidic system is that it does offer the mechanical capacity (which requires syringe pumps and valves) to address the effect of shear stress caused by the tubular flow and blood flow in the in vivo kidney proximal tubules and peritubular microvessels, respectively. A pending design challenge we seek to solve in future studies is to combine shear flow and real time paracrine signaling events in microfluidic coculture models.

4.4.2 *HKMEC and HPTEC Coculture in an Open Microscale Device Preserves Endothelial Morphology*

A central goal of our study is to understand to what extent EC specificity can be modified by parenchymal cells *in vitro*, and potentially to develop a method to maintain kidney specificity of HKMECs *in vitro.* The loss of microvascular endothelium in renal disease progression is directly related to altered local secretion of VEGF *in vivo*, which is mainly produced by proximal tubular epithelium [21, 46, 57]. We utilized the open microscale coculture devices to examine the morphology of HKMECs in four different cultural conditions (Figure 4.2A). Briefly, HKMECs were cultured in the center chambers of the device alone or with HPTECs cultured in the side chambers, both in media with and without exogeneous VEGF. We used immunocytochemistry to

qualitatively compare the expression of vascular endothelial cadherin (VECad), an endothelial integrity marker that is an essential component of endothelial intercellular adherens junctions and critical to endothelium integrity and barrier function [12], and the expression of plasmalemma vesicle associated protein (PV1), a marker critical to the formation of stomatal (in the peri-nuclear cytosol) and fenestral (in the periphery of EC membranes) diaphragms on endothelial cell membranes [50].

As shown in Figure 4.2B, without exogenous VEGF, HKMECs cultured alone (i.e., "Monoculture, VEGF-") lost consistent expression of VECad between adjacent cells, and gaps between the cells were observed (Figure 4.2B, box), indicating disrupted EC barrier. Additionally, in the "Monoculture, VEGF-" condition, majority of PV1 expression is perinuclear, suggesting limited fenestrae formation. Addition of exogenous VEGF in monoculture enabled a contiguous monolayer without gaps (as visualized in the VECad staining) and partially rescued PV1 expression. With the presence of HPTECs in VEGF-free media (i.e., "Coculture, VEGF-"), HKMECs maintained integrated cell-cell contact (VECad staining) and showed clusters of clear PV1 expression (Figure 4.2B, arrows, punctate staining), indicating that soluble factors from the neighboring but physically separated HPTECs helped maintain important endothelial cell function without exogenous VEGF. In addition to qualitatively comparing immunostaining of HKMECs, we also quantitatively compared the cell count and cell size for HKMECs in differential culture conditions. We found that HKMECs cultured with "VEGF+" media yielded higher cell counts than HKMECs in "VEGF-" media, regardless of the presence of HPTECs in the coculture device (***$p<0.001$, ****$p<0.0001$, Figure 4.2C). The increase in cell number corresponding to the addition of exogeneous VEGF in the media suggested that VEGF had essential role in HKMEC proliferation. Moreover, we quantified average HKMEC cell size and found that in the "Coculture,

VEGF-" condition, HKMECs had larger cell size when compared to the "Monoculture, VEGF-", and "Coculture, VEGF+" conditions (****p<0.0001, Figure 4.2D). This suggests that HPTECs co-culture promoted HKMECs quiescence and maturation [35]. Adding VEGF alone did not have the same influence on cell size as the co-culture condition, suggesting that HPTECs affect HKMECs via different or additional small molecule signaling than VEGF alone. The similar trend was observed across donors, and additional data from donor A is provided in Figure 4.8. Taken together, our results show the utility of the coculture device as a simplified *in vitro* platform able to recapitulate key kidney endothelial protein expression and morphology sustained by soluble factor crosstalk with kidney epithelial cells.

4.4.3 *HPTECs Support Expression of Key HKMEC Organ-Specific and Endothelial-Remodeling Genes in Coculture*

Previous studies observed that during organ development, ECs from different organs are heterogeneous in both morphology and gene expression patterns and participate in crosstalk with surrounding microenvironments to form the organ-specific vasculature [14, 39]. Multiple kidney-specific endothelial genes are highly expressed in freshly isolated primary kidney endothelial tissues yet become significantly downregulated in expanded culture [37]. We wanted to determine if coculture with HPTECs could help rescue this loss in parenchymal gene expression by soluble factor signaling. With the same setup shown in Figure 4.2A, we cultured HKMECs under the four different conditions (Figure 4.2A) and collected RNA for quantitative gene expression analysis (RT-qPCR) of selected genes.

We chose to focus on a panel of genes that were previously identified as representative molecular markers for HKMECs [33, 37]. The qPCR data in Figure 4.3 indicate that compared to HKMECs

in monoculture VEGF-free media (red bars), HKMECs in coculture VEGF-free media (green bars) exhibited upregulation of selective kidney-specific genes (top panel), including a 3 to 21-fold increase in Hepatocyte Nuclear Factor 1 Homeobox B (*HNF1B*), a transcription factor important to nephron development; a 7 to 28-fold in Adherens Junctions Associated Protein 1 (*AJAP1*), an adhesion junctional protein precursor crucial to endothelium barrier function; and a 2 to 32-fold in Potassium Voltage-Gated Channel Subfamily J Member 16 (*KCNJ16*), a gene encoding potassium channel protein essential to fluid regulation and pH balance. Key endothelial activation genes (bottom panel) followed a similar trend of upregulation in the coculture (green bars) versus monoculture (red bars) condition, including a 33 to 95-fold increase in *MMP7* and a 2 to 13-fold increase in *MMP10*, two matrix metallopeptidases, and a 6 to 526-fold increase in Vascular Cell Adhesion Molecule 1 (*VCAM1*), which regulates leucocyte adhesion to vascular wall [15, 19, 26, 42, 51]. Additionally, HKMECs from donor C (square symbol) showed 5-fold upregulation of kidney specific gene Contactin 4 (*CNTN4*), which is linked to normal kidney development, and a 6-fold upregulation in endothelial activation gene Angiopoietin 2 (*ANG2*), which regulates angiogenesis and vascular inflammation in coculture versus monoculture [24]. Interestingly, HKMECs cocultured in VEGF-supplemented media (blue bars) showed less upregulation on average of the aforementioned genes except for *ANG2*, as compared to HKMECs cocultured in VEGF-free media (green bars). These data suggest that in coculture, HPTECs secrete not only VEGF but also other soluble factors supporting HKMECs to maintain key kidney endothelial features via paracrine signaling [22, 43, 56].

In contrast to the genes discussed in Figure 4.3, a subset of genes including *PV1*, *VECad*, Nitric Oxide Synthase 3 (*NOS3*, an endothelial proliferation gene), and VEGF Receptor 2 (*VEGFR2*) were upregulated when cultured in “VEGF+” media compared to “VEGF-” media, for both

monoculture (orange vs. red bars) and coculture (blue vs. green bars) conditions (Figure 4.9). The result suggested the critical role of VEGF in HKMEC proliferation and certain aspects of kidney function development.

Figure 4.3 and 4.9 also demonstrate variance across different human donors, which highlights the importance of studying human cell signaling pathways with patient specific cells to understand patient-dependent disease mechanisms. Due to the variation across human donors, only *AJAP1* and *MMP7* show statistical significance between "Monoculture, VEGF-" condition (red bar) and "Coculture, VEGF-" condition (green bar); however, from a biological perspective, it is meaningful that all three human donors show at least 2-fold higher expression in the latter than the former condition for *HNF1B*, *AJAP1*, *KCNJ16*, *VCAM1*, *MMP7*, and *MMP10*. The response among donors for *CNTN4* and *ANG2* was mixed, with only donor C (square symbol) showing upregulated expression. Moreover, donor C showed the most pronounced upregulation in "Coculture, VEGF-" condition than the other two donors across all genes of interest in Figure 4.3.

4.4.4 *HPTECs Induce Key Kidney-Specific Markers in Other Types of ECs*

As shown in the preceding figures, HKMECs display plasticity in the coculture device and demonstrate that paracrine signaling with HPTECs led to enhanced parenchymal properties. Further, we wanted to investigate if parenchymal cells (i.e., HPTECs) have inherent potential to tune human non-kidney ECs through paracrine signaling.

Human umbilical vein ECs (HUVECs) have been widely used as a microvascular endothelial cell surrogate in traditional kidney research [19, 26, 28, 52, 53]. We determined whether coculture with HPTECs could induce parenchymal changes (i.e., kidney-specific expression) in HUVECs

through paracrine signaling. We placed HUVECs in the center chamber of the coculture device with or without HPTECs seeded in the side chamber. After three days of incubation, we used immunocytochemistry to evaluate expression of the platelet-endothelial cell adhesion molecule (PECAM1, also known as CD31), blood glycoprotein von Willebrand Factor (vWF), and actin cytoskeleton molecule (phalloidin staining) in differential culture conditions [16, 47]. Figure 4.4A shows that HUVECs in monoculture had robust PECAM1 localization at intercellular junctions, whereas in coculture, very low levels of PECAM1 resided at the intercellular junctions, suggesting junctional instability and cell activation. In addition, HUVECs in coculture showed less vWF in cell cytosol than in monoculture, and more aligned phalloidin structure, suggesting that HPTECs perturbed endothelial quiescence and led to endothelial activation (4). Together, the data suggest that HPTEC perturbed HUVEC quiescence in coculture, and HPTECs secreted soluble factors that may stimulate endothelial activation in HUVECs.

We also compared the expression of the same panel of kidney-specific and activation genes in HUVECs cultured alone or with HPTECs. Figure 4.4B suggests that similar to HKMECs in coculture with HPTECs, HUVECs expressed higher levels of the kidney organ-specific genes, including AJAP1 (7 to 11-fold), KCNJ16 (7 to 12-fold), and CNTN4 (5 to 22-fold), and the endothelial activation genes, including MMP7 (5 to 17-fold), MMP10 (26 to 99-fold), and VACM1 (148 to 323-fold) in coculture. However, none of the donor cells led to upregulation of ANG2. The expression of HNF1B, a kidney-specific gene was also detected in the HUVECs after coculture, whereas no detectable expression in the HUVEC alone condition (data not shown). Consequently, HPTECs showed potential to induce parenchymal characteristics in HUVECs through paracrine signaling.

Generating ECs *de novo* by using human pluripotent stem cells (hPSC) has emerged as a tool in the past decade to study vascular pathogenesis and construct tissues for drug screening and other therapeutic applications [32, 41]. Here, we explored whether hPSC-derived ECs (hPSC-ECs) can develop kidney specific features when co-cultured with HPTECs. Briefly, we differentiated hPSCs to ECs following the protocol adapted from Palpant et al. [41], and cultured hPSC-ECs in our microscale device in center well alone (monoculture) or co-cultured with HPTECs. We show that compared to in monoculture, hPSC-ECs in coculture exhibited upregulation of *MMP7*, and *VACM1*, whereas no obvious changes of *AJAP1*, *KCNJ16*, *CNTN4*, *MMP10*, and *ANG2* across the three human donors (Figure 4.4C). Similar to HUVECs, the expression of *HNF1B* was not detected in the hPSC-EC monoculture sample, but at a detectable level in the coculture samples (data not shown in the figure). Hence, through the coculture of non-kidney ECs (i.e., HUVECs and hPSC-ECs) with HPTECs, we demonstrated a proof-of-concept that HPTECs can induce changes in EC phenotype, and ECs can acquire kidney specificity by the support of HPTECs in the microenvironment. Moreover, parenchymal tissue coculture (i.e., HPTEC and non-kidney EC coculture) has the potential to tune human generic cells through paracrine signaling to develop organ-specific physiological features. The present open microfluidic coculture system also provides opportunities for future investigation of the effects of paracrine signaling on developing tissue-specific features in other cell types.

It should be noted that cross contamination of the cell types could be a potential issue during the media changing step, as unattached cells or debris could be flushed into the other cell culture chamber when fresh media is pipetted directly from the top of the device; if this occurred, the purity of the cell lysate sample used for qPCR analysis would be affected. In this study, since the immunofluorescence images of the ECs (Figure 4.2) did not show any presence of the HPTECs,

we are confident about the purity of the endothelial cell lysate collected from the center chamber. Further, we have explored this co-culture effect via conditioned media cultures as below, to further support the changes of ECs by HPTECs.

4.4.5 *HPTEC Coculture and Conditioned Media Culture Lead to Different Effects*

Historically, transferring conditioned media from one cell type to another has been a common approach to recapitulating cell-cell interactions via soluble signaling mediators. Although conditioned media experiments have facilitated the understanding of cellular signaling mechanisms and the discovery of biomarkers and therapeutic targets in diseases, they are inadequate to capture the effects of fast-decaying factors or dynamic bidirectional signaling due to the temporal segregation of the cell populations [8, 59]. Using the segregated coculture device, we were able to compare the difference between HKMECs in shared media coculture with HPTECs and HKMECs in HPTEC conditioned media culture. To model conditioned media culture, HPTECs were plated in the side chamber of the device overnight, and conditioned media was collected to feed HKMECs seeded in the center chamber of a separate device. The HPTEC conditioned media was collected every 24 hours, and the freshly collected medium was used to replace HKMEC culture medium. HKMECs were collected for RT-qPCR analysis after three days of culture with HPTEC conditioned medium.

As shown in Figure 4.5, HKMECs in conditioned media culture (red) showed similar trend with noticeable upregulation of kidney specific genes, particularly KCNJ16, MMP7, VCAM1, whereas the changes of HNF1B, AJAP1, and MMP10 are evidently less pronounced in conditioned media culture (red) than in coculture (green). This data suggests that the signaling between HKMECs and HPTECs involves both unidirectional signaling (in conditioned media) and bidirectional signaling

(in shared media) pathways. It is also possible that some of the key signaling factors are short-lived and are therefore lost in the conditioned media experiments while still present in the coculture experiments. Although potential improvement in our system can be made to include the features of tissue-specific architecture, 3D structure, and proximity of two cell populations to better resemble the in vivo condition, our system provides an opportunity to investigate the bidirectional signaling molecule interactions in real time, which is a step forward compared to the traditional one-way signaling in conditioned media studies.

4.5 DISCUSSION

Here, we present an open microscale coculture device that provides spatial segregation for different cell types and supports paracrine signaling in the shared microenvironment. With relatively small cell samples and regular pipetting actions (no sophisticated external pumps or valves), a coculture configuration with operation efficiency can be achieved. Using the microscale device, we cocultured HPTECs with ECs from different sources. We observed that signaling molecules secreted by HPTECs enhance some level of kidney specific characteristics in generic human ECs (HUVECs and hPSC-ECs) and led to endothelial remodeling, indicating a supporting role of HPTECs to the functional development of ECs. Since adult human kidney ECs are similar to fetal kidney ECs in morphology and protein expression profile [33], we expect to see that HPTEC coculture would lead to similar changes in adult human kidney ECs. Future studies would be interesting to examine the different level of genetic modification for different types of ECs in the coculture model.

Moreover, we observed higher upregulation in certain kidney specific genes and endothelial activation genes when HKMECs were cultured with HPTECs in shared media (coculture) than in

conditioned media, suggesting a bidirectional paracrine signaling mechanism in the system. In future work, we envision performing proteomic analysis of the conditioned media collected from HPTEC monoculture and HPTEC-HKMEC coculture, which will provide more specific insight into the mediators of paracrine signaling in the system.

Due to the functional differences among ECs from different organs, it is important to use organ-specific ECs to understand specific vascular injury and regeneration mechanisms. For the study of the interaction between human kidney proximal tubule epithelium and peritubular microvascular endothelium, this is the first time that primary human kidney cell types are cocultured in shared media, more precisely resembling the paracrine signaling effect in the *in vivo* microenvironment. Our findings suggest parenchymal cells have the capability to tune generic human cells *in vitro* through paracrine signaling.

Our culture system is simple to use, and we have translated it to biological collaborators in other application areas who are able to operate the device in their own laboratories without assistance. In future work, we envision that our microscale device will be batch fabricated by injection molding [18, 30, 31] and easily adapted to tune parenchymal characteristics in *in vitro* cell culture studies, and construct patient-specific tissue paracrine signaling models for pathological research and therapeutic applications.

4.6 FIGURES

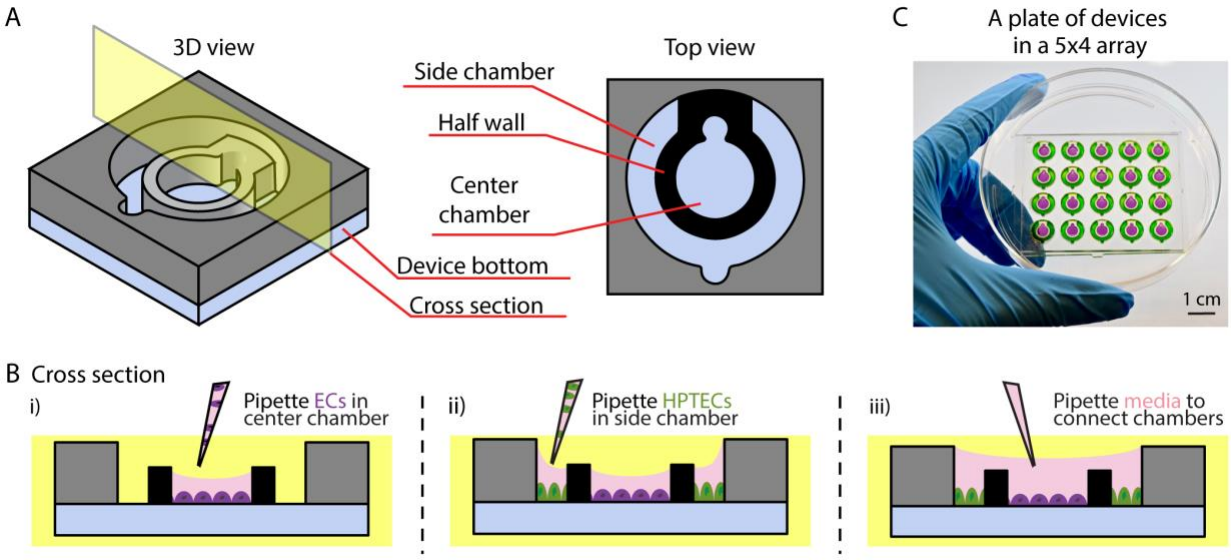

Figure 4.1. Coculture device design and operation.

(A) 3D and top view of device design. (B) Cross section view of device operation: different cell types (endothelial cells (ECs) and HPTECs) are selectively seeded into the separated cell culture chambers (i-ii) and placed into paracrine signaling contact by addition of shared media on top (iii). (C) A photograph of a plate of devices in 5×4 array fitted inside a petri dish. Center and side chambers are loaded with purple and green dye, respectively, to visualize chamber segregation.

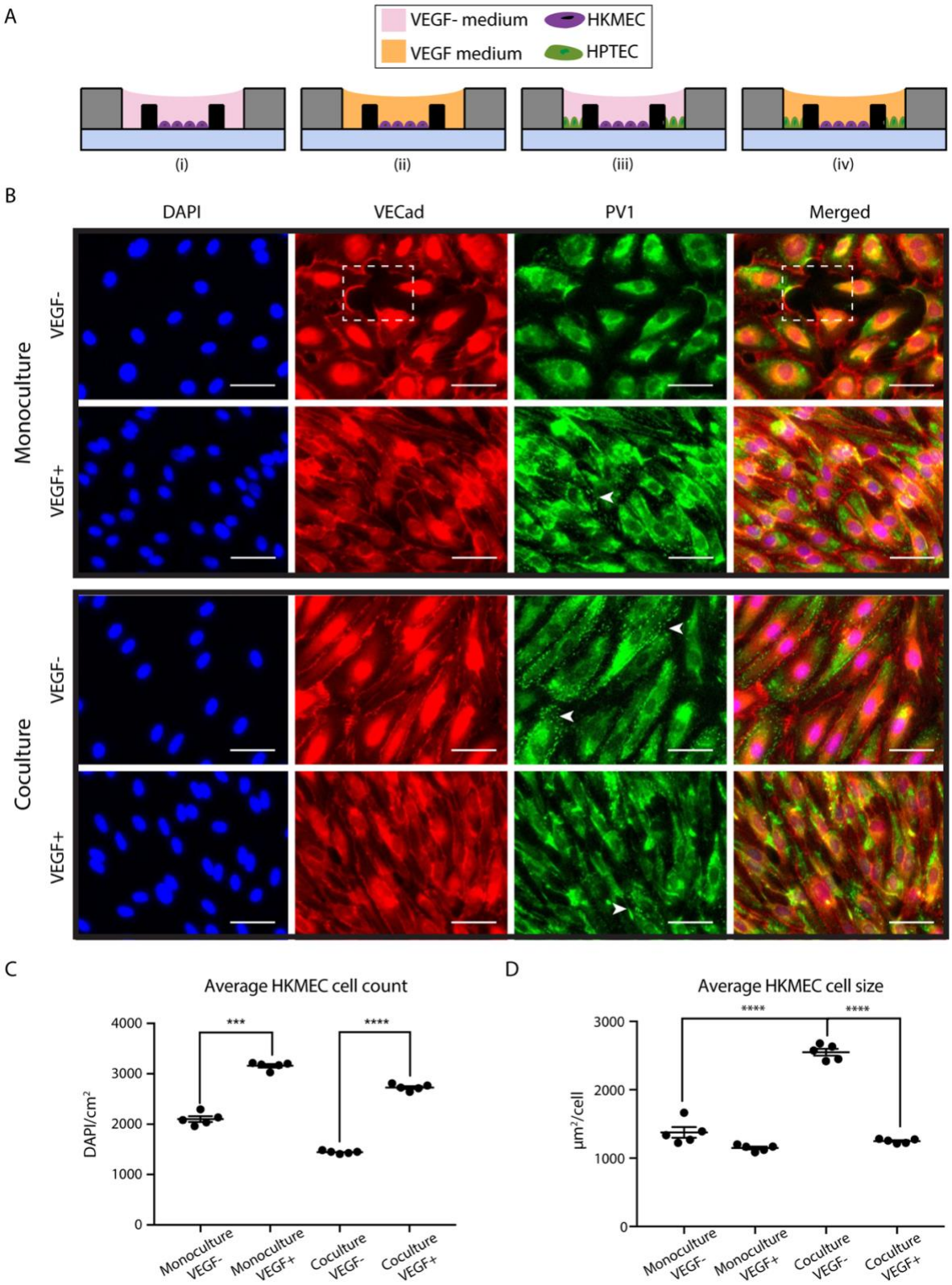

Figure 4.2. Coculture with HPTECs preserves HKMECs morphology in coculture.

(A) Device cross section views showing the four culture conditions of HKMECs and HPTECs: monoculture of HKMECs in media without (i) or with (ii) exogeneous VEGF; segregated coculture of HKMECs and HPTECs in media without (iii) or with (iv) exogeneous VEGF. (B) Immunofluorescence images of HKMECs under differential culture conditions. Blue: nuclear stain (DAPI). Red: vascular endothelial cadherin (VECad); dotted box indicates a region without cells. Green: plasmalemma vesicle associated protein (PV1); arrows indicate example regions with clear PV1 structures (punctate staining). Scale bars: 50 μm. Images shown are from donor C and are representative of experiments with cells from 3 different human donors each with 5 device replicates per experiment. (C) Quantitative comparison of HKMEC cell count between "Monoculture, VEGF-" and "Monoculture VEGF+" conditions; and "Coculture, VEGF-" and "Coculture, VEGF+" conditions. (D) Quantitative comparison of HKMEC cell size between "Coculture, VEGF-" and "Monoculture, VEGF-" conditions; and "Coculture, VEGF-" and "Coculture, VEGF+" conditions. Error bars represent the SEM of 5 device replicates for a single human donor (donor C) in a single experiment. Data sets were analyzed using a one-way ANOVA test; p-values are indicated for Tukey's multiple comparisons tests. (***$p<0.001$, ****$p \leq 0.0001$)

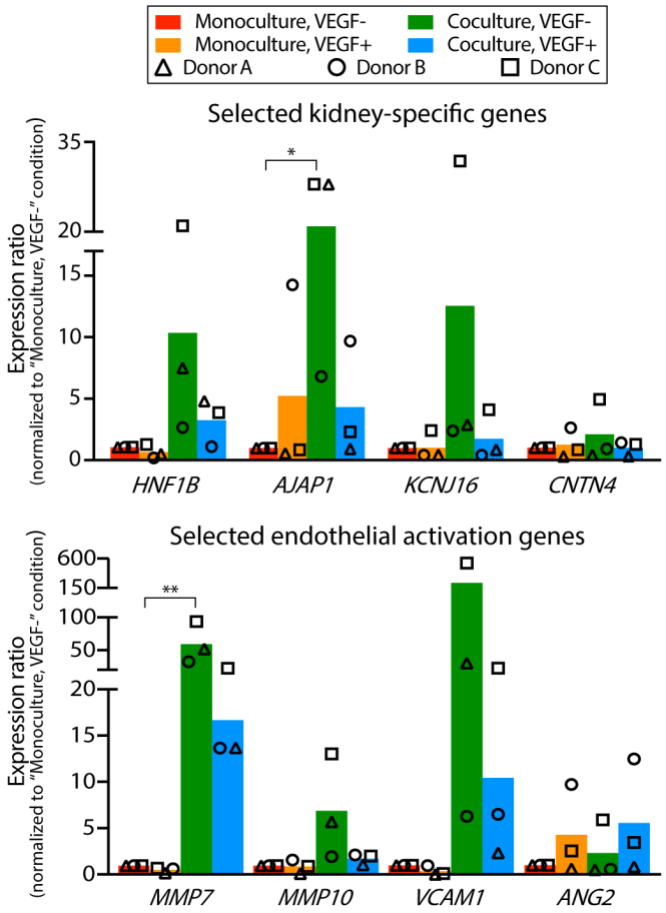

Figure 4.3. Transcriptional changes of HKMECs by coculturing with HPTECs.

RT-qPCR of selected HKMEC-specific genes (top) and activation genes (bottom) show upregulation in "Coculture, VEGF-" condition (green) compared to "Monoculture, VEGF-" condition (red). Each plotted point represents data from an independent human donor (pooled from 5 replicate microculture devices per donor, average of 3 RT-qPCR technical replicates), with each normalized to the "Monoculture, VEGF-" condition (which is set to 1). Each colored bar represents the average ratio of the three donors. Statistical comparisons (as described in the methods section) are shown for genes showing significant differences between "Coculture, VEGF-" and "Monoculture, VEGF-" as described in the methods section (*$p \leq 0.05$, **$p \leq 0.01$).

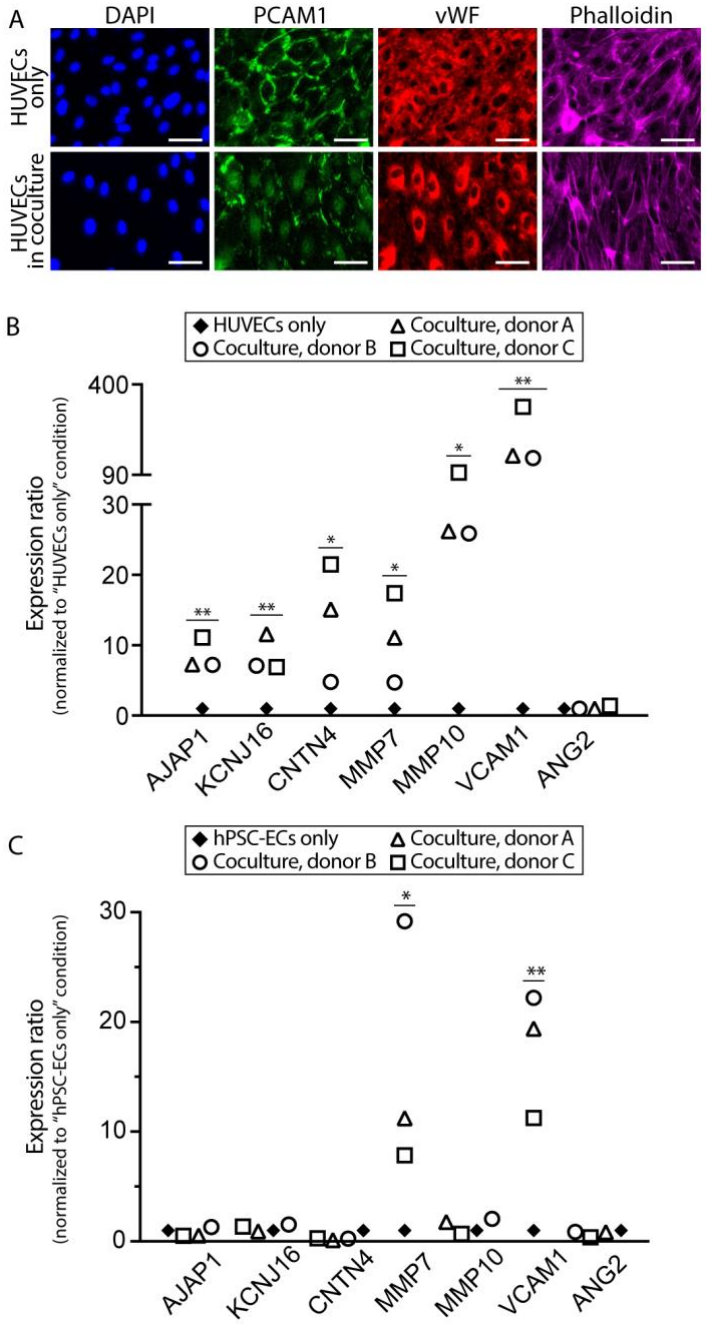

Figure 4.4. HPTECs activate other types of endothelial cells in coculture.

(A) Immunofluorescence images of HUVECs in monoculture and coculture condition with HPTECs. Scale bars: 50 μm. (B) Selected kidney-specific markers and endothelial activation markers in HUVECs cocultured with HPTECs from three different donors. (C) Selected kidney-specific markers and endothelial activation markers in hPSC-ECs cocultured with HPTECs. The RT-qPCR samples were pooled from 5 replicate microculture devices per donor, average of 3 RT-

qPCR technical replicates. Gene expression in both (B) and (C) is normalized to monoculture, which is set to 1. Statistical comparisons (as described in the methods section) are shown for genes showing significant differences between coculture and monoculture (*$p \leq 0.05$, **$p \leq 0.01$).

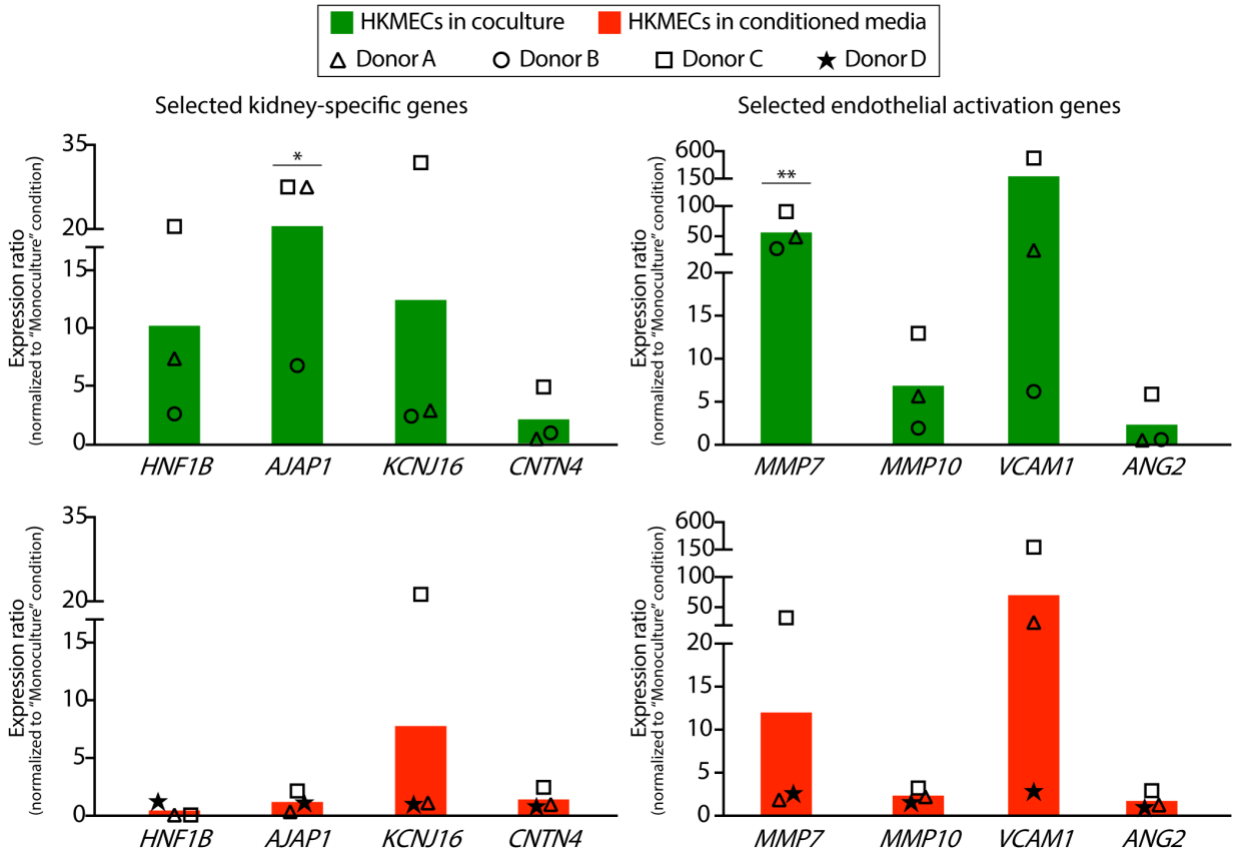

Figure 4.5. Selected gene expression profiles for HKMECs in coculture and conditioned media culture.

HKMECs showed higher upregulation of kidney-specific (left) and endothelial activation (right) genes in coculture with HPTECs (green) compared to in HPTEC conditioned media (red). Each plotted point represents data from an independent human donor (pooled from 5 replicate microculture devices per donor, average of 3 RT-qPCR technical replicates). Each colored bar represents the average of three human donors. Gene expression is normalized to monoculture, which is set to 1.

4.7 SUPPLEMENTARY INFORMATION

Spontaneous capillary flow (SCF) in the device side culture chamber

In an open system fluid flow can occur without the need for external pressure sources, which is described as spontaneous capillary flow (SCF) [22, 24, 33]. SCF occurs when the following inequality is fulfilled:

$$\frac{P_f}{P_w} < \cos(\theta)$$

where the wetted perimeter (Pw) comprises all the solid wetted surfaces in the channel cross-section, the free perimeter (Pf) comprises all the open air-liquid interfaces in the cross-section, and θ represents the contact angle of the liquid on the channel material. In the microfluidic coculture device described in this manuscript, the side chamber cross sectional geometry (Figure 4.6C) fulfills the conditions for spontaneous capillary flow as shown below. The contact angle of cell culture media on device surface (plasma treated polystyrene) is 17.9°±3.0°. (24)

$$cos(17.9°) \approx 0.95,$$

$$\frac{P_f}{P_w} = \frac{1.6\ mm}{(2.0 + 1.5 + 1.4)\ mm} \approx 0.33$$

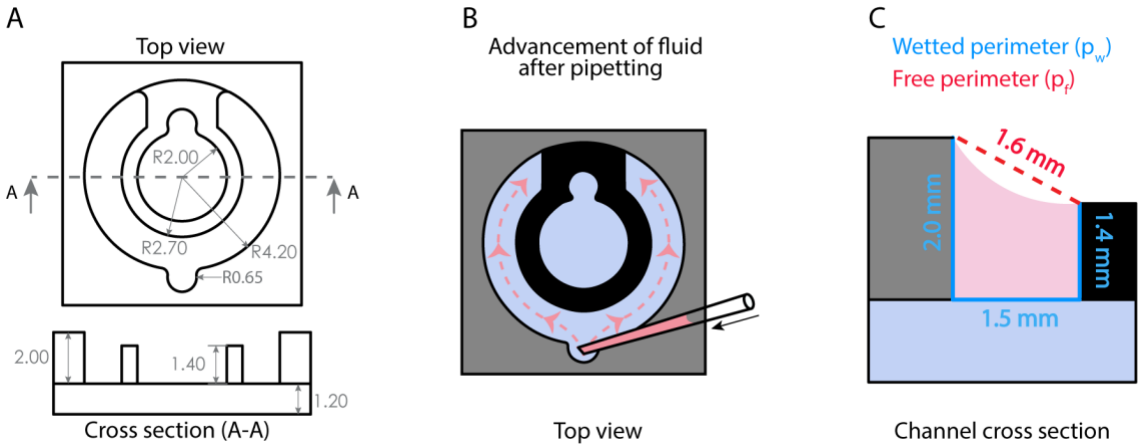

Figure 4.6. Device dimensions and spontaneous capillary flow (SCF) during the microscale device loading.

(A) Top view and cross section illustrating the dimensions of the coculture platform. Unit: mm. Computer aided design (CAD) file is included in the ESI. (B) Top view showing the advancement of fluid in the device side channel. (C) Channel cross section geometry showing the wetted perimeter (pw) and free perimeter (pf), which fulfills the condition for SCF.

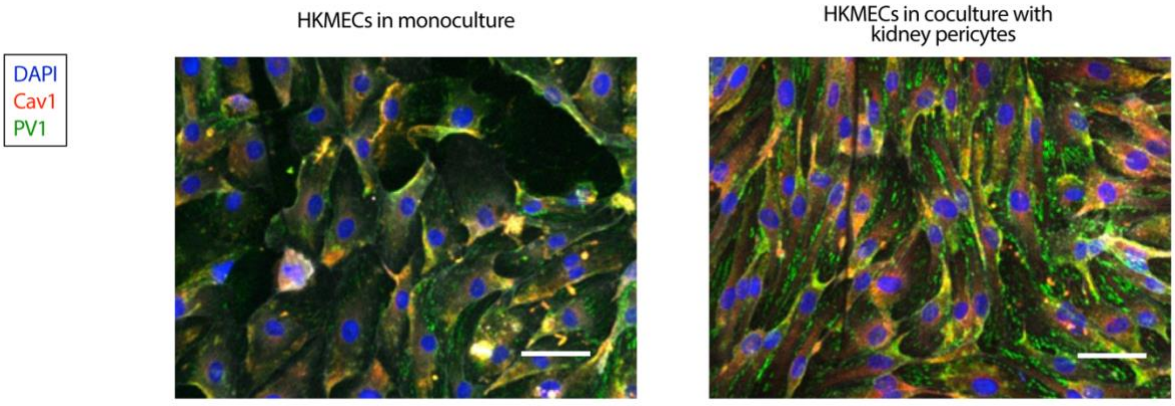

Figure 4.7. Incorporation of kidney pericytes increased HKMEC density in coculture.

Blue: nuclear stain (DAPI). Red: Caveolin- 1 (Cav1); Green: plasmalemma vesicle associated protein (PV1). Scale bars: 50 μm.

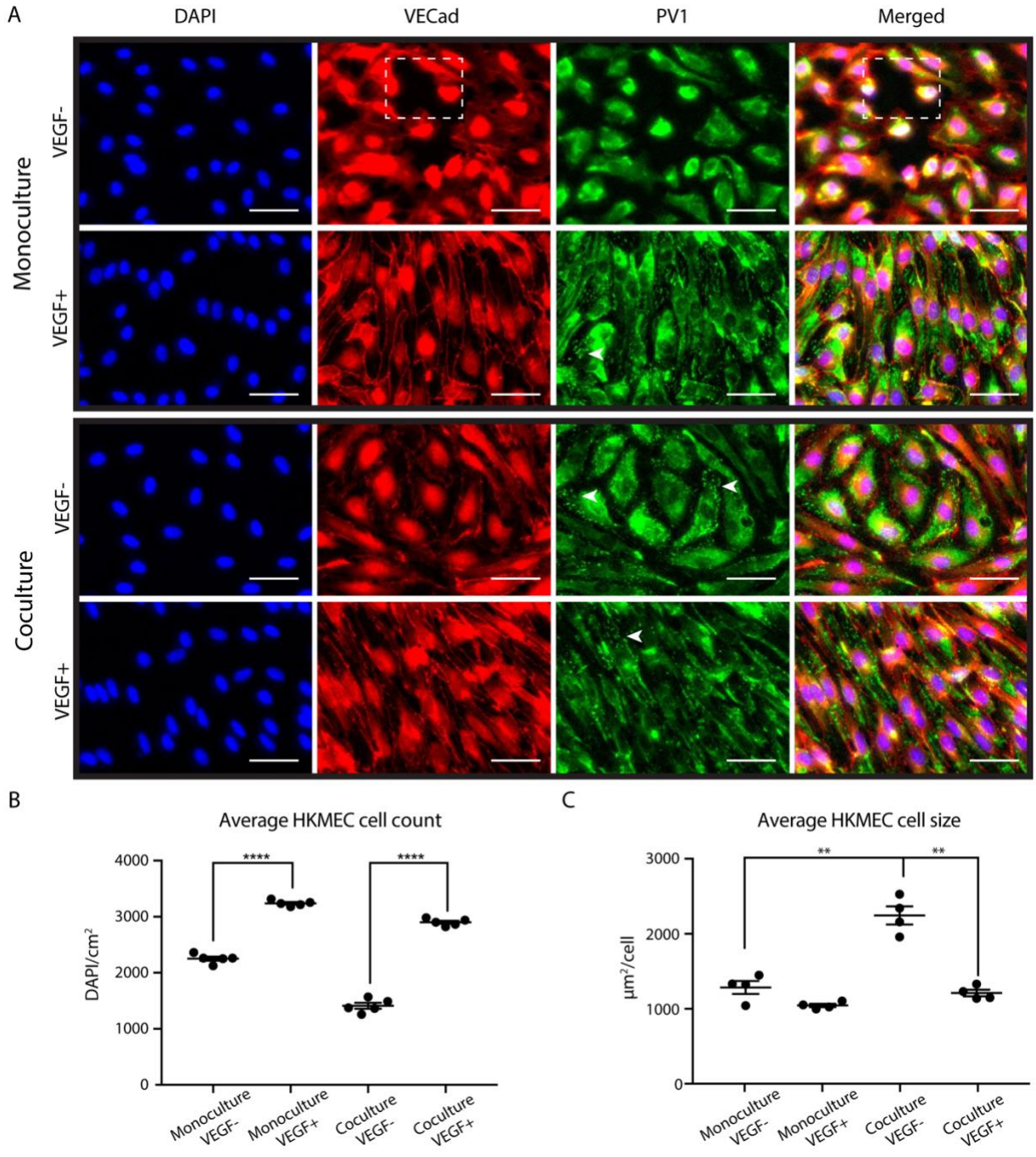

Figure 4.8. Coculture with HPTECs preserves HKMECs morphology in coculture.

(A) Immunofluorescence images of HKMECs under differential culture conditions. Blue: nuclear stain (DAPI). Red: vascular endothelial cadherin (VECad); dotted box indicates a region without cells. Green: plasmalemma vesicle associated protein (PV1); arrows indicate example regions with clear PV1 structures (punctate staining). Scale bars: 50 µm. Images shown are from donor A and

are representative of experiments with cells from 3 different human donors each with 5 device replicates per experiment. (B) Quantitative comparison of HKMEC cell count between "Monoculture, VEGF-" and "Monoculture VEGF+" conditions; and "Coculture, VEGF-" and "Coculture, VEGF+" conditions. (C) Quantitative comparison of HKMEC cell size between "Coculture, VEGF-" and "Monoculture, VEGF-" conditions; and "Coculture, VEGF-" and "Coculture, VEGF+" conditions. Error bars represent the SEM of 5 device replicates for a single human donor (donor A) in a single experiment. Data sets were analyzed using a one-way ANOVA test; p-values are indicated for Tukey's multiple comparisons tests. (**p≤ 0.01, ****p ≤ 0.0001)

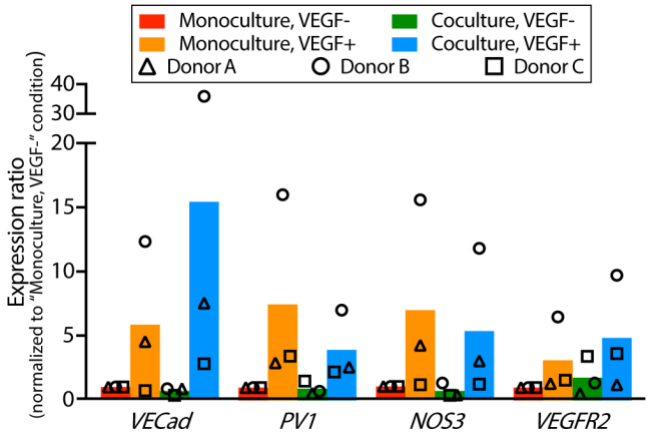

Figure 4.9. RT-qPCR data showing downregulation of selected HKMEC genes in VEGF-free media (red and green bars), suggesting an important role of VEGF in endothelial cell growth and development.

Each plotted point represents data from an independent human donor (pooled from 5 replicate microculture devices per donor, average of 3 RT-qPCR technical replicates), with each normalized to the "Monoculture, VEGF-" condition (which is set to 1). Each colored bar represents the average ratio of the 3 donors.

4.8 REFERENCES

[1] Al-Awqati Q. Goldman's Cecil Medicine. . 2012.

[2] Álvarez-García YR, Ramos-Cruz K, Agostini-Infanzón RJ, Stallcop LE, Beebe DJ, Warrick JW, et al. Open multi-culture platform for simple and flexible study of multi-cell type interactions. *Lab Chip*. 2018;18(**20**):3184-95.

[3] Basile DP. Rarefaction of peritubular capillaries following ischemic acute renal failure: a potential factor predisposing to progressive nephropathy. *Curr Opin Nephrol Hypertens*. 2004 Jan;13(**1**):1-7.

[4] Bayless KJ, Johnson GA. Role of the cytoskeleton in formation and maintenance of angiogenic sprouts. *J Vasc Res*. 2011;48(**5**):369-85.

[5] Berry SB, Zhang T, Day JH, Su X, Wilson IZ, Berthier E, et al. Upgrading well plates using open microfluidic patterning. *Lab Chip*. 2017;17(**24**):4253-64.

[6] Berthier E, Dostie AM, Lee UN, Berthier J, Theberge AB. Open Microfluidic Capillary Systems. *Anal Chem*. 2019;91(**14**):8739-50.

[7] Berthier E, Young EW, Beebe D. Engineers are from PDMS-land, Biologists are from Polystyrenia. *Lab Chip*. 2012 Apr 7;12(**7**):1224-37.

[8] Bhatia SN, Ingber DE. Microfluidic organs-on-chips. *Nat Biotechnol*. 2014 Aug;32(**8**):760-72.

[9] Brenner BM, Falchuk KH, Keimowitz RI, Berliner RW. The relationship between peritubular capillary protein concentration and fluid reabsorption by the renal proximal tubule. *J Clin Invest*. 1969 Aug;48(**8**):1519-31.

[10] Bustin SA, Benes V, Garson JA, Hellemans J, Huggett J, Kubista M, et al. The MIQE guidelines: minimum information for publication of quantitative real-time PCR experiments. *Clin Chem*. 2009 Apr;55(**4**):611-22.

[11] Byrne MB, Leslie MT, Patel HS, Gaskins HR, Kenis PJA. Design considerations for open-well microfluidic platforms for hypoxic cell studies. *Biomicrofluidics*. 2017;11(**5**):054116.

[12] Cao J, Ehling M, Marz S, Seebach J, Tarbashevich K, Sixta T, et al. Polarized actin and VE-cadherin dynamics regulate junctional remodelling and cell migration during sprouting angiogenesis. *Nat Commun*. 2017 Dec 20;8(**1**):221-8.

[13] Casavant BP, Berthier E, Theberge AB, Berthier J, Montanez-Sauri SI, Bischel LL, et al. Suspended microfluidics. *Proceedings of the National Academy of Sciences*. 2013 June 18;110(**25**):10111-6.

[14] Chi JT, Chang HY, Haraldsen G, Jahnsen FL, Troyanskaya OG, Chang DS, et al. Endothelial cell diversity revealed by global expression profiling. *Proc Natl Acad Sci U S A*. 2003 Sep 16;100(**19**):10623-8.

[15] Clissold RL, Hamilton AJ, Hattersley AT, Ellard S, Bingham C. HNF1B-associated renal and extra-renal disease-an expanding clinical spectrum. *Nat Rev Nephrol*. 2015 Feb;11(**2**):102-12.

[16] Cook-Mills J, Deem TL. Active participation of ECs in inflammation. *J Leukoc Biol*. 2005;77(**4**):487-95.

[17] Curtis AS, Forrester JV, McInnes C, Lawrie F. Adhesion of cells to polystyrene surfaces. *J Cell Biol*. 1983 Nov;97(**5 Pt 1**):1500-6.

[18] Day JH, Nicholson TM, Su X, van Neel TL, Clinton I, Kothandapani A, et al. Injection molded open microfluidic well plate inserts for user-friendly coculture and microscopy. *Lab Chip*. 2020;20(**1**):107-19.

[19] Deem TL, Cook-Mills J. Vascular cell adhesion molecule 1 (VCAM-1) activation of endothelial cell matrix metalloproteinases: role of reactive oxygen species. *Blood*. 2004;104(**8**):2385-93.

[20] Dejana E, Hirschi KK, Simons M. The molecular basis of endothelial cell plasticity. *Nature Communications*. 2017; **8**:14361.

[21] Esser S, Wolburg K, Wolburg H, Breier G, Kurzchalia T, Risau W. Vascular endothelial growth factor induces endothelial fenestrations in vitro. *J Cell Biol*. 1998 Feb 23;140(**4**):947-59.

[22] Ferrara N. Molecular and biological properties of vascular endothelial growth factor. *J Mol Med (Berl)*. 1999 Jul;77(**7**):527-43.

[23] Ferrara N. Role of vascular endothelial growth factor in the regulation of angiogenesis. *Kidney Int*. 1999 Sep;56(**3**):794-814.

[24] Ganter MT, Cohen MJ, Brohi K, Chesebro BB, Staudenmayer KL, Rahn P, et al. Angiopoietin-2, marker and mediator of endothelial activation with prognostic significance early after trauma? *Ann Surg*. 2008 Feb;247(**2**):320-6.

[25] Halldorsson S, Lucumi E, Gómez-Sjöberg R, Fleming RMT. Advantages and challenges of microfluidic cell culture in polydimethylsiloxane devices. *Biosensors and Bioelectronics*. 2015; **63**:218-31.

[26] Ito TK, Ishii G, Saito S, Yano K, Hoshino A, Suzuki T, et al. Degradation of soluble VEGF receptor-1 by MMP-7 allows VEGF access to ECs. *Blood*. 2009 Mar 5;113(**10**):2363-9.

[27] Kang DH, Kanellis J, Hugo C, Truong L, Anderson S, Kerjaschki D, et al. Role of the microvascular endothelium in progressive renal disease. *J Am Soc Nephrol*. 2002 Mar;13(**3**):806-16.

[28] Kim BS, Chen J, Weinstein T, Noiri E, Goligorsky MS. VEGF expression in hypoxia and hyperglycemia: reciprocal effect on branching angiogenesis in epithelial-endothelial co-cultures. *J Am Soc Nephrol*. 2002 Aug;13(**8**):2027-36.

[29] Kramann R, Humphreys BD. Kidney pericytes: roles in regeneration and fibrosis. *Semin Nephrol.* 2014 Jul;34(**4**):374-83.

[30] Lee UN, Su X, Guckenberger DJ, Dostie AM, Zhang T, Berthier E, et al. Fundamentals of rapid injection molding for microfluidic cell-based assays. *Lab Chip*. 2018;18(**3**):496-504.

[31] Lee Y, Choi JW, Yu J, Park D, Ha J, Son K, et al. Microfluidics within a well: an injection-molded plastic array 3D culture platform. *Lab Chip*. 2018;18(**16**):2433-40.

[32] Li Y, Wingert RA. Regenerative medicine for the kidney: stem cell prospects & challenges. *Clin Transl Med*. 2013 May 21;2(**1**):1-11.

[33] Ligresti G, Nagao RJ, Xue J, Choi YJ, Xu J, Ren S, et al. A Novel Three-Dimensional Human Peritubular Microvascular System. *J Am Soc Nephrol*. 2016 Aug;27(**8**):2370-81.

[34] Liu Y. Cellular and molecular mechanisms of renal fibrosis. *Nat Rev Nephrol*. 2011 Oct 18;7(**12**):684-96.

[35] Lloyd AC. The regulation of cell size. *Cell*. 2013 Sep 12;154(**6**):1194-205.

[36] Maeshima Y, Makino H. Angiogenesis and chronic kidney disease. *Fibrogenesis Tissue Repair*. 2010 Aug **5**;3:1-13.

[37] Marcu R, Choi YJ, Xue J, Fortin CL, Wang Y, Nagao RJ, et al. Human Organ-Specific Endothelial Cell Heterogeneity. *iScience*. 2018;**4**:20-35.

[38] Nangaku M. Chronic hypoxia and tubulointerstitial injury: a final common pathway to end-stage renal failure. *J Am Soc Nephrol*. 2006 Jan;17(**1**):17-25.

[39] Nolan DJ, Ginsberg M, Israely E, Palikuqi B, Poulos MG, James D, et al. Molecular signatures of tissue-specific microvascular endothelial cell heterogeneity in organ maintenance and regeneration. *Dev Cell*. 2013 Jul 29;26(**2**):204-19.

[40] Oh S, Ryu H, Tahk D, Ko J, Chung Y, Lee HK, et al. "Open-top" microfluidic device for in vitro three-dimensional capillary beds. *Lab Chip*. 2017;17(**20**):3405-14.

[41] Palpant NJ, Pabon L, Friedman CE, Roberts M, Hadland B, Zaunbrecher RJ, et al. Generating high-purity cardiac and endothelial derivatives from patterned mesoderm using human pluripotent stem cells. *Nature Protocols*. 2016;12:15.

[42] Palygin O, Levchenko V, Ilatovskaya DV, Pavlov TS, Pochynyuk OM, Jacob HJ, et al. Essential role of Kir5.1 channels in renal salt handling and blood pressure control. *JCI insight*. 2017;2(**18**):e92331.

[43] Park SA, Jeong MS, Ha K, Jang SB. Structure and function of vascular endothelial growth factor and its receptor system. *BMB reports*. 2018;51(**2**):73-8.

[44] Redd MA, Zeinstra N, Qin W, Wei W, Martinson A, Wang Y, et al. Patterned human microvascular grafts enable rapid vascularization and increase perfusion in infarcted rat hearts. *Nature Communications*. 2019;10(**1**):584.

[45] Regehr KJ, Domenech M, Koepsel JT, Carver KC, Ellison-Zelski SJ, Murphy WL, et al. Biological implications of polydimethylsiloxane-based microfluidic cell culture. *Lab Chip*. 2009 Aug 7;9(**15**):2132-9.

[46] Rudnicki M, Perco P, Enrich J, Eder S, Heininger D, Bernthaler A, et al. Hypoxia response and VEGF-A expression in human proximal tubular epithelial cells in stable and progressive renal disease. *Lab Invest*. 2009 Mar;89(**3**):337-46.

[47] Rusu L, Minshall R. Endothelial Cell von Willebrand Factor Secretion in Health and Cardiovascular Disease. In: ; 2018.

[48] Sackmann EK, Fulton AL, Beebe DJ. The present and future role of microfluidics in biomedical research. *Nature*. 2014 Mar 13;507(**7491**):181-9.

[49] Spontaneous Capillary Flow Between Horizontal Rails. Open Microfluidics. 2016.

[50] Stan R, Tse D, Deharvengt S, Smits N, Xu Y, Luciano M, et al. The Diaphragms of Fenestrated Endothelia: Gatekeepers of Vascular Permeability and Blood Composition. *Developmental Cell*. 2012;23(**6**):1203-18.

[51] Szmitko PE, Wang Chao-Hung, Weisel RD, de Almeida JR, Anderson TJ, Subodh V. New Markers of Inflammation and Endothelial Cell Activation. *Circulatio*n. 2003;108(**16**):1917-23.

[52] Tasnim F, Zink D. Cross talk between primary human renal tubular cells and ECs in cocultures. *Am J Physiol Renal Physiol*. 2012 Apr 15;302(**8**):1055.

[53] Tourovskaia A, Fauver M, Kramer G, Simonson S, Neumann T. Tissue-engineered microenvironment systems for modeling human vasculature. *Exp Biol Med (Maywood)*. 2014 Sep;239(**9**):1264-71.

[54] van Midwoud PM, Janse A, Merema MT, Groothuis GM, Verpoorte E. Comparison of biocompatibility and adsorption properties of different plastics for advanced microfluidic cell and tissue culture models. *Anal Chem*. 2012 May 1;84(**9**):3938-44.

[55] Vedula EM, Alonso JL, Arnaout MA, Charest JL. A microfluidic renal proximal tubule with active reabsorptive function. *PLoS One*. 2017 Oct 11;12(**10**):e0184330.

[56] Vempati P, Popel AS, Mac Gabhann F. Extracellular regulation of VEGF: isoforms, proteolysis, and vascular patterning. *Cytokine Growth Factor Rev*. 2014;25(**1**):1-19.

[57] Villegas G, Lange-Sperandio B, Tufro A. Autocrine and paracrine functions of vascular endothelial growth factor (VEGF) in renal tubular epithelial cells. *Kidney Int*. 2005 Feb;67(**2**):449-57.

[58] Walsh EJ, Feuerborn A, Wheeler JHR, Tan AN, Durham WM, Foster KR, et al. Microfluidics with fluid walls. *Nat Commun*. 2017 Oct 10;8(**1**):81-4.

[59] Winterbourn CC. Reconciling the chemistry and biology of reactive oxygen species. *Nat Chem Biol*. 2008 May;4(**5**):278-86.

[60] Young EW, Berthier E, Beebe DJ. Assessment of enhanced autofluorescence and impact on cell microscopy for microfabricated thermoplastic devices. *Anal Chem*. 2013 Jan 2;85(**1**):44-9.

[61] Young EWK, Beebe DJ. Fundamentals of microfluidic cell culture in controlled microenvironments. *Chem Soc Rev*. 2010;39(**3**):1036-48.

[62] Zhao Y, Zhao H, Zhang Y, Tsatralis T, Cao Q, Wang Y, et al. Isolation and epithelial co-culture of mouse renal peritubular ECs. *BMC cell biology*. 2014;15:40; 4-40.

Chapter 5. DEVELOPING A MICROSCALE COCULTURE PLATFORM TO STUDY AIRWAY FIBROSIS IN ASTHMA

This chapter is preliminary work and will be continued by another group member in Theberge Lab after Tianzi Zhang graduates.

5.1 INTRODUCTION AND MOTIVATION

Asthma is a common inflammatory pulmonary disease with manifestations including wheezing, coughing, and chest tightness, affecting more than 25 million of the US population according to the Centers for Disease Control and Prevention (CDC) in 2019. Although drugs such as corticosteroids can treat the symptoms of asthma effectively, they are unable to prevent or reverse airway remodeling (the structural and compositional changes of the airway wall) [1].

Subepithelial fibrosis is associated with airway wall thickening during the remodeling process. It has been observed that the thickened airway walls contain excessive extracellular matrix (ECM) proteins generated and deposited by myofibroblasts, which are a transdifferentiated form of fibroblasts with enhanced contractility [1-4]. As a tissue repair strategy, myodifferentiation (i.e., differentiation of fibroblasts into myofibroblasts) is regulated by signaling factors in the microenvironment during inflammation [1, 3, 6-9]. However, recent studies indicate that pulmonary macrophages from patients with asthma secrete imbalanced pro-fibrotic leukotriene B4 (LTB4) and anti-fibrotic lipoxin A4 (LXA4) lipid molecules causing myodifferentiation of pulmonary fibroblasts, which triggers fibrosis and ultimately exacerbation of the disease [7, 9].

As an important part of the airway remodeling mechanism, macrophage-induced myodifferentiation should be further studied due to the urgent need to develop effective anti-fibrosis treatments [10-12]. However, traditional pathogenic studies based on mouse models are insufficient to address the phenotypic heterogeneity in patients and complexity of cellular events during airway inflammation [13]. Although some invasive medical procedures including bronchoscopies could harvest small amounts of primary tissue from patients, very limited amount of the cell sample can be utilized for *in vitro* cell culture studies, making it difficult to conduct pathological studies with existing platforms, such as a Petri Dish or Transwell [2, 14].

Therefore, our overall research objective is to use the established microfluidic coculture device described in Chapter 4 to model human lung fibroblast differentiation in asthma. Specifically, human lung fibroblasts are cultured with primary alveolar macrophages from donors with or without asthma diseases to determine if asthmatic alveolar macrophages secrete soluble factors that induce myodifferentiation. Briefly, the first part of this project entails developing a quantitative florescence readout for myodifferentiation in the microscale device. Human lung fibroblasts are differentiated into a more contractile phenotype that can be identified through increased fibronectin uptake or smooth muscle actin expression. Next, human lung fibroblasts and alveolar macrophages are cultured separately in the microfluidic coculture device. The hypothesis for this study is that asthmatic alveolar macrophages will cause an imbalance of pro- and anti-inflammatory factors in the microenvironment which induces lung fibroblast myodifferentiation in airway tissue remodeling.

5.2 MATERIALS AND METHODS

5.2.1 *Device Fabrication*

Open microfluidic devices were designed with Solidworks 2016 ×64 (Solidworks, Waltham, MA) and converted to .TAP files with Sprutcam (Sprutcam, Naberezhnye Chelny, Russia). Devices were milled using a Series 3 PCNC Mill (Tormach, Waunakee, WI). The detailed device milling, solvent bonding and plasma treating procedures can be found in Section 4.3.1. The device employed in this chapter had the similar overall structure of the device described in Chapter 4 but with smaller dimensions (the seeding areas of the center and side chambers are 8 mm^2 and 14 mm^2, respectively).

5.2.2 *Biocompatibility Test*

Primary alveolar fibroblast cell line IMR-90 was purchased from ATCC. Alveolar macrophages from asthma patients were provided by Denlinger's group in University of Wisconsin-Madison. IMR-90 cells were cultured in EMEM (Eagle's Minimum Essential Medium) with 10 % fetal bovine serum (FBS, Gibco), penicillin (100 unit/mL), and streptomycin (100 μg/mL). Expanded populations of fibroblasts were maintained in a 37° C incubator with 5% carbon dioxide and used from passage 2-5. Primary macrophages were thawed and recovered immediately before seeding in RPMI with 10 % fetal bovine serum (FBS, Gibco), penicillin (100 unit/mL), and streptomycin (100 μg/mL). Macrophages and fibroblasts were seeded into the center and the side chamber of the coculture device, respectively. The device was maintained in a 37° C incubator with 5% carbon dioxide for up to two days followed by live/dead labeling (0.01 mM Calcein AM and 2 nM Ethidium homodimer-1 (LIVE/DEAD® Viability/Cytotoxicity Kit for mammalian cells, Invitrogen)).

5.2.3 *Fibronectin Incorporation Assay*

A previously developed fibronectin incorporation assay was modified [2, 15]. IMR-90 cells were plated into the side chamber of the device at 625 cells/mm^2 and allowed to recover overnight in the presence of 10 μM cycloheximide (Sigma-Aldrich) to block endogenous fibronectin expression. On the next day, the media was changed and half of the microwells were treated with 10 ng/mL transforming growth factor-β (TGF-β, Calbiochem) to induce myodifferentiation. Alexa488-labeled Fibronectin (FN 488, Cytoskeleton) was mixed into each microwell at 4 μg/mL. The cells were incubated for 24 h then washed twice with phosphate-buffered saline (PBS), and fixed with 4% paraformaldehyde (PFA) for 20 min at room temperature. A 1:1000 dilution of DAPI (Invitrogen) was added and incubated for 5 min. The samples were washed twice, mounted with PBS, and covered with a glass slip to prevent sample dehydration during imaging. The protected device was fitted directly into the mounting frame for fluorescence microscopy.

5.2.4 *Coculture of Alveolar Macrophages and Lung Fibroblasts*

The procedure was adapted from an established conditioned media experiment [16]. Alveolar macrophages were plated into the center compartment of the microwell at 1316 cells/mm^2. IMR-90 cells were plated as described before. After adherence and spreading overnight, the media in each microwell was withdrawn and replaced with 50 μL of RPMI media containing FN 488 (4 μg/mL) and TCM™ (MP Biomedicals) replacement as serum supplements, in the presence (or absence) of 250 μM Bz-ATP (Sigma-Aldrich). The cells were then incubated for 24 h followed by fixation and fluorescence microscopy.

5.2.5 *Statistical Analysis*

The integrated intensity of both replicate images was averaged. The plotted points represent the average of three images (collected for each of the three replicate wells), and the plotted standard error of the mean (SEM) is the SEM of the three replicate wells. Fluorescence images were quantified with Fiji following the protocol: “Subtract Background > Adjust Brightness/Contrast > Analyze > Measure > IntDen”. Prism (GraphPad Software) was used to conduct a two-tailed unpaired Student's t-test.

5.3 RESULTS AND DISCUSSION

This chapter is preliminary work and will be continued by another group member in Theberge Lab after Tianzi Zhang graduates.

5.3.1 *Biocompatibility of Primary Alveolar Macrophages in the Microfluidic Device*

Figure 5.1 shows the viability result at 72 h for primary macrophages, which are the more sensitive and short-lived cell type in these experiments. With prolonged culture time, more than half of the primary macrophages stayed alive (green), which qualitatively suggested the device is a potential tool to investigate soluble factor signaling and biophysical activities between different cell types.

5.3.2 *Developing FN Incorporation Assay in the Microfluidic Coculture Device*

Fibronectin is secreted and assembled into ECM, which provides structural support for the microenvironment and facilitates biological activities including wound healing and tissue remodeling after injury [2, 15]. Previous studies indicated a correlation between elevated alveolar ECM deposition caused by fibroblast myodifferentiation and fibrosis in asthma [2, 3, 5, 15].

Therefore, FN incorporation levels can be used as a parameter to investigate if asthmatic alveolar macrophages accelerate ECM incorporation by inducing myodifferention [2].

A modified FN incorporation assay was performed in the microscale device, which allowed for quantitative comparison of rates of FN incorporation between native IMR-90 cells and the TGF-β-induced myodifferentiated IMR-90 cells [2, 15]. Briefly, IMR-90 cells were seeded into the side chamber of each microwell in the presence of cycloheximide, a known fibronectin inhibitor to block innate FN expression. After 6 h of incubation, half of the microwells were treated with FN-488 as a control group, and the other half were treated with FN-488 in the presence of TGF-β, an established inducer of myodifferentiation and a pro-fibrotic factor generated by inflammatory cells *in vivo*, as the treatment group. After 24 h of incubation, the FN incorporation of both groups was quantified with fluorescence microscopy.

Figure 5.2 shows the preliminary result of the microscale FN incorporation assay, which suggests that TGF-β treated IMR-90 cells incorporated extracellular fibrillary matrix to a greater extent than the undifferentiated IMR-90 cells (control) after 24 h, independent of endogenous FN expression (p value < 0.05 using Student's t-test). These results are consistent with similar experiments performed in traditional 8-well chamber slides [2]. The microscale FN incorporation assay validated the functionality of the microscale coculture device and could serve as a myodifferentiation readout for the subsequent coculture experiment.

5.3.3 *Developing Human Lung Fibroblasts and Alveolar Macrophages Coculture Assay*

Researchers have discovered that during airway inflammation, alveolar macrophages from patients with asthma release imbalanced lipid mediators *in vivo* which is attributed to attenuated P2X7

nucleotide receptor activities [16-22]. Primarily expressed by leukocytes, including macrophages and dendritic cells, P2X7 is a ligand-gated membrane receptor which has high affinity for extra-cellular ATP (eATP) generated during epithelial injury or pulmonary inflammatory responses [18, 19, 22]. The prolonged exposure of P2X7 to the eATP ligand activates a nonspecific pore on cell membranes allowing small cationic molecules to pass through, inducing subsequent depolarization events including Ca^{2+} influx, which further triggers downstream soluble mediator signaling cascades across different cell types [18, 19]. The normal P2X7 activity in non-asthmatic macrophages upregulates cyclooxygenase-2 (COX2) expression, which is a rate-limiting enzyme required for anti-fibrotic eicosanoid synthesis including anti-inflammatory prostaglandin E2 (PGE2) and anti-fibrotic lipoxin A4 (LXA4) [18-20]. Consequently, the defective pore function also causes dysregulation of dendritic cell-derived recruitment of leukocytes (including eosinophils, neutrophils and lymphocytes) and pro-inflammatory cytokines (including interleukin-1b), all of which play important roles in immune response [17, 19, 20, 21].

Since the stimulation of eATP is required to trigger abnormal P2X7 activity during asthma attacks *in vivo*, we used Bz-ATP, a potent analog of eATP, to activate imbalanced eicosanoid secretion of P2X7 in primary alveolar macrophages from patients with asthma [18]. Because lung fibroblasts express much lower level P2X7 as compared to alveolar macrophages, the exposure to Bz-ATP in the microscale *in vitro* model should not have major impact on fibroblasts [17, 18]. Figure 5.3 shows the preliminary results of the microscale coculture assay, which suggests that IMR-90 had higher rate of FN-488 uptake when cocultured with alveolar macrophages from asthma patients in the presence of Bz-ATP (p value < 0.05 using Student's t-test). This result supports the idea that during inflammation, alveolar macrophages from asthma patients can trigger alveolar fibroblasts to undergo myodifferentiation, resulting in a higher rate of extracellular deposition.

5.4 Conclusion and Future Direction

Most cells in the human body are attached to ECM components, and intercellular communication is implemented by the diffusion of signaling molecules in the surrounding microenvironment. Traditional cell culture platforms allow people to study signaling effects of certain factors *in vitro* and propose specific mechanisms for certain cell activities. However, the relatively large consumption of tissue samples and expensive reagents associated with standard cell culture studies limits the use of primary patient cells in pathological research. Fortunately, the emergence of microscale lab-on-a-chip system has solved some of the problems, as the flexibilities embedded in the design and fabrication process of the device can improve the accuracy and efficiency of the *in vitro* model. The microscale coculture device presented here contributes to the field of microfluidic technology in several aspects. Specifically, (1) the incorporation of an open boundary in the microscale platform improves its accessibility and simplifies the operation requirement; (2) the integration of an optically transparent floor and high-resolution fluorescent microscopy yields measurable readout for quantitative analysis; (3) controllability of the device structure and array pattern accommodates the device to specific applications; and (4) the stability and portability of the fabrication material ensures safety of cell-based research. Our group is currently developing injection molding techniques specifically for open device fabrication, which would significantly increase the fabrication efficiency and reduce the cost of production.

A previous study quantifying enzyme expression in stimulated primary alveolar macrophages and corresponding eicosanoid concentrations in the microenvironment reported that following Bz-ATP treatment, LTB4 and LXA4 were released within 10 min, and PGE2 was released at 12-24 h [16]. The reason for quantifying anti-inflammatory PGE2 was because the defective P2X7 pore function

in asthmatic macrophages would downregulate COX2 expression, which then leads to deficient PGE2 generation [18, 19, 21]. PGE2 has indirect control (through 15lipoxygenase (LO)) over 5LO, a mutual synthetase of pro-fibrotic LTB4 and anti-fibrotic LXA4 [23]. In future experiments, the conditioned media from the coculture experiment should be collected and the concentrations of LTB4, LXA4, and PGE2 could be detected using liquid chromatography–mass spectrometry (LC-MS), which are expected to be on the order of pg/mL. Combined liquid chromatography–electrospray ionization-tandem mass spectrometry (LC–ESI-MS/MS) method established in recent years have brought the detection limits of eicosanoid concentrations down to the order of fg/mL, which can be hard to measure using traditional analytical methods [24]. The quantitative analysis of dynamic small molecule profiles is crucial to pharmacokinetic research and future drug development. It is noteworthy that P2X7 is also expressed in epithelial cells during respiratory inflammation [17], and the generation of eATP would stimulate the endogenous P2X7 receptor to release more eATP *in vivo*.

In summary, the preliminary data of the microscale coculture experiment suggests the capacity of the open microfluidic coculture device to study pulmonary fibrosis and the crosstalk between inflammatory mediators in asthma. The complexities associated with P2X7 and its downstream signaling events are worth studying further, and the proposed open microfluidic coculture system serves as a convenient tool for future investigations.

5.5 FIGURES

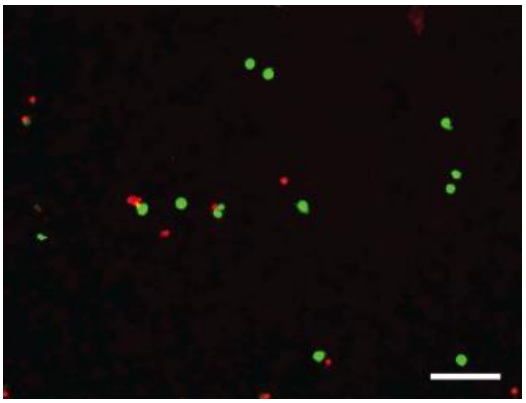

Figure 5.1. Viability test of the primary alveolar macrophages in the central compartment of the microscale device after 72 h.

The cells were treated with 0.01 mM Calcein AM and 2 nM Ethidium homodimer-1 for 20 min immediately before imaging. Live cells were stained green (left) and dead cells were stained red (middle). The two images are merged for qualitative comparison (right). (Scale bar = 100 μM)

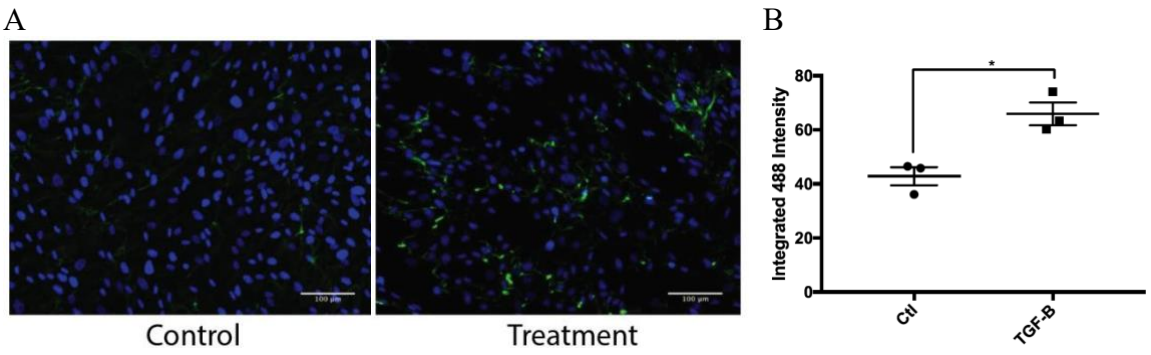

Figure 5.2. FN-488 incorporation by fibroblasts with and without TGF-β treatment in the open microfluidic device at 24 h.

A) Merged images of FN-488 signals (green) and nuclear staining with DAPI (blue). TGF-β treated IMR-90 (treatment) showed higher FN-488 signal than the control (scale bar =100 μm). (B) Quantification of integrated 488 intensity using ImageJ and Student's t-test. Error bars represent the SEM of three replicates from one independent experiment. (* $p < 0.05$).

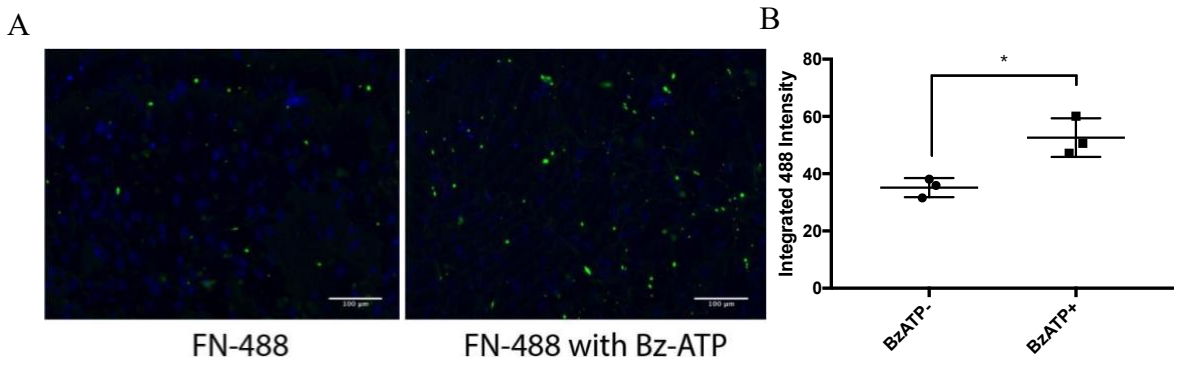

Figure 5.3. Fibroblasts cocultured with alveolar macrophages and treated with Bz-ATP showed increased FN-488 incorporation.

(A) Merged images of FN-488 signals (green) and nuclear staining with DAPI (blue) show IMR-90 had a higher rate of FN-488 uptake in cocuture with alveolar macrophages in the presence of Bz-ATP (left). (Scale bar = 100 μm) (B) Quantification of integrated 488 intensity using ImageJ and Student's t-test. Error bars represent the SEM of three replicates from one independent experiment. (* $p < 0.05$).

5.6 REFERENCES

[1] Hinz B, Phan SH, Thannickal VJ, Galli A, Bochaton-Piallat ML, Gabbiani G. The myofibroblast: One function, multiple origins. *Am J Pathol* 2007 Jun;170(**6**):1807-16.

[2] Torr EE, Ngam CR, Bernau K, Tomasini-Johansson B, Acton B, Sandbo N. Myofibroblasts exhibit enhanced fibronectin assembly that is intrinsic to their contractile phenotype. *J Biol Chem* 2015 Mar 13;290(**11**):6951-61.

[3] Stumm CL, Wettlaufer SH, Jancar S, Peters-Golden M. Airway remodeling in murine asthma correlates with a defect in PGE2 synthesis by lung fibroblasts. *Am J Physiol Lung Cell Mol Physiol* 2011 Nov;301(**5**):L636-44.

[4] Levy BD, Bonnans C, Silverman ES, Palmer LJ, Marigowda G, Israel E, Severe Asthma Research Program, National Heart, Lung, and Blood Institute. Diminished lipoxin biosynthesis in severe asthma. *Am J Respir Crit Care Med* 2005 Oct 1;172(**7**):824-30.

[5] Bonnans C, Fukunaga K, Levy MA, Levy BD. Lipoxin A(4) regulates bronchialepithelial cell responses to acid injury. *Am J Pathol* 2006 Apr;168(**4**):1064-72.

[6] Liu M, Yokomizo T. The role of leukotrienes in allergic diseases. *Allergol Int* 2015 /1;64(**1**):17-26

[7] Ohnishi H, Miyahara N, Gelfand EW. The role of leukotriene B4 in allergic diseases. *Allergol Int* 2008 01/01;57(**4**):291-8.

[8] Miyata J, Arita M. Role of omega-3 fatty acids and their metabolites in asthma and allergic diseases. *Allergol Int* 2015 Jan;64(**1**):27-34.

[9] PlanagumÃ A, Kazani S, Marigowda G, Haworth O, Mariani TJ, Israel E, Bleecker ER, Curran-Everett D, Erzurum SC, Calhoun WJ, et al. Airway lipoxin A(4) generation and lipoxin A(4) receptor expression are decreased in severe asthma. *Am J Respir Crit Care Med* 2008 Sep 15;178(**6**):574-82.

[10] Ignotz RA, Massague J. Transforming growth factor-beta stimulates the expression of fibronectin and collagen and their incorporation into the extracellular matrix. *J Biol Chem* 1986 Mar 25;261(**9**):4337-45.

[11] Halwani R, Al-Muhsen S, Al-Jahdali H, Hamid Q. Role of transforming growth factor-beta in airway remodeling in asthma. *Am J Respir Cell Mol Biol* 2011 Feb;44(**2**):127-33.

[12] Baneyx G, Baugh L, Vogel V. Fibronectin extension and unfolding within cell matrix fibrils controlled by cytoskeletal tension. *Proceedings of the National Academy of Sciences* 2002 April 16;99(**8**):5139-43.

[13] Klein Wolterink RG, Kleinjan A, van Nimwegen M, Bergen I, de Bruijn M, Levani Y, Hendriks RW. Pulmonary innate lymphoid cells are major producers of IL-5 and IL-13 in murine models of allergic asthma. *Eur J Immunol* 2012 May;42(**5**):1106-16.

[14] Michalik M, Pierzchalska M, Legutko A, Ura M, Ostaszewska A, Soja J, Sanak M. Asthmatic bronchial fibroblasts demonstrate enhanced potential to differentiate into myofibroblasts in culture. *Med Sci Monit* 2009 Jul;15(**7**):BR194-201.

[15] Tomasini-Johansson BR, Johnson IA, Hoffmann FM, Mosher DF. Quantitative microtiter fibronectin fibrillogenesis assay: Use in high throughput screening for identification of inhibitor compounds. *Matrix Biol* 2012 Jul;31(**6**):360-7.

[16] Roti Roti EC, Torr EE, Fichtinger P, Guadarrama A, Sandbo N, Denlinger LC. Alveolar macrophages from subjects with asthma release pro-inflammatory LTB4 in ratio excess to LXA4 upon P2X7 stimulation, promoting fibrotic remodeling. In: d101. allergy and asthma: Novel regulatory pathways. *Am Thoracic Soc*; 2016.

[17] Bartlett R, Stokes L, Sluyter R. The P2X7 receptor channel: Recent developments and the use of P2X7 antagonists in models of disease. *Pharmacol Rev* 2014 Jul;66(**3**):638-75.

[18] Gavala ML, Hill LM, Lenertz LY, Karta MR, Bertics PJ. Activation of the transcription factor FosB/activating protein-1 (AP-1) is a prominent downstream signal of the extracellular nucleotide receptor P2RX7 in monocytic and osteoblastic cells. *J Biol Chem* 2010 Oct 29;285(**44**):34288-98.

[19] Denlinger LC, Manthei DM, Seibold MA, Ahn K, Bleecker E, Boushey HA, Calhoun WJ, Castro M, Chinchili VM, Fahy JV, et al. P2X7-regulated protection from exacerbations and loss of control is independent of asthma maintenance therapy. *Am J Respir Crit Care* Med 2013 Jan 1;187(**1**):28-33.

[20] Gudipaty L, Humphreys BD, Buell G, Dubyak GR. Regulation of P2X(7) nucleotide receptor function in human monocytes by extracellular ions and receptor density. *Am J Physiol Cell Physiol* 2001 Apr;280(**4**):C943-53.

[21] Denlinger LC, Shi L, Guadarrama A, Schell K, Green D, Morrin A, Hogan K, Sorkness RL, Busse WW, Gern JE. Attenuated P2X7 pore function as a risk factor for virus-induced loss of asthma control. *Am J Respir Crit Care* Med 2009 Feb 15;179(**4**):265-70.

[22] Riteau N, Gasse P, Fauconnier L, Gombault A, Couegnat M, Fick L, Kanellopoulos J, Quesniaux VF, Marchand-Adam S, Crestani B, et al. Extracellular ATP is a danger signal activating P2X7 receptor in lung inflammation and fibrosis. *Am J Respir Crit Care Med* 2010 Sep 15;182(**6**):774-83.

[23] Kowal-Bielecka O, Kowal K, Distler O, Rojewska J, Bodzenta-Lukaszyk A, Michel BA, Gay RE, Gay S, Sierakowski S. Cyclooxygenase- and lipoxygenase-derived eicosanoids in bronchoalveolar lavage fluid from patients with scleroderma lung disease: An imbalance between proinflammatory and antiinflammatory lipid mediators. *Arthritis Rheum* 2005 Dec;52(**12**):3783-91.

[24] Bollinger JG, Thompson W, Lai Y, Oslund RC, Hallstrand TS, Sadilek M, et al. Improved sensitivity mass spectrometric detection of eicosanoids by charge reversal derivatization. *Anal Chem*. 2010;82(**16**):6790-6.

Chapter 6. SUMMARY AND FUTURE WORK

In conclusion, this dissertation gives an overview of the fundamental development of open microfluidics and our approaches to investigate intercellular signaling interactions underlying human diseases by developing open microfluidic cell culture tools. Our overarching research goal is to use simple engineering design principles to fabricate affordable microscale tools that can be easily adopted by general biological users to address their own research questions.

In Chapter 2, we presented a microfluidic rail-based patterning device, the Monorail Device, which can pattern hydrogel walls inside a conventional well plate to create spatial segregation. Importantly, the Monorail insert allows the use of the native cell culture substrate while creating permeable dividers to support small molecule signaling between the different cell types. In Chapter 3, we developed a microscale collagen gel contraction (CGC) device, which can measure cell-induced hydrogel contractility in a coculture environment. Both the Monorail Device and microscale CGC device function as 3D printed well plate inserts, reflecting that certain aspects of open microfluidic technology could be simply integrated into established cell culture platforms to achieve biological models with greater structural complexity.

In Chapter 4, we developed a microfluidic coculture device to study the paracrine signaling effect of human kidney proximal tubule epithelial cells with human endothelial cells from different sources. The polystyrene-based microfluidic coculture platform allows for culturing precious and sensitive primary human patient cells *in vitro* and conducting standard immunocytochemistry and qPCR studies *in situ*. In Chapter 5, we discussed the possibility of using the same microfluidic coculture device to study the paracrine signaling effect between human lung fibroblasts and primary alveolar macrophages. Based on these preliminary data for the cell coculture experiments

(Chapter 5), it is possible that the present coculture device has the potential to be modified and utilized to investigate macrophage-induced lung fibroblast differentiation; this is an area of ongoing future work.

Moving forward, a future direction for the current research efforts includes understanding the specific soluble factors (proteins, metabolites, and secondary metabolites) in the dynamic microenvironment. With the existing open microfluidic platforms, we provide opportunities for researchers to easily sample conditioned media during the course of the experiment, and also collect cells or extract soluble factors or other cell secretions from hydrogels at the endpoint. The analytes of interest could be captured and assessed with quantification methods such as ELISA or mass spectrometry. A more detailed and dynamic profile for the signaling molecules involved in the biological process could reveal profound disease mechanisms and point to a new direction for translational research.

BIBLIOGRAPHY

A.D. Gracz, I.A. Williamson, K.C. Roche, M.J. Johnston, F. Wang, Y. Wang, P.J. Attayek, J. Balowski, X.F. Liu, R.J. Laurenza, L.T. Gaynor, C.E. Sims, J.A. Galanko, L. Li, N.L.

Allbritton, S.T. Magness, "A high-throughput platform for stem cell niche co-cultures and downstream gene expression analysis", *Nature Cell Biology*, 2015, **17**, 340-349.

A.K. Au, W. Huynh, L.F. Horowitz, A. Folch; "3D-Printed Microfluidics". *Angew. Chem. Int. Ed.* 2016, **55**, 3862 – 3881.

A.K. Au, W. Lee, A. Folch, "Mail-order microfluidics: evaluation of stereolithography for the producton of microfluidic devics." *Lab Chip*, 2014, **14**, 1294.

A.P. Wong, R. Perez-Castillejos, J.C. Love, G.M. Whitesides, "Partitioning microfluidic channels with hydrogel to construct tunable 3-D cellular microenvironments." *Biomaterials*, 2008, **29**, 1853-1861.

Ackerman S. J., Du J., Xin F., Dekoter R., McKercher S., Mak I. R., et al. (2000). Eosinophilopoiesis: to be or not to be (an eosinophil)? That is the question: transcriptional mechanisms regulating eosinophil genes and development. *Respir. Med.* **94**, 1135–1138.

Al-Awqati Q. Goldman's Cecil Medicine. . 2012.

Álvarez-García YR, Ramos-Cruz K, Agostini-Infanzón RJ, Stallcop LE, Beebe DJ, Warrick JW, et al. Open multi-culture platform for simple and flexible study of multi-cell type interactions. *Lab Chip*. 2018;18(**20**):3184-95.

Armistead FJ, Gala De Pablo J, Gadêlha H, Peyman SA, Evans SD. Cells Under Stress: An Inertial-Shear Microfluidic Determination of Cell Behavior. *Biophysical Journal*. 2019;116(**6**):1127-35.

B.P. Casavant, E. Berthier, A.B. Theberge, J. Berthier, S.I. Montanez-Sauri, L.L. Bischel, et al. "Suspended Microfluidics." *PNAS*, 2016, April, **110**, 10111-10116.

Baneyx G, Baugh L, Vogel V. Fibronectin extension and unfolding within cell matrix fibrils controlled by cytoskeletal tension. *Proceedings of the National Academy of Sciences* 2002 April 16;99(**8**):5139-43.

Barkal LJ, Theberge AB, Guo C, Spraker J, Rappert L, Berthier J, et al. Microbial metabolomics in open microscale platforms. *Nature Communications*. 2016;7(**1**):10610.

Baroli B. Photopolymerization of biomaterials: issues and potentialities in drug delivery, tissue engineering, and cell encapsulation applications. *J Chem Technol Biotechnol*. 2006;81(**4**):491-9.

Bartlett R, Stokes L, Sluyter R. The P2X7 receptor channel: Recent developments and the use of P2X7 antagonists in models of disease. *Pharmacol Rev* 2014 Jul;66(**3**):638-75.

Basile DP. Rarefaction of peritubular capillaries following ischemic acute renal failure: a potential factor predisposing to progressive nephropathy. *Curr Opin Nephrol Hypertens*. 2004 Jan;13(**1**):1-7.

Baumann M. A., Paul C. C. (1998). The AML14 and AML14.3D10 cell lines: a long-overdue model for the study of eosinophils and more. *Stem Cells.* **16**, 16–24.

Bayless KJ, Johnson GA. Role of the cytoskeleton in formation and maintenance of angiogenic sprouts. *J Vasc Res*. 2011;48(**5**):369-85.

Beebe DJ, Mensing GA, Walker GM. Physics and Applications of Microfluidics in Biology. *Annu Rev Biomed Eng*. 2002;4(**1**):261-86.

Bell E, Ivarsson B, Merrill C. Production of a tissue-like structure by contraction of collagen lattices by human fibroblasts of different proliferative potential in vitro. *Proc Natl Acad Sci U S A*. 1979;76(**3**):1274-8.

Berry SB, Zhang T, Day JH, Su X, Wilson IZ, Berthier E, et al. Upgrading well plates using open microfluidic patterning. *Lab Chip*. 2017;17(**24**):4253-64.

Berthier E, Dostie AM, Lee UN, Berthier J, Theberge AB. Open Microfluidic Capillary Systems. *Anal Chem*. 2019;91(**14**):8739-50.

Berthier E, Warrick J, Yu H, Beebe DJ. Managing evaporation for more robust microscale assays Part 1. Volume loss in high throughput assays. *Lab Chip*. 2008;8(**6**):852-9.

Berthier E, Young EW, Beebe D. Engineers are from PDMS-land, Biologists are from Polystyrenia. *Lab Chip*. 2012 Apr 7;12(**7**):1224-37.

Berthier J, Brakke KA, Berthier E. Theory of Spontaneous Capillary Flows. In: Open Microfluidics. John Wiley & Sons, Inc.; 2016. p. 13-56.

Bhatia S. N., Ingber D. E. (2014). Microfluidic organs-on-chips. *Nat. Biotechnol*. **32**, 760–772.

Bhatia SN, Ingber DE. Microfluidic organs-on-chips. *Nat Biotechnol*. 2014 Aug;32(**8**):760-72.

Bollinger JG, Thompson W, Lai Y, Oslund RC, Hallstrand TS, Sadilek M, et al. Improved sensitivity mass spectrometric detection of eicosanoids by charge reversal derivatization. *Anal Chem*. 2010;82(**16**):6790-6.

Bonnans C, Fukunaga K, Levy MA, Levy BD. Lipoxin A(4) regulates bronchialepithelial cell responses to acid injury. *Am J Pathol* 2006 Apr;168(**4**):1064-72.

Brenner BM, Falchuk KH, Keimowitz RI, Berliner RW. The relationship between peritubular capillary protein concentration and fluid reabsorption by the renal proximal tubule. *J Clin Invest*. 1969 Aug;48(**8**):1519-31.

Bustin SA, Benes V, Garson JA, Hellemans J, Huggett J, Kubista M, et al. The MIQE guidelines: minimum information for publication of quantitative real-time PCR experiments. *Clin Chem*. 2009 Apr;55(**4**):611-22.

Byrne MB, Leslie MT, Patel HS, Gaskins HR, Kenis PJA. Design considerations for open-well microfluidic platforms for hypoxic cell studies. *Biomicrofluidics*. 2017;11(**5**):054116.

C.J. Flaim, S. Chien, S.N. Bhatia, "An extracellular matrix microarray for probing cellular differentiation." *Nature Methods*, 2005, Feb., **2**, 119-125. Feb. 2005.

C.M. Carney, J.L Muszynski, L.N. Strotman, S.R. Lewis, R.L. O'Connell, D.J. Beebe, A.B. Theberge, J.S. Jorgenson, "Cellular microenvironment dictates androgen production by murine fetal Leydig cells in primary culture", Biol Reprod, 2014, Oct., 91 (4), 85.

C.P. Huang, J. Li, H. Seon, A.P. Lee, L.A. Flanagan, H.Y. Kim, A.J. Putnam, N.L. Jeon, "Engineering microscale cellular niches for three-dimensional multicellular co-cultures". *Lab Chip*, 2009, **9**, 1740-1748.

C.Y. Li, K.R. Stevens, R.E. Schwartz, B.S. Alejandro, J.H. Huang, S.N. Bhatia, "Micropatterned cell-cell interactions enable functional encapsulation of primary hepatocytes in hydrogel microtissues". *Tissue Eng. Part A*, 2014, Aug, **20** (15-16), 2200-2212.

Cao J, Ehling M, Marz S, Seebach J, Tarbashevich K, Sixta T, et al. Polarized actin and VE-cadherin dynamics regulate junctional remodelling and cell migration during sprouting angiogenesis. *Nat Commun*. 2017 Dec 20;8(**1**):221-8.

Casavant BP, Berthier E, Theberge AB, Berthier J, Montanez-Sauri SI, Bischel LL, et al. Suspended microfluidics. *Proceedings of the National Academy of Sciences*. 2013 June 18;110(**25**):10111-6.

Casavant BP, Berthier E, Theberge AB, Berthier J, Montanez-Sauri SI, Bischel LL, et al. Suspended microfluidics. *Proceedings of the National Academy of Sciences*. 2013 June 18;110(**25**):10111-6.

Chan V, Zorlutuna P, Jeong JH, Kong H, Bashir R. Three-dimensional photopatterning of hydrogels using stereolithography for long-term cell encapsulation. *Lab Chip*. 2010;10(**16**):2062-70.

Chapuis J. F., Agache P. (1992). A new technique to study the mechanical properties of collagen lattices. *J. Biomech.* **2**5, 115–120.

Chen H. C., Yang T. H., Thoreson A. R., Zhao C., Amadio P. C., Sun Y. N., et al. . (2013). Automatic and quantitative measurement of collagen gel contraction using model-guided segmentation. *Meas. Sci. Technol.* **24**:85702.

Chen M. Y., Sun Y. L., Zhao C., Zobitz M. E., An K. N., Moran S. L., et al. . (2008). Substrate adhesion affects contraction and mechanical properties of fibroblast populated collagen lattices. *J. Biomed. Mater. Res. B Appl. Biomater.* **84**, 218–223.

Chen T, Saw TB, Mège R, Ladoux B. Mechanical forces in cell monolayers. *J Cell Sci*. 2018;131(**24**):jcs218156.

Chi JT, Chang HY, Haraldsen G, Jahnsen FL, Troyanskaya OG, Chang DS, et al. Endothelial cell diversity revealed by global expression profiling. *Proc Natl Acad Sci U S A*. 2003 Sep 16;100(**19**):10623-8.

Clissold RL, Hamilton AJ, Hattersley AT, Ellard S, Bingham C. HNF1B-associated renal and extra-renal disease-an expanding clinical spectrum. *Nat Rev Nephrol*. 2015 Feb;11(**2**):102-12.

Coluccio ML, Perozziello G, Malara N, Parrotta E, Zhang P, Gentile F, et al. Microfluidic platforms for cell cultures and investigations. *Microelectronic Engineering*. 2019;**208**:14-28.

Cook-Mills J, Deem TL. Active participation of ECs in inflammation. *J Leukoc Biol*. 2005;77(**4**):487-95.

Corning® PureCoat™ Cultureware, Corning Data Sheet CLS-DL-CC-046 REV1, 2013. Web. https://www.corning.com/media/worldwide/cls/documents/CLS-DL-CC-046_REV1.pdf. Accessed 8/12/17.

Curtis AS, Forrester JV, McInnes C, Lawrie F. Adhesion of cells to polystyrene surfaces. *J Cell Biol*. 1983 Nov;97(**5 Pt 1**):1500-6.

D. Patel, Y. Gao, K. Son, C. Siltanen, R.M. Neve, K. Ferrara, A. Revzin. "Microfluidic co-cultures with hydrogel-based ligand trap to study paracrine signals giving rise to cancer drug resistance", *Lab Chip*, 2015, **15**, 4614.

D.A. Lauffenburger, S.H. Zigmond. "Chemotactic factor concentration gradients in chemotaxis assay systems", *Journal of Immunological Methods*, **40**, (1981), 45-60.

D.R. Bogdanowicz and H.H. Lu. "Studying cell-cell communication in co-culture." *Biotechnol. J*. 2013, April, 8(**4**), 395-396.

D.R. Church, E. Lee, T.A. Thompson, H.S. Basu, M.O. Ripple, E.A. Ariazi, G. Wilding. "Induction of AP-1 Activity by Androgen Activation of the Androgen Receptor in LNCaP Human Prostate Carinoma Cells". *The Prostate*, 2005, **63**,155-168.

Dallon J. C., Ehrlich H. P. (2008). A review of fibroblast-populated collagen lattices. *Wound Repair Regen*. **16**, 472–479.

Day JH, Nicholson TM, Su X, van Neel TL, Clinton I, Kothandapani A, et al. Injection molded open microfluidic well plate inserts for user-friendly coculture and microscopy. *Lab Chip*. 2020;20(**1**):107-19.

de Groot TE, Veserat KS, Berthier E, Beebe DJ, Theberge AB. Surface-tension driven open microfluidic platform for hanging droplet culture. *Lab Chip*. 2016;16(**2**):334-44.

Deem TL, Cook-Mills J. Vascular cell adhesion molecule 1 (VCAM-1) activation of endothelial cell matrix metalloproteinases: role of reactive oxygen species. *Blood*. 2004;104(**8**):2385-93.

Dejana E, Hirschi KK, Simons M. The molecular basis of endothelial cell plasticity. *Nature Communications*. 2017; **8**:14361.

Denlinger LC, Manthei DM, Seibold MA, Ahn K, Bleecker E, Boushey HA, Calhoun WJ, Castro M, Chinchili VM, Fahy JV, et al. P2X7-regulated protection from exacerbations and loss of control is independent of asthma maintenance therapy. *Am J Respir Crit Care* Med 2013 Jan 1;187(**1**):28-33.

Denlinger LC, Shi L, Guadarrama A, Schell K, Green D, Morrin A, Hogan K, Sorkness RL, Busse WW, Gern JE. Attenuated P2X7 pore function as a risk factor for virus-induced loss of asthma control. *Am J Respir Crit Care* Med 2009 Feb 15;179(**4**):265-70.

Derby B. Bioprinting: inkjet printing proteins and hybrid cell-containing materials and structures. *J Mater Chem*. 2008;18(**47**):5717-21.

Duval K., Grover H., Han L. H., Mou Y., Pegoraro A. F., Fredberg J., et al. . (2017). Modeling physiological events in 2D vs. 3D cell culture. *Physiology (Bethesda)*. **32**, 266–277.

E. Berthier, E.W. Young, D.J. Beebe, "Engineers are from PDMS-land, biologists are from polystyrenia." *Lab Chip*, 2012, 12(**7**), 1224-37.

E. Mowat, R. Rajendran, C. Williams, E. McCulloch, B. Jones, S. Lang, G. Ramage. "*Pseudomonas aeruginosa* and their small diffusible extracellular molecules inhibit *Aspergillus fumigatus* biofilm formation", *FEMS Microbiol Lett*, 2010, **313**, 96-102.

E.E. Hui, S.N. Bhatia, “Micromechanical control of cell-cell interactions”. *PNAS*, 2007, April, **104**, 5722-5726.

E.W.K. Young, C. Pak, B.S. Kahl, D.T. Yang, N.S. Callander, S. Miyamoto, D.J. Beebe, “Microscale functional cytomics for studying hematologic cancers” *Blood*, 2012, **119**, e76-e85.

Epa A. P., Thatcher T. H., Pollock S. J., Wahl L. A., Lyda E., Kottmann R. M., et al. . (2015). Normal human lung epithelial cells inhibit transforming growth factor-β induced myofibroblast differentiation via prostaglandin E2. *PLoS ONE* **10**:e0135266.

Esnault S., Jarzembowski J. A., Malter J. S. (1998). Stabilization of granulocyte-macrophage colony-stimulating factor RNA in a human eosinophil-like cell line requires the AUUUA motifs. *Proc. Assoc. Am. Physicians.* **110**, 575–584.

Esser S, Wolburg K, Wolburg H, Breier G, Kurzchalia T, Risau W. Vascular endothelial growth factor induces endothelial fenestrations in vitro. *J Cell Biol*. 1998 Feb 23;140(**4**):947-59.

Ferrara N. Molecular and biological properties of vascular endothelial growth factor. *J Mol Med (Berl)*. 1999 Jul;77(**7**):527-43.

Ferrara N. Role of vascular endothelial growth factor in the regulation of angiogenesis. *Kidney Int*. 1999 Sep;56(**3**):794-814.

Flueckiger J, Bazargan V, Stoeber B, Cheung KC. Characterization of postfabricated parylene C coatings inside PDMS microdevices. *Sensors and Actuators B: Chemical*. 2011;160(**1**):864-74.

Forgacs G., Newman S. A., Hinner B., Maier C. W., Sackmann E. (2003). Assembly of collagen matrices as a phase transition revealed by structural and rheologic studies. *Biophys. J*. **84,** 1272–1280.

Franco, M. Jiang, D. W. Strand, J. Peacock, S. Fernandez, R.S. Jackson II, et al. “Altered TGF-β Signaling in a Subpopulation of Human Stromal Cells Promotes Prostatic Carcinogenesis”. *Cancer Res*., 2011, Feb., 71 (**4**), 1272-1281.

Fredriksson K., Lundahl J., Palmberg L., Romberger D. J., Liu X. D., Rennard S. I., et al. . (2003). Red blood cells stimulate human lung fibroblasts to secrete interleukin-8. *Inflammation.* **27**, 71–78.

Fujii T. PDMS-based microfluidic devices for biomedical applications. *Microelectronic Engineering*. 2002;**61-62**:907-14.

G.B. Huffnagle, M.C. Noverr. “The emerging world of the fungal microbiome”. *Trends Microbiol*, 2013, July, 7 (**21**), 334-341.

Ganter MT, Cohen MJ, Brohi K, Chesebro BB, Staudenmayer KL, Rahn P, et al. Angiopoietin-2, marker and mediator of endothelial activation with prognostic significance early after trauma? *Ann Surg.* 2008 Feb;247(**2**):320-6.

Gavala ML, Hill LM, Lenertz LY, Karta MR, Bertics PJ. Activation of the transcription factor FosB/activating protein-1 (AP-1) is a prominent downstream signal of the extracellular nucleotide receptor P2RX7 in monocytic and osteoblastic cells. *J Biol Chem* 2010 Oct 29;285(**44**):34288-98.

Grinnell F. (1994). Fibroblasts, myofibroblasts, and wound contraction. J. *Cell Biol*. **124**, 401–404.

Grinnell F. (2000). Fibroblast-collagen-matrix contraction: growth-factor signalling and mechanical loading. *Trends Cell Biol*. **10**, 362–365.

Guckenberger DJ, de Groot T,E., Wan AMD, Beebe DJ, Young EWK. Micromilling: a method for ultra-rapid prototyping of plastic microfluidic devices. *Lab chip*. 2015;15(**11**):2364-78.

Gudipaty L, Humphreys BD, Buell G, Dubyak GR. Regulation of P2X(7) nucleotide receptor function in human monocytes by extracellular ions and receptor density. *Am J Physiol Cell Physiol* 2001 Apr;280(**4**):C943-53.

Gullberg D., Tingstrom A., Thuresson A. C., Olsson L., Terracio L., Borg T. K., et al. . (1990). Beta 1 integrin-mediated collagen gel contraction is stimulated by PDGF. *Exp. Cell Res*. **186**, 264–272.

H. Zheng, J. Kim, M. Liew, J.K. Yan, O. Herrera, J.W. Bok, N.L. Kelleher, N.P. Keller, Y. Wang. "Redox metabolites signal polymicrobial biofilm development via the NapA oxidative stress cascade in *Aspergillus*", *Current Biology*, 2015, **25**, 29-37.

H.J. Kim, J.Q. Boedicker, J.W. Choi, R.F. Ismagilov, "Defined spatial structure stabilizes a synthetic multispecies bacterial community." *PNAS*, 2008, Nov., **105**, 18188-18193.

Halldorsson S, Lucumi E, Gómez-Sjöberg R, Fleming RMT. Advantages and challenges of microfluidic cell culture in polydimethylsiloxane devices. *Biosensors and Bioelectronics*. 2015;**63**:218-31.

Halwani R, Al-Muhsen S, Al-Jahdali H, Hamid Q. Role of transforming growth factor-beta in airway remodeling in asthma. *Am J Respir Cell Mol Biol* 2011 Feb;44(**2**):127-33.

Hatherell K, Couraud P, Romero IA, Weksler B, Pilkington GJ. Development of a three-dimensional, all-human in vitro model of the blood–brain barrier using mono-, co-, and tri-cultivation Transwell models. *Journal of Neuroscience Methods*. 2011;199(**2**):223-9.

Hinz B, Phan SH, Thannickal VJ, Galli A, Bochaton-Piallat ML, Gabbiani G. The myofibroblast: One function, multiple origins. *Am J Pathol* 2007 Jun;170(**6**):1807-16.

Huang G., Wang S., He X., Zhang X., Lu T. J., Xu F. (2013). Helical spring template fabrication of cell-laden microfluidic hydrogels for tissue engineering. *Biotechnol. Bioeng*. **110**, 980–989.

Huang G., Zhang X., Xiao Z., Zhang Q., Zhou J., Xu F., et al. (2012). Cell-encapsulating microfluidic hydrogels with enhanced mechanical stability. *Soft Matter*. **8**, 10687–10694.

Humayun M, Chow C, Young EWK. Microfluidic lung airway-on-a-chip with arrayable suspended gels for studying epithelial and smooth muscle cell interactions. *Lab Chip*. 2018;18(**9**):1298-309.

Ignotz RA, Massague J. Transforming growth factor-beta stimulates the expression of fibronectin and collagen and their incorporation into the extracellular matrix. *J Biol Chem* 1986 Mar 25;261(**9**):4337-45.

Ilagan R., Guthrie K., Quinlan S., Rapoport H. S., Jones S., Church A., et al. . (2010). Linear measurement of cell contraction in a capillary collagen gel system. *BioTechniques*. 48, 153–155.

Ito TK, Ishii G, Saito S, Yano K, Hoshino A, Suzuki T, et al. Degradation of soluble VEGF receptor-1 by MMP-7 allows VEGF access to ECs. *Blood*. 2009 Mar 5;113(**10**):2363-9.

J. Berthier, K.A. Brakke, E. Berthier, "Open Microfluidics". Wiley; 2016

J.N. Lee, C. Park, G.M. Whitesides, “Solvent compatibility of poly(dimethylsiloxane)-based microfluidic devices”, *Anal. Chem*, 2003, 75 (**23**), pp 6544-6554.

Jeffery P. (2001). Remodeling in asthma and chronic obstructive lung disease. *Am. J. Respir. Crit. Care Med.* **164**, S2–S38.

Jin T., Li L., Siow R. C. M., Liu K. (2015). A novel collagen gel-based measurement technique for quantitation of cell contraction force. *J. R. Soc. Interface*. **12**. 10.1098

Jonas O., Duschl C. (2010). Force propagation and force generation in cells. *Cytoskeleton (Hoboken)*. **67**, 555–563.

K. Hatherell, P.O. Couraud, I.A. Romero, B. Weksler, G.J. Pilkington, “Development of a three-dimensional, all-human *in vitro* model of the blood-brain barrier using mono-, co-, and tri-cultivation Transwell models”. *Journal of Neuroscience Methods*, 2011, **199**, 223-229.

K. Shimizu, N.P. Keller. “Genetic involvement of a cAMP-dependent protein kinase in a G protein signaling pathway regulating morphological and chemical transitions in Aspergillus nidulans”. Genetics, 2001, 157, 591–600.

K. Smith, R. Rajendran, S. Kerr, D. Lappin, W.G. Mackay, C. Williams, G. Ramage. “*Aspergillus fumigatus* enhances elastase production in *Pseudomonas aeruginosa* co-cultures”, *Medical Mycology*, 2015, **53**¸645-655.

K.H. Spencer, M.Y. Kim, C.C.W. Hughes, E.E. Hui, “A screen for short-range paracrine interactions”, *Integr. Biol.*, 2014, **6**, 382.

K.J. Regehr, M. Domenech, J.T. Koepsel, K.C. Carver, S.J. Ellison-Zelski, W.L. Murphy, L.A. Schuler, E.T. Alarid, D.J. Beebe, “Biological implications of polydimethylsiloxane-based microfluidic cell culture”, *Lab Chip*, 2009, Aug., 9 (**15**), 2132-2139.

K.J. Son, P. Gheibi, G. Stybayeva, A. Revzin. “Detecting cell-secreted growth factors in microfluidic devices using bead-based biosensors”, *Microsystems and Nanoengineering* (2017), **3**, 17025.

Kang DH, Kanellis J, Hugo C, Truong L, Anderson S, Kerjaschki D, et al. Role of the microvascular endothelium in progressive renal disease. *J Am Soc Nephrol*. 2002 Mar;13(**3**):806-16.

Kendall R. T., Feghali-Bostwick C. (2014). Fibroblasts in fibrosis: novel roles and mediators. *Front. Pharmacol*. **5**:123.

Khetan S., Burdick J. A. (2011). Patterning hydrogels in three dimensions towards controlling cellular interactions. *Soft Matter*. **7**, 830–838.

Kim BS, Chen J, Weinstein T, Noiri E, Goligorsky MS. VEGF expression in hypoxia and hyperglycemia: reciprocal effect on branching angiogenesis in epithelial-endothelial co-cultures. *J Am Soc Nephrol*. 2002 Aug;13(**8**):2027-36.

Kim HJ, Boedicker JQ, Choi JW, Ismagilov RF. Defined spatial structure stabilizes a synthetic multispecies bacterial community. *Proc Natl Acad Sci USA*. 2008;105(**47**):18188.

Klein Wolterink RG, Kleinjan A, van Nimwegen M, Bergen I, de Bruijn M, Levani Y, Hendriks RW. Pulmonary innate lymphoid cells are major producers of IL-5 and IL-13 in murine models of allergic asthma. *Eur J Immunol* 2012 May;42(**5**):1106-16.

Koh G. C., Shek L. P., Goh D. Y., Van Bever H., Koh D. S. (2007). Eosinophil cationic protein: is it useful in asthma? A systematic review. *Respir. Med.* **101**, 696–705

Kowal-Bielecka O, Kowal K, Distler O, Rojewska J, Bodzenta-Lukaszyk A, Michel BA, Gay RE, Gay S, Sierakowski S. Cyclooxygenase- and lipoxygenase-derived eicosanoids in bronchoalveolar lavage fluid from patients with scleroderma lung disease: An imbalance between proinflammatory and antiinflammatory lipid mediators. *Arthritis Rheum* 2005 Dec;52(**12**):3783-91.

Kramann R, Humphreys BD. Kidney pericytes: roles in regeneration and fibrosis. *Semin Nephrol.* 2014 Jul;34(**4**):374-83.

L. Goers, P. Freemont, K.M. Polizzi, "Co-culture systems and technologies: taking synthetic biology to the next level." *J. R. Soc. Interface*, 2014, **11**, 0065.

L.J. Barkal, A.B. Theberge, C.J. Guo, J. Spraker, L. Rappert, J. Berthier, et al., "Microbial metabolomics in open microscale platforms." *Nature Com*. 2016, Feb, **7**, 10610.

L.J. Barkal, C.L. Procknow, Y.R. Alvarez-Garcia, M. Niu, J.A. Jimenez-Torres, R.A. Brockman-Schneider, et al. "Microbial volatile communication in human organotypic lung models", *Nat. Comm.*, Accepted.

L.J. Barkal, E. Berthier, A.B. Theberge, N.P. Keller, D.J. Beebe. "Multikingdom microscale models", *PLoS Pathog*, 2017, **13**, 8: e1006424.

L.M. Borland, S. Kottegoda, K.S. Phillips, N.L. Allbritton, "Chemical analysis of single cells", *Annu. Rev. Anal. Chem.*, 2008, **1**, 191-227.

Lauffenburger DA, Zigmond SH. Chemotactic factor concentration gradients in chemotaxis assay systems. *Journal of Immunological Methods*. 1981;40(**1**):45-60.

Lee SH, Heinz AJ, Shin S, Jung Y, Choi S, Park W, et al. Capillary Based Patterning of Cellular Communities in Laterally Open Channels. *Anal Chem*. 2010;82(**7**):2900-6.

Lee UN, Su X, Guckenberger DJ, Dostie AM, Zhang T, Berthier E, et al. Fundamentals of rapid injection molding for microfluidic cell-based assays. *Lab Chip*. 2018;18(**3**):496-504.

Lee Y, Choi JW, Yu J, Park D, Ha J, Son K, et al. Microfluidics within a well: an injection-molded plastic array 3D culture platform. *Lab Chip*. 2018;18(**16**):2433-40.

Leung B. M., Moraes C., Cavnar S. P., Luker K. E., Luker G. D., Takayama S. (2015). Microscale 3D collagen cell culture assays in conventional flat-bottom 384-well plates. *J. Lab. Autom.* **20**, 138–145.

Levy BD, Bonnans C, Silverman ES, Palmer LJ, Marigowda G, Israel E, Severe Asthma Research Program, National Heart, Lung, and Blood Institute. Diminished lipoxin biosynthesis in severe asthma. *Am J Respir Crit Care Med* 2005 Oct 1;172(**7**):824-30.

Li Y, Wingert RA. Regenerative medicine for the kidney: stem cell prospects & challenges. *Clin Transl Med*. 2013 May 21;2(**1**):1-11.

Ligresti G, Nagao RJ, Xue J, Choi YJ, Xu J, Ren S, et al. A Novel Three-Dimensional Human Peritubular Microvascular System. *J Am Soc Nephrol*. 2016 Aug;27(**8**):2370-81.

Lijnen P., Petrov V., Fagard R. (2001). In vitro assay of collagen gel contraction by cardiac fibroblasts in serum-free conditions. *Methods Find. Exp. Clin. Pharmacol*. **23**, 377–382.

Ling Y., Rubin J., Deng Y., Huang C., Demirci U., Karp J. M., et al. . (2007). A cell-laden microfluidic hydrogel. *Lab Chip*. **7**, 756–762.

Liu M, Yokomizo T. The role of leukotrienes in allergic diseases. *Allergol Int* 2015 /1;64(**1**):17-26

Liu Y. Cellular and molecular mechanisms of renal fibrosis. *Nat Rev Nephrol*. 2011 Oct 18;7(**12**):684-96.

Lloyd AC. The regulation of cell size. *Cell*. 2013 Sep 12;154(**6**):1194-205.

M. Domenech, H. Yu, J. Warick, N.M. Badders, I. Meyvantsson, C.M. Alexander, D.J. Beebe, "Cellular observations enabled by microculture: paracrine signaling and population demographics." *Integr. Biol*., 2009, **1**, 267-274.

M. Verhulsel, M. Vignes, S. Descroix, L. Malaquin, D.M. Vignjevic, J.L. Viovy. "A review of microfabrication and hydrogel engineering for micro-organs on chips", *Biomaterials*, **35**, (2014), 1816-1832.

M.S. Liberio, M.C. Sadowski, C. Soekmadji, R.A. Davis, C.C. Nelson; "Differential effects of tissue culture coating substrates on prostate cancer cell adherence, morphology, and behavior". *PLoS ONE*, 2014, 9(**11**): e112122.

Maeshima Y, Makino H. Angiogenesis and chronic kidney disease. *Fibrogenesis Tissue Repair*. 2010 Aug **5**;3:1-13.

Marcu R, Choi YJ, Xue J, Fortin CL, Wang Y, Nagao RJ, et al. Human Organ-Specific Endothelial Cell Heterogeneity. *iScience*. 2018;**4**:20-35.

Margulis A., Nocka K. H., Wood N. L., Wolf S. F., Goldman S. J., Kasaian M. T. (2009). MMP dependence of fibroblast contraction and collagen production induced by human mast cell activation in a three-dimensional collagen lattice. *Am. J. Physiol. Lung Cell. Mol. Physiol*. 296:236.

Mehling M, Tay S. Microfluidic cell culture. *Current Opinion in Biotechnology*. 2014;**25**:95-102.

Michalik M, Pierzchalska M, Legutko A, Ura M, Ostaszewska A, Soja J, Sanak M. Asthmatic bronchial fibroblasts demonstrate enhanced potential to differentiate into myofibroblasts in culture. *Med Sci Monit* 2009 Jul;15(**7**):BR194-201.

Mikami Y., Matsuzaki H., Takeshima H., Makita K., Yamauchi Y., Nagase T. (2016). Development of an in vitro assay to evaluate contractile function of mesenchymal cells that underwent epithelial-mesenchymal transition. *J. Vis. Exp*. 2016:53974.

Miki Y, Ono K, Hata S, Suzuki T, Kumamoto H, Sasano H. The advantages of co-culture over mono cell culture in simulating in vivo environment. *The Journal of Steroid Biochemistry and Molecular Biology*. 2012;131(**3**):68-75.

Miyata J, Arita M. Role of omega-3 fatty acids and their metabolites in asthma and allergic diseases. *Allergol Int* 2015 Jan;64(**1**):27-34.

Moraes C., Simon A. B., Putnam A. J., Takayama S. (2013). Aqueous two-phase printing of cell-containing contractile collagen microgels. *Biomaterials*. **34**, 9623–9631.

N. Bhattacharjee, A. Urrios, S. King, A. Folch. "The upcoming 3D-printing revolution in microfluidics", *Lab Chip*, 2016, **16**, 1720.

N. Rao, G.N. Grover, L.G. Vincent, S.C. Evans, Y.S. Choi, K.H. Spencer, E.E. Hui, A.J. Engler, K.L. Christman, "A co-culture device with a tunable stiffness to understand combinatorial cell-cell and cell-matrix interactions", *Integr. Biol.*, 2013, **5**¸1344.

Nangaku M. Chronic hypoxia and tubulointerstitial injury: a final common pathway to end-stage renal failure. *J Am Soc Nephrol*. 2006 Jan;17(**1**):17-25.

Nash, C., Mavria, G., Baxter, E., Holliday, D., Tomlinson, D., Treanor, D., Novitskaya, V., Berditchevski, F., Hanby, A., Speirs,V. Development and characterisation of a 3D multi-cellular *in vitro* model of normal human breast: a tool for cancer initiation studies. *Oncotarget*. 2015;6(**15**).

Nolan DJ, Ginsberg M, Israely E, Palikuqi B, Poulos MG, James D, et al. Molecular signatures of tissue-specific microvascular endothelial cell heterogeneity in organ maintenance and regeneration. *Dev Cell*. 2013 Jul 29;26(**2**):204-19.

Oh S, Ryu H, Tahk D, Ko J, Chung Y, Lee HK, et al. "Open-top" microfluidic device for in vitro three-dimensional capillary beds. *Lab Chip*. 2017;17(**20**):3405-14.

Ohnishi H, Miyahara N, Gelfand EW. The role of leukotriene B4 in allergic diseases. *Allergol Int* 2008 01/01;57(**4**):291-8.

Oliveira NM, Vilabril S, Oliveira MB, Reis RL, Mano JF. Recent advances on open fluidic systems for biomedical applications: A review. *Materials Science and Engineering*: C. 2019;**97**:851-63.

P. Concus, R. Finn; "On the behavior of a capillary surface in a wedge". *PNAS*, 1969, June, 2 (**63**), 292-299.

P. Gheibi, K.J. Son, G. Stybayeva, A. Revzin. "Harnessing endogenous signals from hepatocytes using a low-volume multi-well plate", *Integr. Biol.*, 2017, 9, 427.

Palpant NJ, Pabon L, Friedman CE, Roberts M, Hadland B, Zaunbrecher RJ, et al. Generating high-purity cardiac and endothelial derivatives from patterned mesoderm using human pluripotent stem cells. *Nature Protocols*. 2016;12:15.

Palygin O, Levchenko V, Ilatovskaya DV, Pavlov TS, Pochynyuk OM, Jacob HJ, et al. Essential role of Kir5.1 channels in renal salt handling and blood pressure control. *JCI insight*. 2017;2(**18**):e92331.

Park SA, Jeong MS, Ha K, Jang SB. Structure and function of vascular endothelial growth factor and its receptor system. *BMB reports*. 2018;51(**2**):73-8.

PlanagumÃ A, Kazani S, Marigowda G, Haworth O, Mariani TJ, Israel E, Bleecker ER, Curran-Everett D, Erzurum SC, Calhoun WJ, et al. Airway lipoxin A(4) generation and lipoxin A(4) receptor expression are decreased in severe asthma. *Am J Respir Crit Care Med* 2008 Sep 15;178(**6**):574-82.

R. Hatoum, S. Labrie, I. Fliss. "Antimicrobial and probiotic properties of yeasts: from fundamental to novel applications". *Front. Microbiol*., 2012, **3**, 421.

Redd MA, Zeinstra N, Qin W, Wei W, Martinson A, Wang Y, et al. Patterned human microvascular grafts enable rapid vascularization and increase perfusion in infarcted rat hearts. *Nature Communications*. 2019;10(**1**):584.

Redden R. A., Doolin E. J. (2003). Collagen crosslinking and cell density have distinct effects on fibroblast-mediated contraction of collagen gels. *Skin Res. Technol*. **9**, 290–293.

Regehr KJ, Domenech M, Koepsel JT, Carver KC, Ellison-Zelski SJ, Murphy WL, et al. Biological implications of polydimethylsiloxane-based microfluidic cell culture. *Lab Chip*. 2009 Aug 7;9(**15**):2132-9.

Riteau N, Gasse P, Fauconnier L, Gombault A, Couegnat M, Fick L, Kanellopoulos J, Quesniaux VF, Marchand-Adam S, Crestani B, et al. Extracellular ATP is a danger signal activating P2X7 receptor in lung inflammation and fibrosis. *Am J Respir Crit Care Med* 2010 Sep 15;182(**6**):774-83.

Roti Roti EC, Torr EE, Fichtinger P, Guadarrama A, Sandbo N, Denlinger LC. Alveolar macrophages from subjects with asthma release pro-inflammatory LTB4 in ratio excess to LXA4 upon P2X7 stimulation, promoting fibrotic remodeling. In: d101. allergy and asthma: Novel regulatory pathways. *Am Thoracic Soc*; 2016.

Royce S. G., Cheng V., Samuel C. S., Tang M. L. K. (2012). The regulation of fibrosis in airway remodeling in asthma. *Mol. Cell. Endocrinol*. **351**, 167–175.

Rudnicki M, Perco P, Enrich J, Eder S, Heininger D, Bernthaler A, et al. Hypoxia response and VEGF-A expression in human proximal tubular epithelial cells in stable and progressive renal disease. *Lab Invest*. 2009 Mar;89(**3**):337-46.

Rusu L, Minshall R. Endothelial Cell von Willebrand Factor Secretion in Health and Cardiovascular Disease. In: ; 2018.

Ruth J. H., Esnault S., Jarzembowski J. A., Malter J. S. (1999). Calcium ionophore upregulation of AUUUA-specific binding protein activity is contemporaneous with granulocyte macrophage colony-stimulating factor messenger RNA stabilization in AML14.3D10 cells. *Am. J. Respir. Cell Mol. Biol.* **21**, 621–628.

S. Bersini, J.S. Jeon, G. Dubini, C. Arrigoni, S. Chung, J.L. Charest et al. "A microfluidic 3D *in vitro* model for specificity of breast cancer metastasis to bone", *Biomaterials*, **35**, (2014), 2454-2461.

S. March, V. Ramanan, K. Trehan, S. Ng, A. Galstain, N. Gural. et al, "Micropatterned coculture of primary human hepatocytes and supportive cells for the study of hepatotropic pathogens". *Nature Protocols*, 2015, **10**, 2027-2053.

S. Saegusa, M. Totsuka, S. Kaminogawa, T. Hosoi; "*Saccharomyces cerevisiae* and *Candida albicans* stimulate cytokine secretion from human neutrophil-like HL-60 cells differentiated with retinoic acid or dimethylsulfoxide". *Biosci. Biotechnol. Biochem*., 2009, 73, (**12**), 2600-2608.

S. Takayama, J.C. McDonald, E. Ostuni, M.N. Liang, P.J. Kenis, R.F. Ismagilov, G.M. Whitesides, "Patterning Cells and Their Environments Using Multiple Laminar Fluid Flows in Capillary Networks." *PNAS*, 1999, May, **96**, 5545-5548

S.H. Lee, A.J. Heinz, S. Shin, Y.G. Jung, S.E. Choi, W. Park, J.H. Roe, S. Kwon. "Capillary based patterning of cellular communities in laterally open channels", *Anal. Chem.*, 2010, **82**, 2900-2906.

S.N. Bhatia, D.E. Ingber. *Nature Biotechnology*, 2014, **32**, 760–772.

S.N. Bhatia, U.J. Balis, M.L. Yarmush, M. Toner, "Microfabrication of hepatocyte/fibroblast co-cultures: Role of homotypic cell interactions." *Biotechnol. Prog*., 1998, May-Jun, **14** (3), 378-387.

Sackmann E. K., Fulton A. L., Beebe D. J. (2014). The present and future role of microfluidics in biomedical research. *Nature*. **507**, 181–189.

Schierbaum N., Rheinlaender J., Schäffer T. E. (2019). Combined atomic force microscopy (AFM) and traction force microscopy (TFM) reveals a correlation between viscoelastic material properties and contractile prestress of living cells. *Soft Matter*. **15**, 1721–1729.

Sia SK, Whitesides GM. Microfluidic devices fabricated in Poly(dimethylsiloxane) for biological studies. *Electrophoresis*. 2003;24(**21**):3563-76.

Sköld C. M., Liu X. D., Umino T., Zhu Y. K., Ertl R. F., Romberger D. J., et al. . (2000). Blood monocytes attenuate lung fibroblast contraction of three-dimensional collagen gels in coculture. *Am. J. Physiol. Lung Cell. Mol. Physiol*. 279:667.

Spontaneous Capillary Flow Between Horizontal Rails. Open Microfluidics. 2016.

Stan R, Tse D, Deharvengt S, Smits N, Xu Y, Luciano M, et al. The Diaphragms of Fenestrated Endothelia: Gatekeepers of Vascular Permeability and Blood Composition. *Developmental Cell*. 2012;23(**6**):1203-18.

Stone HA, Stroock AD, Ajdari A. Engineering Flows in Small Devices: Microfluidics Toward a Lab-on-a-Chip. *Annu Rev Fluid Mech*. 2004;*36*(**1**):381-411.

Stumm CL, Wettlaufer SH, Jancar S, Peters-Golden M. Airway remodeling in murine asthma correlates with a defect in PGE2 synthesis by lung fibroblasts. *Am J Physiol Lung Cell Mol Physiol* 2011 Nov;301(**5**):L636-44.

Szmitko PE, Wang Chao-Hung, Weisel RD, de Almeida JR, Anderson TJ, Subodh V. New Markers of Inflammation and Endothelial Cell Activation. *Circulatio*n. 2003;108(**16**):1917-23.

T. Kojima, C. Moraes, S.P. Cavnar, G.D. Luker, S. Takayama, "Surface templated hydrogel patterns prompt matrix-dependent migration of breast cancer cells towards chemokine-secreting cells." *Acta Biomaterialia,* 2015, **13**, 68-77.

T.M. Keenan, A. Folch. "Biomolecular gradients in cell culture systems", *Lab Chip*, 2008, **8**, 34-57.

Tan SH, Nguyen N, Chua YC, Kang TG. Oxygen plasma treatment for reducing hydrophobicity of a sealed polydimethylsiloxane microchannel. *Biomicrofluidics*. 2010;4(**3**):32204.

Tasnim F, Zink D. Cross talk between primary human renal tubular cells and ECs in cocultures. *Am J Physiol Renal Physiol*. 2012 Apr 15;302(**8**):1055.

The Human Microbiome Project Consortium. “Structure, function, and diversity of the healthy human microbiome”. *Nature*, 2012, June, **486**, 207-214.

Timpson P., McGhee E. J., Erami Z., Nobis M., Quinn J. A., Edward M., et al. (2011). Organotypic collagen I assay: a malleable platform to assess cell behaviour in a 3-dimensional context. *J. Vis. Exp.* 2011:e3089.

Tomasini-Johansson BR, Johnson IA, Hoffmann FM, Mosher DF. Quantitative microtiter fibronectin fibrillogenesis assay: Use in high throughput screening for identification of inhibitor compounds. *Matrix Biol* 2012 Jul;31(**6**):360-7.

Torr EE, Ngam CR, Bernau K, Tomasini-Johansson B, Acton B, Sandbo N. Myofibroblasts exhibit enhanced fibronectin assembly that is intrinsic to their contractile phenotype. *J Biol Chem* 2015 Mar 13;290(**11**):6951-61.

Tourovskaia A, Fauver M, Kramer G, Simonson S, Neumann T. Tissue-engineered microenvironment systems for modeling human vasculature. *Exp Biol Med (Maywood)*. 2014 Sep;239(**9**):1264-71.

V.V. Abhyankar, D.J. Beebe, “Spatiotemporal micropatterning of cells on arbitrary substrates”. *Anal. Chem*., 2007, **79**, 4066-4073.

van Midwoud PM, Janse A, Merema MT, Groothuis GM, Verpoorte E. Comparison of biocompatibility and adsorption properties of different plastics for advanced microfluidic cell and tissue culture models. *Anal Chem*. 2012 May 1;84(**9**):3938-44.

Vedula EM, Alonso JL, Arnaout MA, Charest JL. A microfluidic renal proximal tubule with active reabsorptive function. *PLoS One*. 2017 Oct 11;12(**10**):e0184330.

Velve-Casquillas G, Le Berre M, Piel M, Tran PT. Microfluidic tools for cell biological research. *Nano today*. 2010;5(**1**):28-47.

Vempati P, Popel AS, Mac Gabhann F. Extracellular regulation of VEGF: isoforms, proteolysis, and vascular patterning. *Cytokine Growth Factor Rev*. 2014;25(**1**):1-19.

Vernon R. B., Gooden M. D. (2002). An improved method for the collagen gel contraction assay. *In Vitro Cell. Dev. Biol. Anim*. **38**, 97–101.

Villegas G, Lange-Sperandio B, Tufro A. Autocrine and paracrine functions of vascular endothelial growth factor (VEGF) in renal tubular epithelial cells. *Kidney Int*. 2005 Feb;67(**2**):449-57.

Walsh EJ, Feuerborn A, Wheeler JHR, Tan AN, Durham WM, Foster KR, et al. Microfluidics with fluid walls. *Nat Commun*. 2017 Oct 10;8(**1**):81-4.

Weisgrab G, Ovsianikov A, Costa PF. Functional 3D Printing for Microfluidic Chips. *Adv Mater Technol*. 2019;4(**10**):1900275.

Whitesides G. M. (2006). The origins and the future of microfluidics. *Nature*. **442**, 368–373.

Winterbourn CC. Reconciling the chemistry and biology of reactive oxygen species. *Nat Chem Biol*. 2008 May;4(**5**):278-86.

Wygrecka M. F. A. U. D. B., Kosanovic D. F., Petersen F. F., Taborski B, FAU, von Gerlach, von Gerlach S. F., et al. . (2013). Mast cells and fibroblasts work in concert to aggravate pulmonary fibrosis: role of

transmembrane SCF and the PAR-2/PKC-alpha/Raf-1/p44/42 signaling pathway. *Am. J. Pathol*. **182**, 2094–2108.

Xu T, Zhao W, Zhu J, Albanna MZ, Yoo JJ, Atala A. Complex heterogeneous tissue constructs containing multiple cell types prepared by inkjet printing technology. *Biomaterials*. 2013;34(**1**):130-9.

Y. Gao, D. Majumdar, B. Jovanovic, C. Shaifer, P.C. Lin, A. Zijlstra et al. "A versatile valve-enabled microfluidic cell co-culture platform and demonstration of its applications to neurobiology and cancer biology", *Biomed Microdevices*, (2011), **13**:539-548.

Y. Miki, K. Ono, S. Hata, T. Suzuki, H. Kumamoto, H. Sasano, "The advantages of co-culture over mono cell culture in simulating *in vivo* environment". *Journal of Steroid Biochemistry and Molecular Biology*, 2012, **131**, 68-75.

Y. Torisawa, B. Mosadegh, G.D. Luker, M. Morell, K.S. O'Shea, S. Takayama "Microfluidics hydrodynamic cellular patterning for systematic formation of co-culture spheroids." *Integr. Bio.*, 2009, **1**, 649-654.

Y.S. Torisawa, B Mosadegh, S.P. Cavnar, M. Ho, S. Takayama, "Transwells with microstamped membranes produce micropatterned two-dimensional and three-dimensional cocultures." *Tissue Eng Part C Methods*, 2011, Jan, 17 (**1**), 61-67.

Young EW, Berthier E, Beebe DJ. Assessment of enhanced autofluorescence and impact on cell microscopy for microfabricated thermoplastic devices. *Anal Chem*. 2013 Jan 2;85(**1**):44-9.

Young EWK, Beebe DJ. Fundamentals of microfluidic cell culture in controlled microenvironments. *Chem Soc Rev*. 2010;39(**3**):1036-48.

Young EWK, Berthier E, Guckenberger DJ, Sackmann E, Lamers C, Meyvantsson I, et al. Rapid Prototyping of Arrayed Microfluidic Systems in Polystyrene for Cell-Based Assays. *Anal Chem*. 2011;83(**4**):1408-17.

Yun H, Kim K, Lee WG. Cell manipulation in microfluidics. *Biofabrication*. 2013;5(**2**):022001.

Zagai U., Dadfar E., Lundahl J., Venge P., Sköld C. M. (2007). Eosinophil cationic protein stimulates TGF-beta1 release by human lung fibroblasts in vitro. *Inflammation.* **30**, 153–160.

Zagai U., Sköld C. M., Trulson A., Venge P., Lundahl J. (2004). The effect of eosinophils on collagen gel contraction and implications for tissue remodelling. *Clin. Exp. Immunol*. **135**, 427–433.

Zervantonakis IK, Kothapalli CR, Chung S, Sudo R, Kamm RD. Microfluidic devices for studying heterotypic cell-cell interactions and tissue specimen cultures under controlled microenvironments. *Biomicrofluidics*. 2011;5(**1**):13406.

Zhang T, Day JH, Su X, Guadarrama AG, Sandbo NK, Esnault S, et al. Investigating Fibroblast-Induced Collagen Gel Contraction Using a Dynamic Microscale Platform. *Frontiers in Bioengineering and Biotechnology*. 2019;7:196.

Zhang T, Lih D, Nagao RJ, Xue J, Berthier E, Himmelfarb J, et al. Open microfluidic coculture reveals paracrine signaling from human kidney epithelial cells promotes kidney specificity of endothelial cells. *Am J Physiol Renal Physiol.* 2020 May 11.

Zhang X, Huk DJ, Wang Q, Lincoln J, Zhao Y. A microfluidic shear device that accommodates parallel high and low stress zones within the same culturing chamber. *Biomicrofluidics.* 2014;8(**5**):054106.

Zhao Y, Zhao H, Zhang Y, Tsatralis T, Cao Q, Wang Y, et al. Isolation and epithelial co-culture of mouse renal peritubular ECs. *BMC cell biology*. 2014;15:40; 4-40.

Zhou J, Khodakov DA, Ellis AV, Voelcker NH. Surface modification for PDMS-based microfluidic devices. *Electrophoresis.* 2012;33(**1**):89-104.

Zhu Y. K., Liu X. D., Sköld M. C., Umino T., Wang H., Romberger D. J., et al. (2001). Cytokine inhibition of fibroblast-induced gel contraction is mediated by PGE2 and NO acting through separate parallel pathways. *Am. J. Respir. Cell. Mol. Biol*. **25**, 245–253.

Zimmermann M, Bentley S, Schmid H, Hunziker P, Delamarche E. Continuous flow in open microfluidics using controlled evaporation. *Lab Chip*. 2005;5(**12**):1355-9.

VITA

Tianzi Zhang was born and raised in Xi'an, China. She studied at the High School Affiliated to Shaanxi Normal University. After high school, Tianzi attended Cornell College in Mount Vernon, IA, where she graduated with a BA in chemistry in 2015. Tianzi then decided to pursue a PhD in Chemistry at University of Washington-Seattle, where she worked in Theberge Lab to develop microfluidic cell culture platforms and understand cell signaling mechanisms underlying human diseases, such as chronic kidney disease and pulmonary fibrosis in asthma.